Master Thesis

Wik Breure

Towards Improved Design of Rock Reinforcement Systems for Underground Excavations Subjected to Strain Bursting

August, 2017

Graduation committee:

Prof. Dr.	C. Jommi	Chair Delft University of Technology, department Geo-Engineering
Dr. Ir.	D.J.M Ngan-Tillard	Daily Supervisor Delft University of Technology, department Geo-Engineering
Dr.	J.H.L. Voncken	External Supervisor Delft University of Technology, department Resource Engineering
Prof. Dr.	C.C. Li	External supervisor Norwegian University of Science and Technology, department of Geoscience and Petroleum

Summary

This thesis report presents a concept methodology to quantify the energy release associated with strain bursting in underground excavations based on the size of the failed zone and the elastic strain energy stored in the rock mass prior to failure. A strain burst implies potential harm to people and machinery and may lead to economic loss. An increased understanding of the amount of released energy rock support systems are subjected to allows for more convenient excavation design and risk mitigation.

Rock tunnels subjected to high in situ stresses may host strain bursts, a stress induced failure mechanism where elastic strain energy is released with the failing rock through the violent ejection of fragments. As it is often not practicable to prevent the occurence of strain bursts mitigation measures are required so that the consequences can be kept at an acceptable level. This means that the energy released with the failing rock has to be dissipated by a rock reinforcement system (e.g. rock bolts and steel wire mesh) to obtain a stable situation after a burst. To date quantification of the released kinetic energy (E_{tot}) is assessed based on the equation $E_{tot} = \frac{1}{2} m_{rock} v_e^2$, in which m_{rock} is the mass of the ejected rock and v_e the ejection velocity. Because v_e is squared in this formulation E_{tot} is most dependent on this parameter. Therefore, effords were made to back calculate its quantity from the trajectory of ejected rock (Tannant et al. (1993)). It was found that burst damage becomes evident if the ejection velocity exceeds $3m/s$, is most likely to be in the range of $4 - 6m/s$ but can be up to $10m/s$ for small rock fragments. This large variety makes approximation of the total energy release uncertain and implies a need for an alternative method to assess energy release associated with strain bursting.

According to the methodology proposed in this thesis the total energy release is calculated as: $E_{tot} = E_1 V$. In this formulation E_1 equals the energy release per unit of failing rock and V the volume of failing rock. In order to investigate this approach case studies from Sweden, China and Peru were selected to get realistic input parameters of conditions in which strain bursts occur (e.g. stress state, excavation geometry, rock mass strength).

The energy release per unit of failing rock is determined by the surface under the elastic share of the stress strain curve in a unconfined compressive strength (UCS) test up to the loading rate corresponding with the in situ strength. When elaborating data from test tunnels presented by Martin et al. (1999) it showed that the in situ strength amounts approximately 40% of the UCS. A major advantage of the proposed approach is that the energy release is a function of just the UCS and the stiffness E_{mod} of the rock mass, parameters that are relatively easy to derive.

Support systems consisting of (dynamic) rock bolts and steel mesh are considered most effective in burst prone conditions. Therefore steel mesh and a bolting pattern of $1m \times 1m$ using split-set, rebar and D-Bolts were considered to study the response of the support system to dynamic loading from strain bursting. An analytic analysis of the convergence-confinement equilibrium for burst prone rock masses was set up. It showed that because of the low stiffness and support pressure derived from such support systems the only purpose it serves is retaining the failed rock by dissipating the released energy. Because mesh supplies so called "loose retention" the rock mass will shift before being retained. This makes it uncertain whether there is a support stress from the failed rock on the intact rock. Therefore the depth of failure from an unsupported excavation is considered a proper estimator for the depth of failure in a supported excavation.

To assess the size and geometry of the localised failed zone by means of numerical analyis the methodology as proposed by Martin et al. (1999) was adopted. Based on this approach the depth of failure in unsupported excavations can be derived using the generalised Hoek-Brown failure criterion with $m = 0$ and $s = 0.11$

assuming linear elastic material behavior. A major advantage of this approach is that the geometry of the failed zone is approximated as a part of the solution. This allows for assessment of sufficient bolt length, and the number of bolts that are considered responsible for stabilising the failing rock mass (n_{bolt}). With the dynamic performance (e.g. Energy Dissipation Capacity, EDC_b) of the bolts being approximated from lab tests, deriving the dynamic performance of the system as a whole is a very straight forward exercise. The factor of safety (FOS) in engineering design can be calculated according to:

$$FOS = n_{bolt} EDC_b / E_{tot} \tag{1}$$

It is suggested in recent publications that for excavations made by means of drilling and blasting the in situ strength may be underestimated because stress concentrations are more localised increasing the overal brittle strength of the rock mass (e.g. Cai and Kaiser (2014a)). Case studies of underground excavations where strain bursts occured are adopted to get an understanding of the setting in which such events happen (excavation geometry, stress state and rock mass properties). The results from all these cases show that the total energy release decreases with an increasing in situ rock mass strength σ_f. This means that a potential underestimation of the in situ strength when an excavation realised by means of drilling and blasting is considered leads to a conservative assessment with regard to the total released energy.

In order to verify whether the output of the alternative method is satisfactory, or in short *'makes sense'*, the output of the analysis is compared with a physical quantity that is measured: the ejection velocity v_e. For all cases, with an in situ strength ranging from $40-60\%$ of the UCS, ejection velocities were back calculated and values ranging from $3.3-7.1 m/s$ were found, which is in good agreement with the measured ejection velocities.

Acknowledgments

I would like to express my sincere gratitude to Dominque Ngan-Tillard, Charlie Chunlin Li, Christina Jommi and Jack Voncken for their supervision and constructive feedback during my master thesis project. I am grateful that you have given me the opportunity to write my thesis on a topic that appealed to me and enjoyed the discussions we had on the theory, literature and which approach to apply.

Finishing my master thesis is a milestone, which makes it a good moment to thank my parents for their support throughout my life. You showed me it is fun to know about different things and always gave me the freedom to make my own decisions. It is hard to put into words how thankful I am for this.

Studying at Delft University of Technology has been an inspiring experience which has brought me far beyond just Delft and the university itself. I would like to thank everybody that has been on this adventure with me for the great times and lessons learned.

List of Symbols

Symbol	Definition
Acronyms	
AE	Acoustic Event
EDC	Energy Dissipation Capacity
EDC_b	Energy Dissipation Capacity - single rock bolt
FOS	Factor of Safety
GRC	Ground Response Curve
GSI	Geological Strength Index
HB	Hoek-Brown
LDP	Longitudinal Deformation Profile
$LEBP$	Linear Elastic Brittle Plastic
$LEPP$	Linear Elastic Perfectly Plastic
MC	Mohr-Coulomb
RQD	Rock Quality Designation
RMR	Rock Mass Rating
UCS	Unconfined Compression Strenght (σ_{ci})
PLT	Point Load Test
PSI	Pounds per Square Inch ($1psi \approx 6.89kPa$)
SL	Stress Level
SRC	Support Response Curve
$SS46$	Split Set bolt with 46mm cross section diameter
TBM	Tunnel Boring Machine

Symbol	Definition	Unit
Latin letters		
a	Hoek Brown exponent a	$-$
a_r	Residual Hoek Brown exponent a	$-$
A	Surface area	m^2
c	Cohesion	MPa
c_r	Residual cohesion	MPa
d	horizontal distance	m
d_b	Diameter rock bolt cross section	m
D	Disturbance factor	$-$
E_b	Modulus of elasticity Bolt steel	MPa
E_{mod}	Modulus of elasticity rock mass	MPa
E_s	Modulus of elasticity steel	MPa
E_{tot}	Total energy release failing rock	kJ
E_1	Energy release per unit of failing rock	kJ/m^3
f	Plastic strain ratio ϵ_1 over ϵ_3	$-$
F	Force	MN
G	Shear modulus rock mass	MPa
h	Height	m
H	Depth below surface	m
k_b	Elastic rock bolt stiffness	MN/m
k_r	Elastic rock mass unloading stiffness	MN/m
k_s	Elastic stiffness rock reinforcement system	MN/m
K_0	Coefficient of horizontal stress (k also used)	$-$
l	Length (bolt)	m
m	Hoek Brown parameter m	$-$
m_{dil}	Hoek Brown dilation parameter	$-$
m_i	Hoek Brown parameter m for intact rock	$-$
m_r	Residual Hoek Brown parameter m	$-$
m_{rock}	Mass failed rock	kg
m_{drop}	Mass dropped weight	kg
n_{bolt}	Amount of rock bolts	$-$
p	In-situ hydrostatic pressure	MPa
$p_{i,cr}$	Critical support pressure	MPa
p_i	Internal support pressure	MPa
p_z	Vertical in situ stress ($= \sigma_v$)	MPa
$P_{sb,max}$	In situ strength rock reinforcement system	MPa
r	Radius	m
r_i	Radius circular tunnel	m
$r_{i,eq}$	Equivalent radius circular tunnel	m
r_e	Radius plastic zone around circular tunnel	m
R_f	Equivalent tunnel radius plus depth of failure	m
s	Hoek Brown parameter s	$-$
s_c	Circumferential bolt spacing	$-$
s_l	Longitudinal bolt spacing	$-$
s_r	Residual Hoek Brown parameter s	$-$
u	Deformation	m
u_{i0}	Rock mass deformation prior to installation reinforcement	m
u_b	Deformation rock bolt	m
u_{ie}	Deformation reinforcement system	m
T_{bf}	(Dynamic) bolt axial strength	m
v_{drop}	Striking velocity dropped weight	m/s
v_e	Ejection velocity failing rock	m/s
v_f	Final velocity ejected rock	m/s
V	Volume	m^3
w	Width	m

Symbol	Definition	Unit
Greek letters		
α	Share of strain energy available at failure	kN/m^3
γ	Density rock material $\approx 27kN/m^3$	kN/m^3
θ	Ejection angle rock block	$^\circ$
ϵ	Strain	-
$\epsilon_1 = \epsilon_\theta$	Elastic strain major principal stress	-
$\epsilon_3 = \epsilon_r$	Elastic strain minor principal stress	-
ϵ_1^p	Plastic strain major principal stress	-
ϵ_3^p	Plastic strain minor principal stress	-
ϵ_{1e}	Strain major principal stress elastic/plastic boundary	-
ϵ_{3e}	Strain minor principal stress elastic/plastic boundary	-
ν	Poisson's ratio	-
ρ	Density rock ($\approx 2700kg/m^3$)	kg/m^3
σ	Stress	MPa
σ_{ci}	UCS intact rock	MPa
σ_{cm}	UCS rock mass	MPa
σ_{di}	Damage initiation stress	MPa
σ_f	Unconfined strength rock mass	MPa
σ_h	Horizontal in-situ stress	MPa
$\sigma_{max,r}$	Maximum roof stress	MPa
σ_p	Peak stress during UCS test ($= \sigma_{ci}$)	MPa
σ_r	Radial stress	MPa
σ_{res}	Residual strength	MPa
$\sigma_{max,s}$	Maximum sidewall stress	MPa
σ_{sd}	Systematic damage stress	MPa
σ_t	Tensile strength intact rock	MPa
σ_v	Vertical in-situ stress	MPa
σ_z	Out of plane in-situ stress	MPa
σ_θ	Tangential or circumferential stress	MPa
$\sigma_{\theta,max}$	Maximum tangential or circumferential stress	MPa
$\sigma_{\theta r}$	Shear stress	MPa
σ_1	Major principal stress	MPa
σ_2	Intermediate principal stress	MPa
σ_3	Minor principal (confining) stress	MPa
ϕ	Friction angle rock mass	$^\circ$
ϕ_r	Friction angle failed rock mass	$^\circ$

Contents

List of Figures

List of Tables

Chapter 1

Introduction

There is a large interest in understanding the behavior of underground excavations through massive rock masses subjected to high in situ stresses. In such a setting stress induced failure mechanisms, such as strain bursting, may be triggered. In a tunnel or mine drift this violent failure mechanism is the result of accumulated elastic strain energy that is released from the rock mass after excavation through the ejection of fragments. In underground operations a rock burst implies a danger to people and machinery, may cause downtime and potential economic loss.

When excavating highly stressed rock masses it is often not practicable to prevent the occurrence of a rock burst. In such cases mitigation measures that keep the consequences at an acceptable level are required. Rock bursting is associated with energy release from the rock mass when failure occurs, which means that sufficcient energy dissipation by the reinforcement system has to take place in order to obtain a stable situation after failure. At this moment measures are available to mitigate the consequences of strain bursting. For example dynamic rock support is already applied in some burst prone settings (e.g. D-bolt in the Kiruna mine, Sweden, Li (2010)).

1.1 Problem Definition

Currently the recommended way to assess energy release associated with strain bursting is based on the kinetic energy of the ejected rock mass, according to: $E_{tot} = \frac{1}{2} m_{rock} v_e^2$ (e.g. Kaiser et al. (1996)). From test results a large variety in ejection velocities are found, which leads to difficulties when selecting appropriate input parameters. Also, assessment of the mass of rock that is involved in the burst event is up to the engineering judgment of the person designing the excavation. From a physical point of view the stated relationship to derive the energy release is not considered wrong, but the derivation of the input parameters (m_{rock}, v_e) is very unsatisfying.

1.2 Research Question

In this research an alternative method to approximate the energy release is proposed, based on the energy release per unit of failing rock (E_1) and the volume of rock (V) involved with failure ($E_{tot} = E_1 V$). From this the following research questions follow:

- Can input parameters for this proposed method be derived, and how?
- Is the derivation procedure for the input parameters convenient?
- Is the outcome of energy release assessment satisfactory when using the proposed method?
- How can the proposed method be implemented in support design and excavation design?

1.3 Hypothesis

A method to approximate the energy release during strain bursting based on the volume of failing rock and the energy release per unit of failing rock will allow for better assessment than based on $E_{tot} = m_{rock} v_e^2$. The

size of the failed zone and the energy release at failure are a function of the depth of failure when a burst occurs, the stress strain behavior of the rock and the in situ strength of the rock mass. These parameters can be quantified with sufficient accuracy using currently available methods and knowledge to allow for (*preliminary*) assessment of the total energy release.

1.4 Definition of Strain Burst

When consulting different literature sources, various definitions on strain bursting are found. Examples of definitions are: *"Violent spalling with ejection of fragments"* - Ortlepp and Stacey (1994), *"A sudden and violent failure of overstressed rock resulting in the instantaneous release of large amounts of accumulated energy"* - Whyatt et al. (2002), *"Strain bursting is the violent rupture of a volume of wall rock under high stress (...) it is the instability created by the formation of paralell and thin spall slabs that provides for the sudden energy release"* - Diederichs (2007). Spalling is described by Fairhurst and Cook (1966) as tensile splitting parallel to the major principal compressive stress.

Summarizing these definitions the following becomes clear:

- Strain bursting is associated with brittle spalling.
- The release of energy that is associated with a strain burst is causing the failing rock mass to be ejected from the excavation boundary into the drift or tunnel.
- The development of a strain burst is a sequential process that starts with the formation of spall slabs and eventually followed by failure of these slabs.

Simply adding up the different elements presented in these definitions gives a proper but elaborate definition of a strain burst: *"A failure event that originates from an highly stressed rock mass in which tensile splitting has taken place after which the accumulated strain energy is suddenly released from a formed slab through ejection into the tunnel."* A visual representation of this mechanism is given in Figure 1.1.

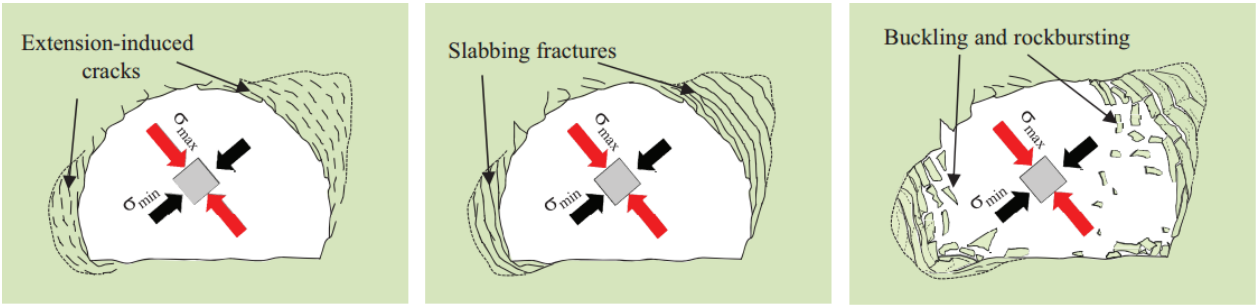

Figure 1.1: Development of strain burst failure (from: Qiu et al. (2014))

A characteristic of rock masses is that the quality tends to increase with depth, which means in practice that they become more massive (Martin (1994)). In the research described in this thesis massive rock masses in high stress conditions are considered, as they tend to facilitate spalling and strain bursting (Broch and Sørheim (1984)).

Two forms of rock burst can be distinguished in practice, being strain bursting and fault slip type bursts. Only the prior is considered in this research. In the case of a fault slip rock burst energy is released when shear slip occurs along a fault, causing damage to an excavation situated at a distance from the slipping fault (Ortlepp and Stacey (1994)).

Chapter 2

Theoretical Background

This chapter presents an overview of the theory on which this research is based. When a more elaborate explanation is given in an appendix, a reference is stated.

2.1 Rock Mass Failure

In underground excavations through rock generally two modes of failure can be identified, being structurally controlled failure (e.g. wedge failure) and stress induced failure (e.g. shear failure and spalling). Stress induced failure of brittle and moderately jointed to massive rock masses (GSI 70) loaded in compression will occur in the form of spalling (Diederichs (2007)). According to Kaiser (2006) the dominant mode of failure depends on the ratio between the maximum tangential stress around the underground opening (σ_θ) divided by the uniaxial compressive strength (UCS) of the intact rock (σ_{ci}). This ratio is denoted using the dimensionless stress level parameter SL, as shown in Equation 2.1.

$$SL = \frac{\sigma_\theta}{\sigma_{ci}} \tag{2.1}$$

Stress induced failure starts to be the dominant failure mechanism rather than structurally controlled failure when $SL \gtrsim 0.8$. When $SL \gtrsim 1.15$, stress induced failure is commonly the critical failure mechanism. Strain burst, being a violent form of spalling, is associated with high stress levels (Palmström (1995)).

Failure of brittle rocks in compression is characterized by a sudden drop in mobilised strength. Linear elastic brittle plastic (LEBP) behavior as opposed to linear elastic perfectly plastic (LEPP) behavior is displayed in Figure 2.1. The residual strength of a failed brittle rock mass is a function of the confinement the failed rock experiences. This topic will be discussed in detail later in this chapter. When failed rock does not experience confinement (e.g. UCS testing or unsupported excavation) the residual rock mass strength is zero.

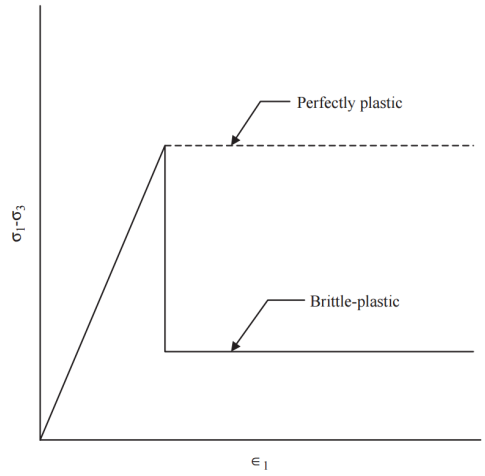

Figure 2.1: LEPP and LEBP behavior (from: Sharan (2003))

Before excavation an in situ stress is acting on a rock mass at a certain depth. After excavation the rock mass is subjected to a compressive tangential stress ($\sigma_\theta = \sigma_1$) parallel to the excavation boundary in combination with no confining radial stress ($\sigma_r = \sigma_3 = 0$) when the excavation is unsupported. For example, when considering a hydrostatic in situ stress $\sigma_h = \sigma_v = p$, a circular excavation and plain strain conditions, the tangential stress σ_θ equals two times the in situ stress (Figure 2.2, see Appendix C). It is because of this stress state that the behavior of brittle rocks in UCS testing is of major importance to understand the in situ behavior of a brittle rock mass close to the excavation boundary in high stress conditions after excavation.

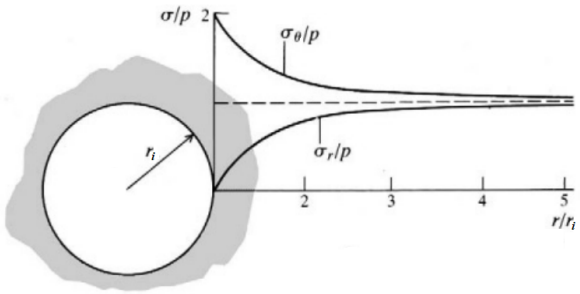

Figure 2.2: Stress distribution elastic material behavior, *note:* $a = r_i$, (from: Brady and Brown (2007), *adjusted*)

In order to understand the behavior of brittle rock in compression, it is important to comprehend that processes in which tensile cracks are formed play a major role. The boundaries between grains are flaws or micro defects, and act as zones of weakness from where tensile cracks will start to form when rock is loaded in compression (Griffith (1921)). The occurrence of tensile forces at a grain boundary under compressive loading is visualized in Figure 2.3.

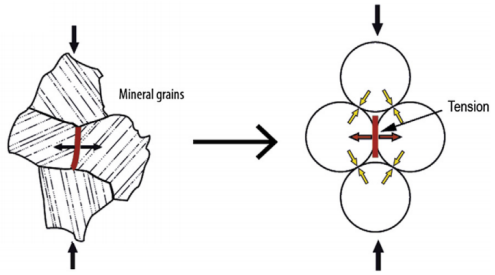

Figure 2.3: Tensile stresses in rock under compressive loading (from: Hoek and Martin (2014))

Cracks start to form when the compressive stress in a rock mass is sufficiently high. It is well documented that the in situ crack initiation stress in brittle rock masses corresponds with the crack initiation stress in UCS testing and amounts 30-50% of the UCS of an intact rock sample (Goodman (1989), Diederichs (2007), Hoek and Martin (2014), Cai and Kaiser (2014b) and Appendix A). In the crack initiation stage the cracks are formed randomly and are mostly separated from each other (Eberhardt et al. (1998)). When compression increases the cracks start to propogate, which tends to happen in the direction parallel to the major principal stress (Hoek and Bieniawski (1965)). When in the roof or wall of a tunnel tensile cracking occurs on a micro scale, the formed cracks can develop to a macro scale causing the formation of rock slabs parallel to both the major principal stress and excavation boundary (Fairhurst and Cook (1966)). Failure of the formed slabs is referred to as spalling. When considering the definition of strain bursting presented in chapter 1 the phenomenon is referred to as a form of violent spalling. When cracks have formed in the rock mass, it can still carry loads paralell to the formed slabs Diederichs (2007). When stresses built up in the slab sudden and violent failure can occur as the result of buckling: a strain burst. The sequence of tensile cracking, slab formation and slab buckling is displayed in the introduction of this report (Figure 1.1).

As opposed to strain bursting non violent failure of spall slabs may occur as well, when lower stresses accumulate prior to failure. This is referred to as slabbing (Li (2017b)). An example of mild spalling in a hard and massive rock mass is shown in Figure 2.4. If an underground excavation is subjected to a non hydrostatical in situ stress state the damaged area tends to develop along the direction of minimum principal

in situ stress due to stress concentrations, resulting in the characteristic triangular shaped failed area like displayed in Figure 2.4.

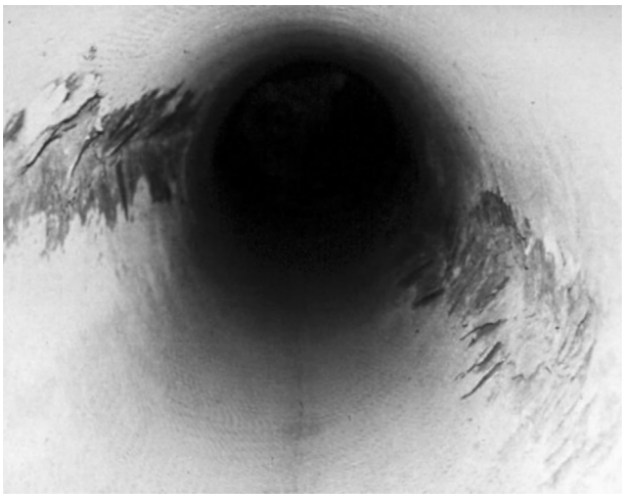

Figure 2.4: Mild spalling of wall rock in a raise boring shaft (from: Hoek and Brown (1980b))

2.2 Modeling Spalling Behavior

Strength criteria such as the Mohr-Coulomb (MC) and Hoek-Brown (HB) failure are based on the idea that the ultimate strength of rock is a function of a cohesive and the frictional component. Both criteria are not elaborated in this chapter but an explanation can be found in Appendix B. The MC criterion is based on c and ϕ denoting the cohesion and friction angle respectively. The Hoek-Brown failure criterion is an emperical strength criterion based on a large set of tensile, uniaxial and triaxial test data on different rock types and describes the ratio between the principal stresses σ_1 and σ_3 at failure (Hoek and Brown (1980a), Appendix B). As a consequence the parameters s and m are also empirical and unitless. However, s and m are often referred to as the HB version of the frictional and cohesive parameter respectively. This is because s determines whether the rock has a tensile strength capacity and m determines the slope of the failure envelope (Equation 2.2). Both the MC and HB failure criterion are explained in detail in Appendix B.

$$\sigma_1 = \sigma_3 + \sigma_{ci}\left(m\frac{\sigma_3}{\sigma_{ci}} + s\right)^a \tag{2.2}$$

When using the MC or HB criterion it is indirectly assumed that the cohesive and frictional component of the rock mass strength are simultaniously available, which is not in agreement with the behavior of rock masses that fail through spalling. This is because cracking of rock is considered a loss on internal cohesion whereas the frictional component does not play a significant role in this process leading to spalling failure (Martin et al. (1999)). Since the frictional strength of brittle rock masses is not mobilised in situ, the original HB peak strength envalope is suppressed in low confinement conditions (Figure 2.5). After failure the broken rock is expected to behave as a rock fill with a certain friction angle but all internal cohesion is lost (Hoek and Brown (1997)).

Crack propagation and therefore in situ spalling behavior is limited by the so called spalling limit, denoted by the point where the in situ strength envelope starts to bend towards the original HB peak strenght envelope. This is due to the fact that crack propagation at higher degrees of confinement is suppressed. At higher degrees of confinement a stress state compared to the stress state in a triaxial test setting is obtained, which causes the rock mass to fail through shearing.

In order to find the in situ peak strength of brittle rock masses case studies on different excavations were studied and summarised by Martin et al. (1999). A data set is compiled out of observations from several

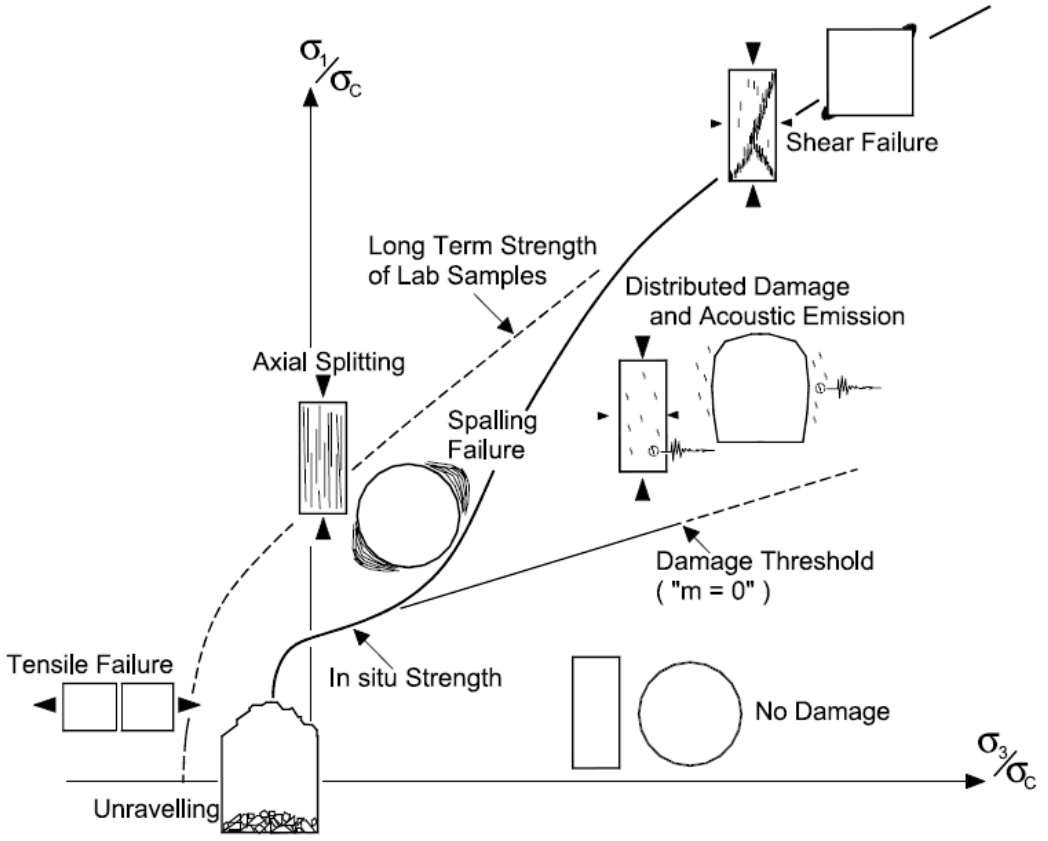

Figure 2.5: In situ failure mechanism brittle rock mass, solid line = origininal HB peak strength envalope, dashed line = in situ HB peak strength envalope brittle rock mass, $\sigma_c = \sigma_{ci}$, (from: Diederichs (2003))

unsupported (test) tunnels in which spalling occurred (Kaiser et al. (1996), Kirsten et al. (1979), Jiayou et al. (1989), Martin et al. (1989), Ortlepp and Gay (1984), Pelli et al. (1991) and Stacey (1977)). When the depth of failure with respect to the tunnel radius is plotted as a function of the maximum tangential stress at the excavation boundary $\sigma_{\theta,max}$ over the UCS (σ_{ci}) the image presented at the left hand side of Figure 2.6 is obtained.

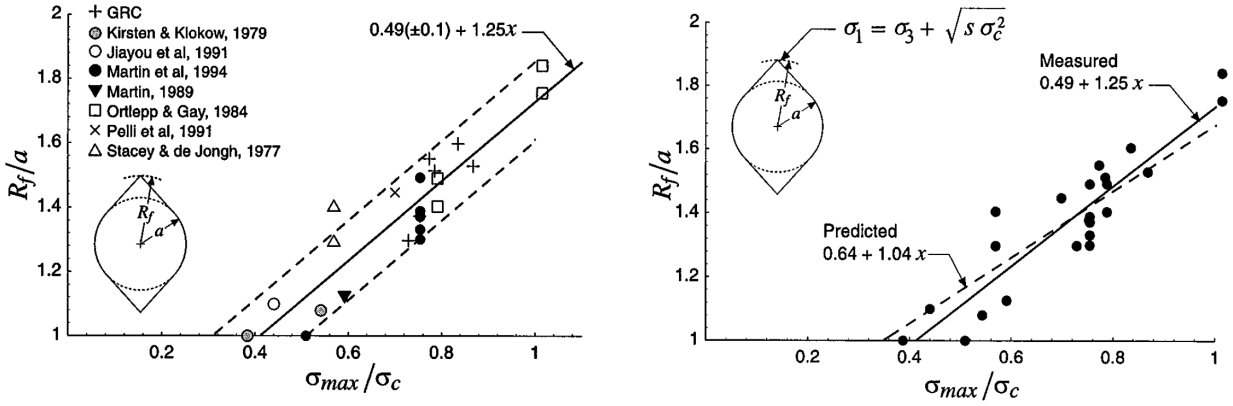

Figure 2.6: (L) Relation depth of failure and stresses. (R) Approximation based on proposed HB elastic parameters. (*Note:* $x = \sigma_{max}/\sigma_{ci}$, $\sigma_c = \sigma_{ci}$, $\sigma_{\theta,max} = \sigma_{max}$ *and* $a = r_i$) *from: Martin et al. (1999))*

From Figure 2.6 it can be derived that stress induced damage at the excavation initiates ($R_f/r_i = 1$) when $\sigma_{\theta,max} \approx 0.4\sigma_{ci}$. An approach to assess the depth of failure in spalling tunnels using the Hoek-Brown failure criterion is presented below.

As discussed the process of spalling is dominated by the cohesive strength of the rock mass. In line with this observation m, earlier described as the HB version of the friction angle ϕ, is taken to be 0. With this m value the expression for the peak strength of the rock mass (Equation 2.2) becomes as displayed in Equation 2.3. As suggested earlier the unconfined strength ($\sigma_3 = 0$) amounts approximately 40% of σ_{ci}, this corresponds with $s = 0.16$.

$$\sigma_1 = \sqrt{s}\sigma_{ci} + \sigma_3 \tag{2.3}$$

From a hypothesis stated and researched by Cai and Kaiser (2014a) and Guo et al. (2016) it follows that the aforementioned derivation of the in situ strength underestimates the brittle strength of tunnels and drifts excavated by means of drilling and blasting. Due to the rough excavation surface as the result of over break the stress concentrations at the excavation boundary will be local, rather than along a certain stretch of a smooth excavation boundary. This discontinuous stress state causes tensile cracks under compressive loading to be formed only locally, while a higher stress is required to cause brittle failure on a larger scale (spalling). As a result, tunnels excavated by means of drilling and blasting can have a higher in situ strength than would be predicted based on current practice. This hypothesis is discussed in chapter 5.

When LEBP rock mass behavior is applied, like in the analytic analysis in this thesis research, the residual frictional strength is a function of the confinement the failed rock experiences. Crowder and Bawden (2004) present guidelines suggested by Hoek on the resedual strength of brittle rock masses. As discussed it is assumed that there is no cohesion in failed brittle rock. In line with this the residual cohesion $s_r = 0$, and the residual frictional strength parameter m_r is proposed to be put to 1. This assumed value for m_r is introduced by Hoek et al. (2000) and according to the author an educated guess based on the thought that the internal cohesion is lost in combination with a strong reduction of the m with respect to the value of m_i due to the fact that the rock has failed (e.g. for quartzite, $m_i = 20 \pm 3$, Figure B.4). Because the UCS of intact rock is used in the residual strength criterion, m_r being reduced value with respect to m should be looked at as a 'penalty' given to the failed rock mass (see Appendix B). With these m_r and s_r values the expression for the residual strength of the rock mass (Equation 2.2) becomes as displayed in Equation 2.4. An example plot of the peak and residual strength envelope are given in the model output presented in Figure 4.5.

$$\sigma_1 = \sigma_3 + \sigma_{ci}\left(\frac{\sigma_3}{\sigma_{ci}}\right)^a \tag{2.4}$$

2.3 Localised Failure

When the in situ stress state is not hydrostatic failure is localised and the analytic models cannot be applied. Efforts were made by the author to implement LEBP material behavior in numerical finite element models (FEM), but without success. A discussion on the shortcomings of the obtained trial results is presented in chapter 5.

Alternatively numerical models based on purely elastic rock mass behavior were set up trying to find a value for the cohesional strength s corresponding with the closest fit so that the depth of failure could be approximated. It was found that the depth of failure could be approximated reasonably well when a value of 0.11 is adopted for s (Figure 2.6, right hand side). The corresponding failure envelope with these input parameters is shown in Figure 2.7.

When using the proposed values for s and m the size and geometry of the damaged or plastic zone around an excavation is not the same as that of the zone involved when spalling or strain bursting occurs, but does describe the depth of failure (Figure 2.8). Only in the exceptional theoretical case of a circular excavation through a homogeneous massive rock mass subjected to a hydrostatic in situ stress state the failed zone is formed around the entire excavation.

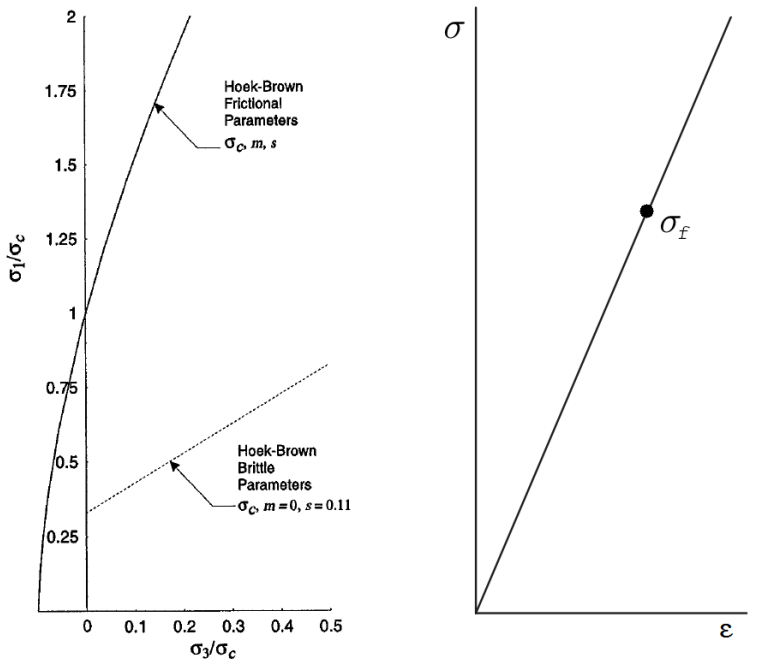

Figure 2.7: (L) Failure envelope generalised HB with $s = 0.11$ and $m = 0$ (from: Martin et al. (1999)) (R) Linear stress strain behavior

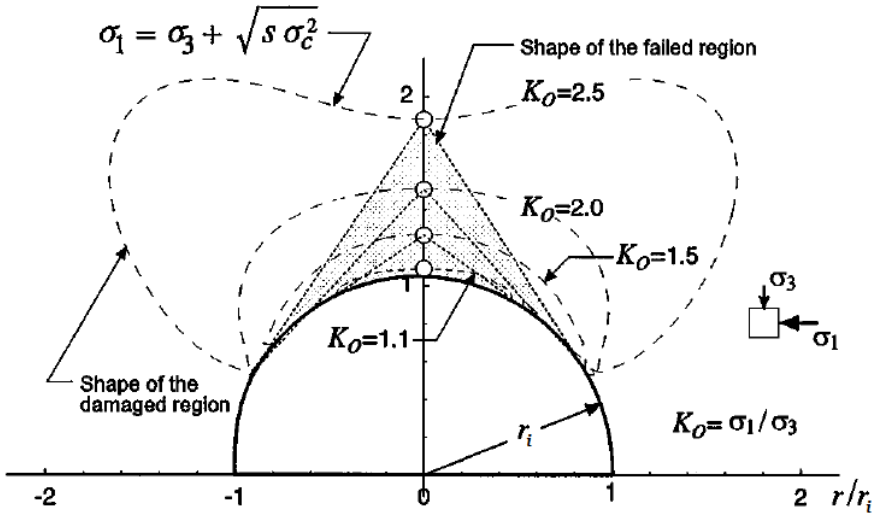

Figure 2.8: Damage and failure zone as a function of principal stress ratio K_0 (from: Martin et al. (1999))

As shown in Figure 2.8 the size and geometry of the failed zone are derived as a part of the solution. However, the amount of rock involved in a strain burst is denoted as a volume V. This volume is derived based on the surface area of the failed zone (A) in combination with the out of plane bolt spacing s_l, which determines the length of the section along the tunnel to be supported by an in plane row of bolts (Equation 2.5). This means that the calculated volume is not the absolute volume of failing rock but the volume of failing rock which is supported by a single row of bolts. Bolt types and the assumed bolt spacing are introduced later in this chapter.

$$V = As_l \tag{2.5}$$

2.4 Energy Release at Failure

In a lab setting a stress-strain curve will be obtained when conducting a UCS test on a cylindrical rock sample. The amount of energy consumed per volume of rock material is equal to the surface under this curve up to that point (deformation from point A to point B on the curve, according to Equation 2.6 and Figure 2.9).

$$E_1 = \alpha \int_A^B \sigma(\epsilon) d\epsilon \tag{2.6}$$

Deformation can be either elastic (reversible) or plastic (permanent) and during testing of a rock sample both will occur. Elastic energy can be described as a form of spring energy that is released when the rock fails in a brittle manner.

Lee et al. (2004) state that from intact volcanic and metamorphic rocks little plastic behavior is obtained when conducting a cyclic uniaxial compressive test. This is confirmed by Li (2017b), stating that approximately 90% of the deformation is elastic and recoverable at failure of such rock types. A consequence of this observation is that the primary loading curve and unloading curve roughly overlap prior to failure. From this it is assumed that the modulus of elasticity E_{mod} of the material can be approximated from the primary loading curve (Martin (1994)).

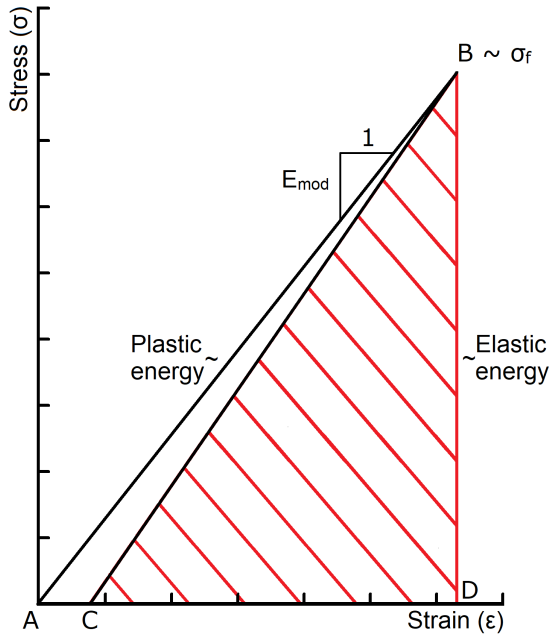

Figure 2.9: Energy released per unit of brittle failing rock (modified from Li (2017b))

The difference in angle between the primary loading line AB and unloading line BC originates from the fact that only elastic deformation is recovered when unloading, as plastic deformation is permanent. As discussed, $\alpha = 0.9$ is considered an appropriate value for a first estimation. Note that E_1 then equals the surface of the area designated with diagonal red stripes (BCD) displayed in Figure 2.9 and can be approximated with Equation 2.7. Note that as mentioned before the unit of E_1 is kJ/m^3. Likewise, the white area ABC in the latter image represents the plastic energy absorbed per unit volume of rock mass prior to failing.

$$E_1 = \alpha \frac{\sigma_f^2}{2E_{mod}} \tag{2.7}$$

In the latter formula σ_f equals the in situ unconfined strength of the rock mass. The value of σ_f is found by putting $\sigma_3 = 0$ in Equation 2.3, which leads to Equation 2.8. It is important to comprehend that confinement does increase the in situ strength of the rock but has no influence on E_1. This is because the additional strength due to confinement leads to the formation of additional cracks in the rock

(i.e. plastic deformation) which does not lead to additional elastic strain energy release at failure (Li (2017b)).

$$\sigma_f = \sqrt{s}\sigma_{ci} \tag{2.8}$$

With the the average energy released per unit of rock and size of the failure zone, respectively E_1 and V, calculated the total energy released at failure can be calculated according to Equation 2.9.

$$E_{tot} = VE_1 \tag{2.9}$$

The energy dissipation capacity (EDC) of a single in plane row of bolts equals the energy dissipation capacity of a single bolt (EDC_b) multiplied by the number of bolts that are involved in stabilising the ejected rock mass (Equation 2.10). In Figure 2.10 an example is given where two rock bolts are considered responsible for stabilising the ejected rock, displayed as a triangular block. Note that the volume (V) of ejected rock stabilised by these two bolts is a function of the out of plane bolt spacing (Equation 2.5). Between the bolts wire mesh has to be installed in order to retain broken rock and direct the released energy to the bolts. Because it is assumed that the wire mesh is only a retaining element (i.e. does not dissipate energy) it is not displayed in the image below. Different bolt types and retaining elements to be applied are introduced in the next section.

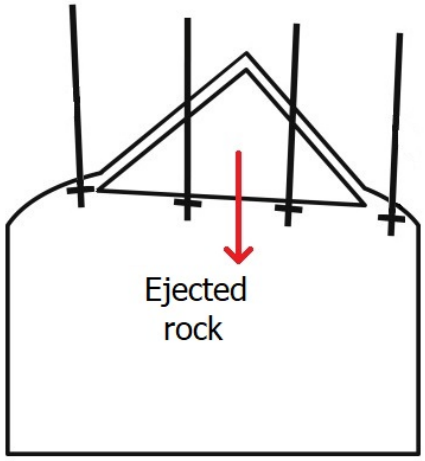

Figure 2.10: Roof bolting patern responsible for arresting ejected rock block, image from: Li (2017a), *adjusted*

$$EDC = n_{bolt}EDC_b \tag{2.10}$$

If EDC is larger than the released energy the dissipation has been successful, and a stable situation is obtained. This is the case if the following condition is met (Equation 2.11):

$$EDC > E_{tot} \tag{2.11}$$

Alternatively, a stable situation is obtained in theory if the factor of safety (FOS) exceeds 1 (Equation 2.12):

$$FOS = \frac{n_{bolt}EDC_b}{E_{tot}} = \frac{EDC}{E_{tot}} \tag{2.12}$$

However, it is strongly advised to design a reinforcement system aiming for a factor of safety which is higher (e.g. $FOS = 2$). A discussion on the considerations involved in selecting a factor of safety is presented in chapter 5.

2.5 Rock Reinforcement Systems

A rock reinforcement system consists out of multiple components, for instance: rock bolts, (reinforced) shotcrete and steel wire mesh. As discussed in chapter 5 systems including shotcrete are excluded from this research. This is because experience points out that shotcrete is unlikely to successfully retain bursting rock. A discussion on the applicability of shotcrete is presented in chapter 5. When support systems consisting out of bolts and steel wire mesh are considered it is assumed that the dynamic performance of the rock bolts is critical for the rock reinforcement system as a whole. In other words, it is assumed that bolt failure is considered failure of the system.

Three bolt types are considered, being: split set, grouted rebar and the D-bolt. These are all so called passive bolt types, which means that the support pressure is mobilised through deformation of the rock mass they are installed into. The response of a bolt to strain bursting in a lab setting can be modeled as a crack opening up by installing the bolt through two concrete blocks that are moved apart during a test. This can be done slowly or quickly in order to obtain either the static or dynamic response of the bolt (Appendix E). The characteristic static stress strain curve of these bolts is shown in Figure 2.11. The area under the load-deformation curve up till failure equals the amount of energy a particular bolt can consume before failing.

The three named rock bolt types exist in various geometries and versions (e.g. galvanised, non-galvanised, lengths and cross section diameter) which has an influence on strength properties. Also, when bolts are tested in a lab setting a certain variation in these properties is obtained. In this research a single but representative value for the strength, stiffness and energy dissipation capacity of the considered bolt types when loaded dynamically is used.

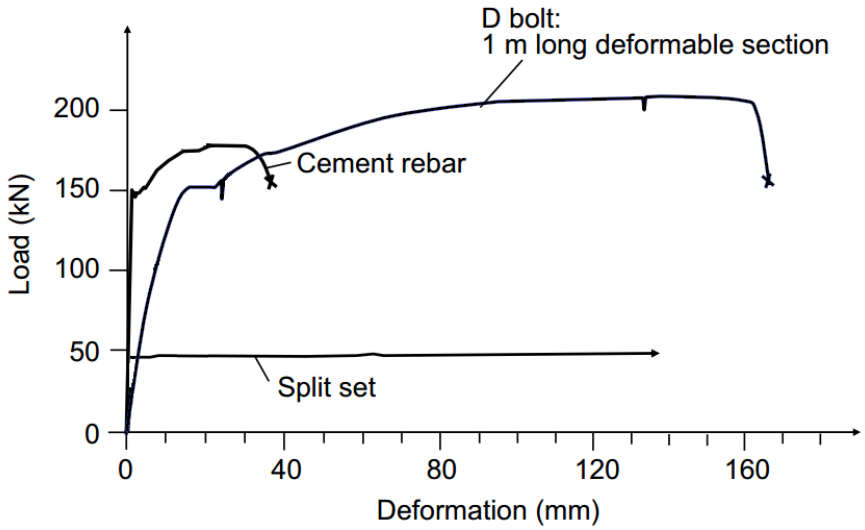

Figure 2.11: Static pull test split set bolt, $d_s = 20mm$ grouted rebar and 1 meter section of a D-bolt (from: Li (2010), *adjusted*)

Background theory on how the dynamic performance of bolts and their stiffness is derived can be found in Appendix E. Application of the reinforcement system in the confinement curve of the convergence confinement method is elaborated in Appendix D.

2.5.1 Split Set bolt

The split set bolt is a rock bolt that is installed by pushing it into an undersized hole, causing a tight interlock between the bolt steel and the rock mass. When loaded axially, the bearing capacity of the bolt is the result of the skin friction that is mobilised (Scott et al. (1977)). A typical characteristic of the bolt is that the stress remains constant when the peak is reached, meaning that the bolt is slipping through the hole. In this way a split set bolt is capable of withstanding large deformations without the bolt itself failing.

An image of a split set bolt is displayed in Figure 2.12.

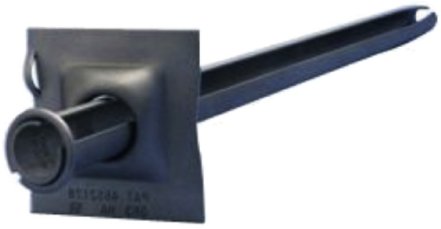

Figure 2.12: Split set bolt (image from: Li et al. (2014))

When testing Split set bolts in either a static or dynamic test a large variety in strength is obtained (Tomory et al. (1998), Player et al. (2009)). Li et al. (2014) presents observations by Stjern (1995) that for a 1 meter long SS46 (Split Set 46mm cross section diameter) bolt a pull out strength of approximatelly 50kN/m is representative. According to Player et al. (2009), the peak strength per meter of bolt has to be reduced by 50% to obtain a representative value for the peak strength in the case of dynamic loading (i.e. 25kN/m). On top of that, it was found that the energy dissipation capacity of an galvanised SS46 is approximately 11kJ per meter of embedment. In this research 2.5 meter long galvanised SS46 bolts are considered. Based on the aforementioned properties of the bolt the strength and energy dissipation capacity of this bolt is assumed to be as presented in Table 2.1.

2.5.2 D-Bolt

The D-Bolt is a smooth bar with multiple anchors along its length that is fully grouted when installed. The schematic layout of the D-Bolt is presented in Figure 2.13. When the bolt is loaded as the result of a burst (simualated as a crack opening up in a lab setting, Figure E.1) the stress is distributed evenly along the loaded smooth section between two anchors, which allows for full mobilisation of the strength and deformation capacity of the steel material (Li (2010), Li and Doucet (2012), Li (2012)).

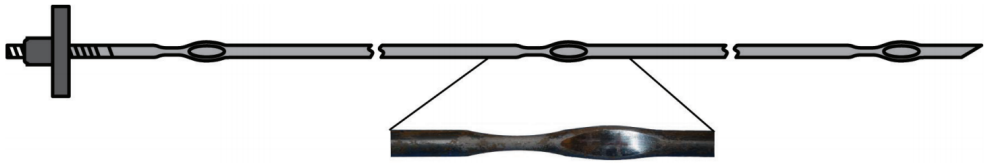

Figure 2.13: Layout of the D-bolt (image from: Normet (2014))

When a strain burst occurs the rock reinforcement system is subjected to dynamic loading, which causes the dynamic properties of the system to be mobilised. Normet (2014) presents typical responses of D-Bolts in static and dynamic conditions, as displayed in Figure 2.14. Visual assessment of these stress strain curves do show slight variations between both cases, but generally speaking it can be stated that the dynamic stress strain curve can be approximated with the stress strain curve representing the static performance.

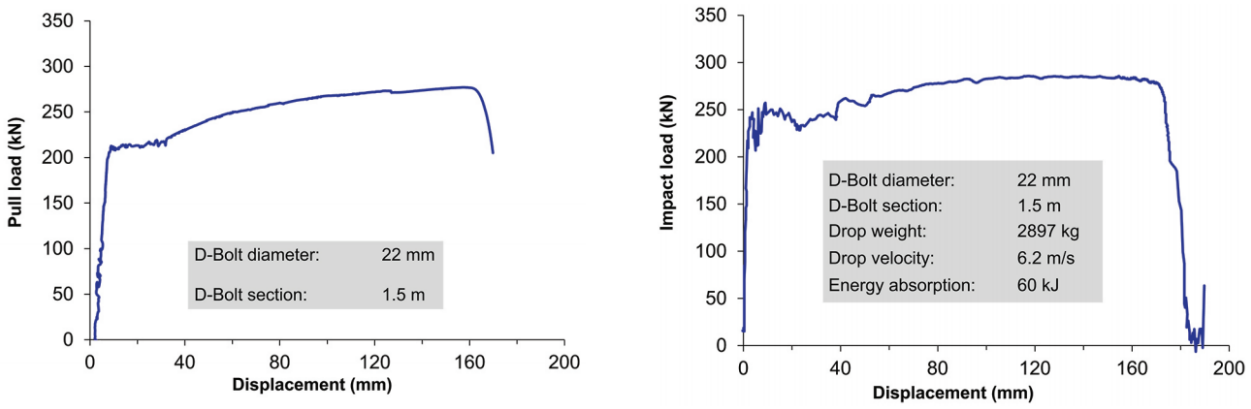

Figure 2.14: Typical static and dynamic performance D-bolt (from: Normet (2014))

2.5.3 Grouted Rebar Bolt

A grouted rebar (short for reinforcement bar, Figure 2.15) bolt is a rock bolt with a relatively high load bearing capacity but low deformation capacity once yielded (Figure 2.11). This behavior is the result of the fact that the stress accumulates in a short loaded section, causing the bolt to respond in a stiff manner. The deformation of a grouted rebar before failure is in the order of 30mm, regardless of the initial length of the bolt. Logically, the tensile strength of the bolt is directly proportional to the size of the cross section. It is assumed that the rebar bolt fails through the bolt steel.

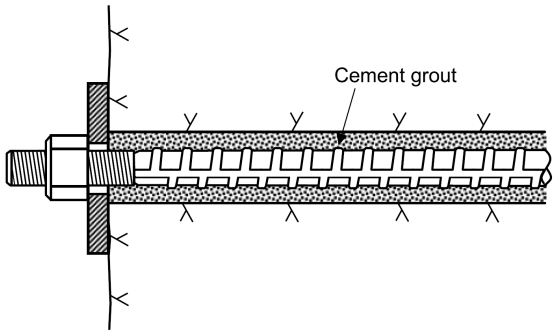

Figure 2.15: Schematic layout of an installed grouted rebar bolt (from: Li (2007))

For the D-Bolt it is displayed in Figure 2.14 that the static performance is a good estimator for the dynamic performance of the bolt. It is assumed that the static performance is a good estimator for the dynamic performance of grouted rebar bolts as well, when both bolt types fail through the bolt steel.

2.5.4 Bolt Property Summary

The maximum dynamic load as well as the energy absorbing capacity of the considered bolt types is summarized in Table 2.1. In this table T_{bf} represent the strength of the bolt when loaded dynamically. The stated parameters are based on the considerations presented in the previous sections. For all bolts a stiffness $E_b = 150MN/m$ is used (see Appendix E).

Bolt type	T_{bf} [kN]	EDC_b [kJ]	source	note
Grouted Rebar	200	5	Ortlepp and Stacey (1994)	$d_s = 22mm$
Split Set	62.5	27.5	Player et al. (2009), Li et al. (2014)	SS46
D-bolt	200	56	Li and Doucet (2012)	$d_s = 22mm$

Table 2.1: Dynamic peak load and energy absorbing capacity considered bolt types (length=2.5m)

2.6 Rock Mass Support Interaction

A visual representation of the required support pressure to stabilise the excavation as a function of the tunnel wall displacement is referred to as the convergence curve. This curve represents the tunnel deformation (u) as a function of the support pressure (p_i) for the considered cross section. Because support stress is derived from the presence of the face, this method allows for the inclusion of 3D effects in a 2D analysis. Figure 2.16 shows the theoretical Longitudinal Deformation Profile (LDP) along a tunnel in front of and behind the face. Convergence of the rock mass initiates at a distance of approximatelly one time the tunnel diameter ahead of the face. Roughly $\frac{1}{3}$ of the final displacement has taken place at the face and at a distance of two to three times the tunnel diameter (D) from the face the unsupported final displacement is obtained. The loss of support pressure or confinement as the result of the face moving away from the considered cross section explains this observation. Vlachopoulos and Diederichs (2009) point out that the convergence that has taken place when the rock reinforcement system is installed depends on the distance from the face at which this is done.

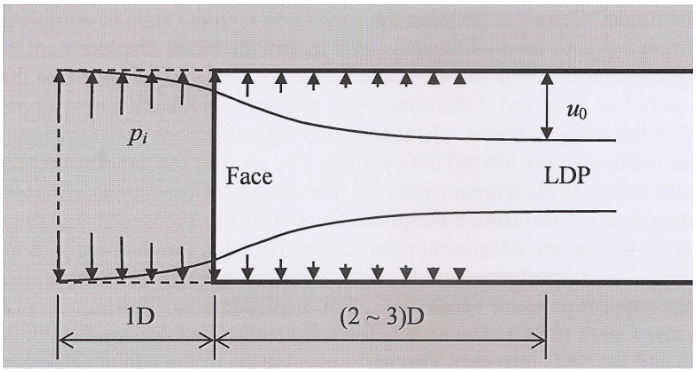

Figure 2.16: Support stress derived from the presence of the face, (from: Li (2016))

In theory the support stress will become zero if no rock support is applied. When the convergence curve is presented by a straight line the unloading behavior is linear. When the support pressure is reduced after the critical support pressure is reached plasticity occurs forming a plastic zone around the excavation. Deformation of the tunnel mobilises the support pressure of the reinforcement system. The origin of the support reaction curve (SRC) depends on distance from the face at which the support is installed. In the analytic analysis in this study it is assumed that reinforcement system is installed right at the face when $\frac{1}{3}$ of the final deformation has taken place already (installation at a certain distance from the face will cause the SRC to shift to the right). When equilibrium is reached tunnel wall deformation does not proceed. An example of such a convergence curve and convergence confinement equilibrium are shown in Figure 2.17. The formulation of the confinement curve is given and explained in Appendix D.

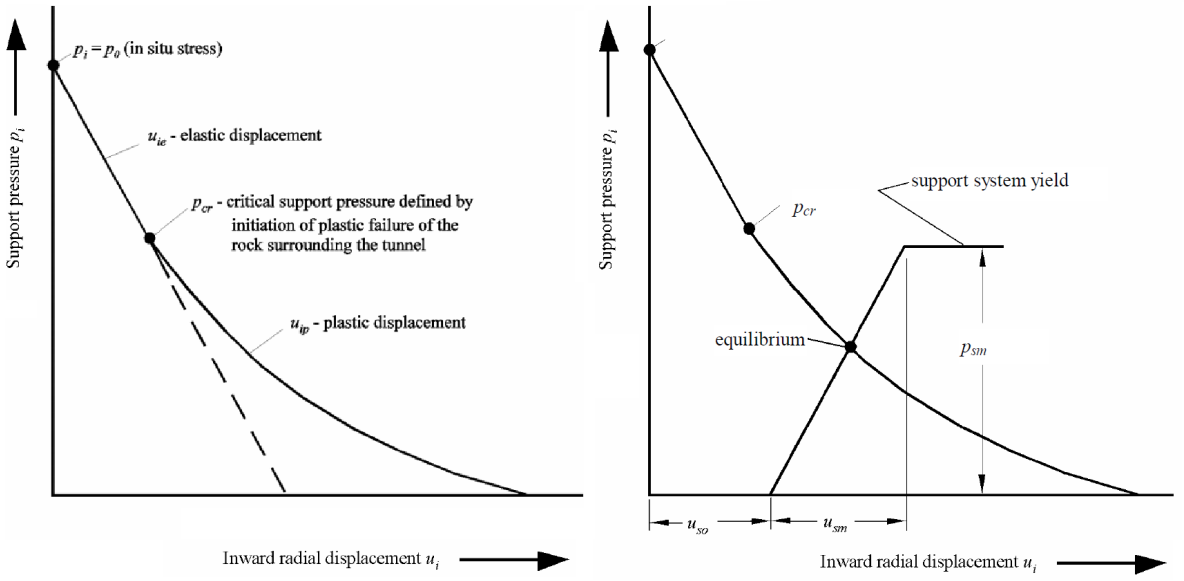

Figure 2.17: Convergence of tunnel (L) Convergence-Confinement equilibrium (R) (from: Hoek et al. (2000))

McCreath and Kaiser (1992) summarise that rock reinforcement systems serve three purposes, being: reinforcing, stabilising and retaining the rock mass. All purposes are briefly discussed individually underneath:

- **Reinforcing:** Deformation of the rock mass after excavation (convergence) causes the support stress of the reinforcement system to be mobilised. Since strength is confinement dependent the rock mass strength will increase when subjected to a confining support stress.

- **Stabilising:** When the support pressure from the reinforcement system equals the support pressure required to keep the rock mass from deforming any further a stable situation is obtained. Therefore the presence of a reinforcement system in theory limits deformation of the rock mass compared to a scenario in which no rock reinforcement is installed.

- **Retaining:** When rock yields while deforming it can be so that loose fragments are ejected from the excavation boundary. The rock reinforcement system supplies a physical barrier that keeps these fragments from entering the excavation (Figure 2.18).

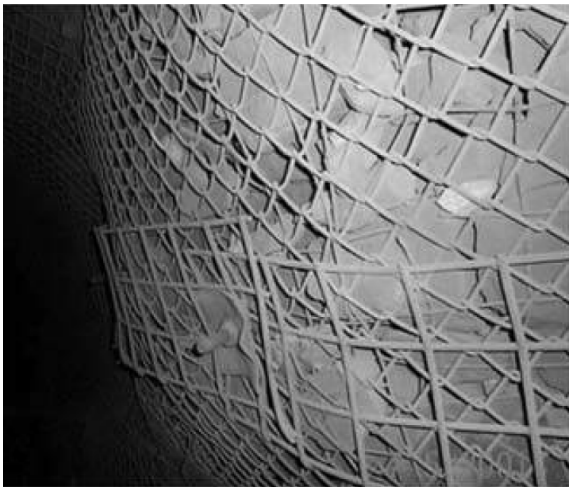

Figure 2.18: Loose rock fragments retained by mesh and bolts (from: Simser (2001))

2.7 Past Attempts To Assess Energy Release

When a strain burst occurs the accumulated strain energy is turned into kinetic energy and released with the failing rock. In the past efforts have been made trying to quantify the kinetic energy release based on Equation 2.13.

$$E_{tot} = \frac{1}{2} m_{rock} v_e^2 \tag{2.13}$$

In line with this approach the ejection velocity was backcalculated after a burst based on the trajectory of the ejected rock, as displayed in Figure 2.19. The ejection velocity was then estimated according to Equation 2.14 (Tannant et al. (1993)).

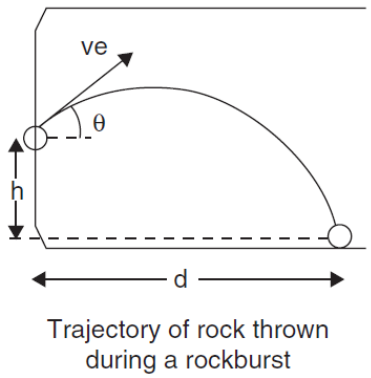

Figure 2.19: Back calculation ejection velocity from trajectory ejected rock (Tannant et al. (1993))

$$v_e = d\sqrt{\frac{g}{2h\cos^2\theta + \sin\theta}} \tag{2.14}$$

From these tests it was found that burst damage becomes evident from an ejection velocity of 3 m/s. The ejection velocity of large rock blocks was 4-6 m/s and could be up to 10 m/s for small pieces. As the velocity is squared in Equation 2.13, this range of possible ejection velocities also presents a wide range of possible quantities of energy released.

Ortlepp and Stacey (1994) provide a practical example giving an insight in the importance of a dynamic approach when assessing the performance of rock reinforcement systems. When considering a single rebar bolt with a static loading capacity of 190kN, the energy dissipation capacity amounts approximately 5kJ (Figure 2.20, right hand side). The theoretical static loading capacity allows the bolt to carry the dead weight of a freely hanging 19,000kg rock block. When this bolt is expected to arrest a 2000kg rock block ejected at a velocity of 10m/s, 100kJ has to be dissipated (Figure 2.20, left hand side). This is about 20 times the energy dissipation capacity of the bolt which will snap as a consequence, whereas carrying the dead weight of the rock block would not have been a problem.

The measured ejection velocities are applied in tests to determine the dynamic response of rock bolts in lab tests. As explained in Appendix E the dynamic response is measured by dropping a weight from a certain height which loads the bolt dynamically when striking the bolt with a certain velocity simulating a rock burst (Figure E.2). Dynamic tests on the D-Bolt were set up such that the block strikes at an velocity of 5,4m/s, which is within the presented range of expected ejection velocities (Li and Doucet (2012)).

2.8 Backcalculation Ejection Velocity

Based on the alternative method to calculate the energy release presented in this thesis work based on the size of the failed zone (V) and the amount of energy released per unit of failing rock (E_1) a new expression can be derived to explain the ejection velocity (Equation 2.15, Equation 2.16, Equation 2.17, Equation 2.18, Equation 2.19, Equation 2.20, Equation 2.21):

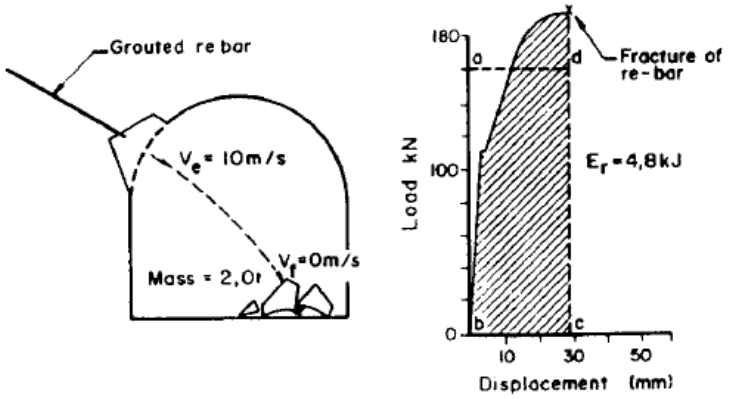

Figure 2.20: Hypothetical case to assess energy release (from Ortlepp and Stacey (1994))

$$E_{tot} = VE_1 \tag{2.15}$$

$$E_{tot} = \frac{1}{2} m_{rock} v_e^2 \tag{2.16}$$

$$VE_1 = \frac{1}{2} m_{rock} v_e^2 \tag{2.17}$$

$$m_{rock} \rho E_1 = \frac{1}{2} m_{rock} v_e^2 \tag{2.18}$$

$$\rho E_1 = \frac{1}{2} v_e^2 \tag{2.19}$$

$$v_e = \sqrt{\frac{2E_1}{\rho}} \tag{2.20}$$

with:

$$E_1 = \alpha \frac{\sigma_f^2}{2E_{mod}} \tag{2.21}$$

Chapter 3

Formulation of the Model

The derivation of the methodology to assess the energy release based on the size of the failed zone and the elastic strain energy stored in the rock mass prior to failure is presented in this chapter. This is done by combining the outcome of an analytic analysis and a numerical analysis, which are introduced individually.

3.1 Step I: Analytic Analysis

The convergence confinement equilibrium of reinforced brittle rock masses can be described by means of an analytic solution under the assumption that a circular excavation through a massive rock mass under a hydrostatic stress state is considered. When the stress in the rock mass exceeds the in situ strength a plastic or broken zone is formed around the excavation. The in situ strength is defined in the previous chapter based on the HB failure criterion (see Equation 2.2). After failure the stress in the broken zone is limited by the residual strength of the rock mass (see Equation 2.4). The considered situation is displayed in Figure 3.1.

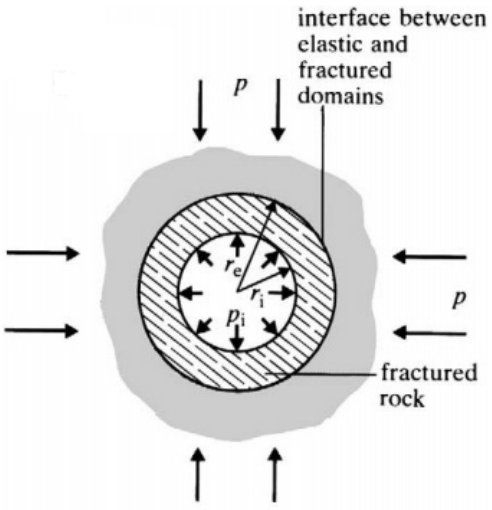

Figure 3.1: Pressures that influence the radial displacement of a tunnel wall (from: Hoek et al. (2000))

The analytic method that describes the static equilibrium presented in the situation displayed above is given in Appendix C after the derivation and explanation given by Hoek and Brown (1980b), Brown et al. (1983), Brady and Brown (2007). In this analysis the Hoek-Brown linear elastic brittle plastic strength criterion is applied (Appendix B). According to this criterion the strength of a rock mass can be expressed in terms of the two strength parameters m and s, denoting the Hoek-Brown version of the friction angle and cohesion respectively as discussed in chapter 2. The Hoek-Brown failure criterion is stated in Equation 3.1. In this expression the parameter σ_{ci} represents the theoretical UCS of intact rock as well as the rock mass, because a massive rock mass is assumed.

$$\sigma_1 = \sigma_3 + \sigma_{ci}\left(m\frac{\sigma_3}{\sigma_{ci}} + s\right)^a \tag{3.1}$$

In Appendix D the stress equilibrium method according to the convergence confinement principal is derived and explained. This analysis shows that the radius of the broken rock zone can be calculated according to Equation 3.2, Equation 3.3 and Equation 3.4. In these equations p_i equals the support pressure at the convergence confinement equilibrium. Also, it is shown that the axial and tangential stress distribution around the circular opening are as displayed in Figure 3.2 when a failed zone exists around the excavation.

$$r_e = r_i \exp\left[N - \frac{2}{m_r\sigma_{ci}}(m_r\sigma_{ci}p + s_r\sigma_{ci}^2)^{0.5}\right] \tag{3.2}$$

with:

$$N = \frac{2}{m_r\sigma_{ci}}(m_r\sigma_{ci}p + s_r\sigma_{ci}^2 - m_r\sigma_{ci}^2M)^{0.5} \tag{3.3}$$

and:

$$M = \frac{1}{2}\left[\frac{m}{4} + m\frac{p}{\sigma_{ci}} + s\right]^{0.5} - \frac{m}{8} \tag{3.4}$$

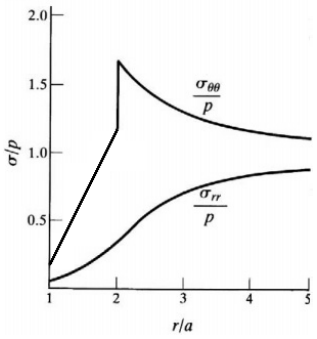

Figure 3.2: Stress distribution around circular opening according to elastic brittle plastic material behavior (from Brady and Brown (2007), *adjusted*), *Note:* $a = r_i$

From the analysis the surface (A) of failed rock is derived. As explained in the previous chapter this surface is transferred into a volume based on the longitudinal spacing of the bolts (Equation 3.5):

$$V = (\pi r_e^2 - \pi r_i^2)s_l \tag{3.5}$$

In order to repetitively run the model with varying input parameters (UCS, p) in a convenient manner a Python code was written. This code is provided in Appendix D.

3.1.1 Limitations to the Model

When executing the models from the previous sections the outcome is considered invalid in two situations:

1. The maximum confining stress (σ_r or σ_3) in the failed zone exceeds the $\frac{1}{10}\sigma_{ci}$. It is stated by Kaiser and Kim (2015) that when the confining stress is higher than this threshold spalling is surpressed (spalling limit) and the model does not account for spalling behavior anymore as the failure mechanism starts to change towards shear failure (Figure 2.5).

2. The unrealistic situation in which the residual strength (defined by Equation 2.4) at the boundary between the broken and the intact rock exceeds the peak strength of the rock mass (defined by Equation 2.2).

3.2 Step II: Numerical 2D Solution

This section describes the considerations based on which the numerical analysis was set up.

3.2.1 Analysis Type and Rock Mass Parameters

The software package RS2 9.0 is used to set up a numerical model to analyse the depth of failure and geometry of the failed zone. The rock mass is modeled to be massive using the elastic generalised HB failure criterion. In order to derive the size and geometry of the failed zone the required input parameters are: σ_{ci}, m, s, E_{mod} and ν. As part of the analysis s and m are fixed to be 0.11 and 0 respectively (see chapter 2).

3.2.2 Excavation Geometry

The excavation shapes can be defined using the so called "Tunnel Wizard" option available in RS2 9.0. Selecting the wanted geometry can then be done easily. Circular excavations can be set up easily by selecting: excavation boundary > circ > radius.

3.2.3 Excavation Boundary

A so called radial mesh (8 noded square elements) is used creating a circular shaped outer boundary. Throughout this research a element length and width of 0.1m is applied, which are the smallest possible dimensions. Excavations that are made by means of the excavation wizard option as described in the previous subsection are defined as so called material boundaries. In order to be able to use the radial mesh option the excavation has to be converted to an excavation boundary, which can be done by selecting the option boundary > convert boundary. The size of the mesh is defined using the so called expansion factor. In this research an expansion factor of 10 is applied. This factor locates the boundary at a distance of 10 times the equivalent diameter of the excavation. Fixed boundaries are used by default, which means that the horizontal and vertical movement are restricted at the boundary whereas free rotation is allowed. An expansion factor of 10 was maintained throughout, which makes the model large, potentially slow to compute, but guarantees that boundary effects do not influence the outcome of the analysis. However, because linear elastic material behavior is applied the model computes within seconds.

3.2.4 Field Stress

The center of excavations subjected to strain bursting are usually located at relatively large depth, which means that the stress increase along the height of the model is small with respect to the in situ stress at the excavation. It is assumed that the stress increase which occurs along the height of the model does not have a significant influence on the outcome of the analysis. Therefore a constant field stress is applied throughout this research.

3.3 Realisation Sequence

The model is run after being set up according to the procedure described in the previous sections. When the execution is successful the interpret environment of RS2 is selected. In this environment the option is selected that the strength factor contour around the excavation is displayed. The depth of failure is defined by the depth of the *strength factor = 1* contour along the direction of the minor principal stress (As explained in Figure 2.8). A polygon is drawn to find the triangular shape of the failed zone. When turning on the so called data tip option the area of the failed zone is displayed when hovering over the drawn polygon. From the output of the analysis the number of bolts considered responsible for retaining the bursting rock can be derived. An representative example of a model output is given in chapter 4.

3.4 Outcome Validation

In order to check whether the model output is realistic data from tunnels in which strain bursts occurred and the corresponding performance of the rock reinforcement system is required (see chapter 5). Though, as such data is not available an alternative approach is adopted to make a preliminary validation. As explained in chapter 2 the rock ejection velocity is in the range of 3-10 m/s and most likely to be in the range of 4-6 m/s.

Using the alternative derivation for the ejection velocity, as reproduced underneath, the ejection velocity is back calculated. When the back calculated velocities are within the range found from tests this is considered an indication that the applied method is valid (Equation 3.6 and Equation 3.7).

$$v = \sqrt{\frac{2E_1}{\rho}} \tag{3.6}$$

with:

$$E_1 = \alpha \frac{(\sqrt{s}\sigma_{ci})^2}{2E_{mod}} \tag{3.7}$$

Chapter 4

Model Validation

In order to validate the approach introduced in the previous chapter ($E_{tot} = E_1 V$) three cases have been adopted in this study. First the different cases are introduced followed by a step wise explanation of the obtained model output for every case.

4.1 Considered Cases

The setting at every individual case is discussed in the upcoming sub sections. Note that the major principal stress is the horizontal stress ($\sigma_h = \sigma_1$) as its magnitude exceeds the value of the vertical in situ stress, which is the minor principal stress ($\sigma_v = \sigma_3$, see chapter 2). In this report every case is referred to using the name of the country the case is from.

4.1.1 Case Sweden

The case study presents a strain burst event which occurred at an underground mining operation in Sweden (Li (2017b)). For exploration drilling purposes a drift was made at a depth of 1000 meters through massive quartzite. The cross section of the drift was horse shoe shaped and both the height and a width were 6 meters (Figure 4.1).

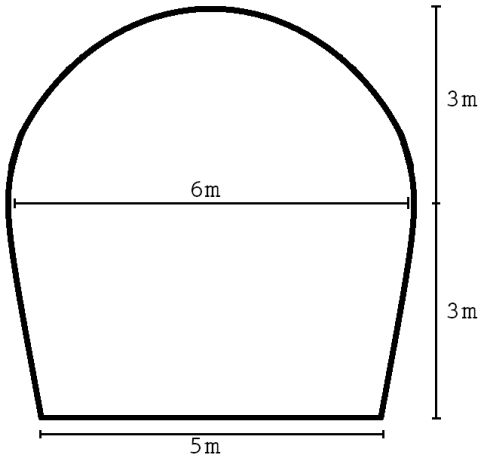

Figure 4.1: Geometry of exploration drift case Sweden

The strength of intact rock was measured by means of point load tests (PLT), where an average UCS of 140 MPa was found. The in situ stresses were as displayed in Table 4.1.

As outlined in chapter 2 stress induced damage tends to develop along the direction of the minor principal stress, which is the vertical stress in the considered case. In this case the principal stresses had rotated 25 degrees. The applied rock reinforcement system consisted out of grouted rebars in combination with steel

Parameter rock mass	orientation	value	unit
σ_h	Horizontal, perpendicular strike drift	38	[MPa]
σ_v	Vertical	27	[MPa]
σ_z	Horizontal, out-of-plane stress	62	[MPa]

Table 4.1: Principal stresses at 1000 meters depth, case Sweden

fiber reinforced shotcrete. This system not was capable of retaining the failed rock mass after a strain burst occurred. As a consequence, a new rock reinforcement system had to be installed to stabilise the excavation.

The rock mass parameters are elaborated in Table 4.2. Equivalent MC parameters are provided in Appendix B.

Parameter	Value	unit
UCS	140	MPa
E_{mod}	$46,000$	MPa
ν	0.2	$-$
γ	27	kN/m^3

Table 4.2: Rock mass properties, case Sweden

Not all input parameters required to model the stated case are provided. In order to overcome this issue representative values for quartzite are used from literature. Based on data from UCS tests on scandinavian quartzite Nilsen and Palmström (2000) state the relationship displayed in Equation 4.1 between the elasticity modulus and UCS.

$$E_{mod} = 328\sigma_{ci} \tag{4.1}$$

In the analytic analysis of the convergence confinement equilibrium only case Sweden is considered in this report. An explanation and discussion on this decision are presented in the next section of this chapter and chapter 5. In order to find a hydrostatic in situ stress p which corresponds with the non hydrostatic in situ stress from case Sweden a value was selected such that the maximum tangential stress right at the excavation boundary (σ_θ) is the same for both in situ stress states. From this $p = 40MPa$ was found to correspond with the in situ stress state for case Sweden (see Appendix C). The analysis was also run with a p value ranging from 20 to 70 MPa to research how the energy release behaves as a function of the in situ stress and allow for comparison with results from the numerical analysis.

4.1.2 Case Peru

As part of realisation of a Hydro power plant a waterway tunnel was constructed through massive granite and gneiss (Sayah et al. (2016)). The tunnel was constructed by means of drilling and blasting and grouted rebar bolts were applied in combination with short cone bolts and shotcrete. At a depth of 800 meters a severe strain burst occurred completely destroying the rock reinforcement system. An image of the situation right after the burst is shown in Figure 4.2:

The vertical in situ stress is not given in the paper in which the case is described. However, it is stated that the burst occured at a depth of 830 meter below the surface. The vertical in situ stress (σ_v) is a function of the density of the overlying geology and the considered depth. The vertical stress (σ_v) is the product of the depth (H) and the average density of the overlying geology (γ), as displayed in Equation 4.2 (Goodman (1989)). For granite rock, a density of 27 kN/m^3 is considered appropriate (**?**).

$$\sigma_v = \gamma H \tag{4.2}$$

It is stated that the coefficient of horizontal stress K_0 equals 1.5, from which the horizontal in situ stress σ_h can be calculated (Equation 4.3):

$$K_0 = \frac{\sigma_h}{\sigma_v} \tag{4.3}$$

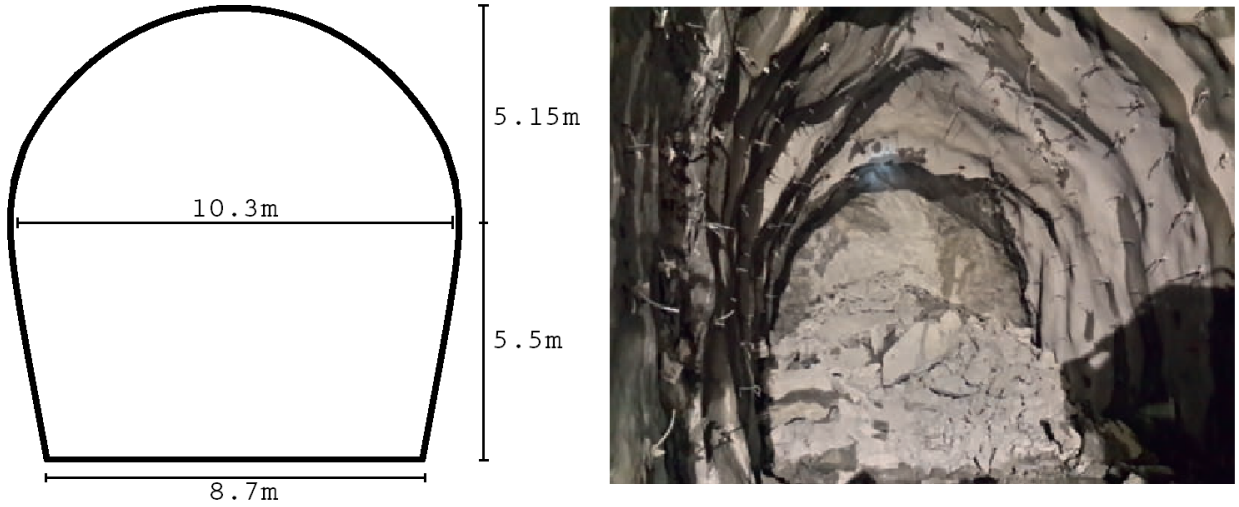

Figure 4.2: Situation after strain burst occured in roof of the waterway tunnel of the Cerro del guila Hydro Power Plant (from: Sayah et al. (2016))

The approximate stresses at the location of the burst are as displayed in Table 4.3. Note that the major principal stress is the horizontal stress as its quantity exceeds the vertical in situ stress, which is the minor principal stress in the considered case. Because the out of plane stress is not given a stress level equal to σ_h is assumed.

Parameter rock mass	orientation	value	unit
σ_h	Horizontal, perpendicular strike drift	33	[MPa]
σ_v	Vertical	22	[MPa]
σ_z	Horizontal, out-of-plane stress	33	[MPa]

Table 4.3: Principal stresses at 830 meters depth, case Peru

The Rock Mass Rating (RMR) of the granite rock was assessed to be around 60-90, which qualifies as a good to very good quality rock mass (Bieniawski (1989)). The modulus of elasticity E_{mod} is not given for the granite rock mass, posting the need for an estimate to be made based on literature. Waltham (2009) suggests that roughly a linear relationship exists between σ_{ci} and E_{mod} for different rock types. It is stated that the average σ_{ci} and E_{mod} for granite amount 200MPa and 70,000MPa respectively, which comes down to a E_{mod}/σ_{ci} ratio of 375. Goodman (1989) states that the E_{mod}/σ_{ci} ratio for Pikes Peak granite equals 312 and a value of 523 was found for Navada test site granite, which averages to 418. This average value is of the same order of magnitude as the value suggested by Waltham (2009). A rounded intermediate value is selected to determine to the value for E_{mod} for case Peru (Equation 4.4).

$$E_{mod} \approx 400\sigma_{ci} \tag{4.4}$$

The used rock mass properties are given to be as presented in Table 4.4.

Parameter	Value	unit
UCS	100	MPa
E_{mod}	$40,000$	MPa
ν	0.2	–
γ	27	kN/m^3

Table 4.4: Rock mass properties, case Peru

4.1.3 Case China

During the construction of a waterway tunnel through dense bedded limestone as part of a hydropower station multiple strain burst events were encountered (Jiayou et al. (1989)). The considered tunnel has a diameter of 10 meters and was constructed by means of a tunnel boring machine (TBM) and left unsupported afterwards. The damage to the excavation as the result of strain bursting occurred in both the roof and the floor, but in this research only the roof is considered. A schematic image of the geometry of the cross section of the tunnel after the strain burst is presented in Figure 4.3.

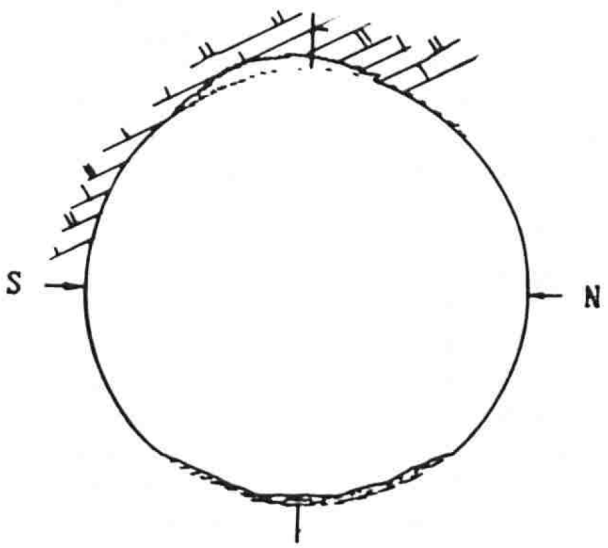

Figure 4.3: Situation after strain burst occured in roof of the waterway tunnel of a Hydro Power Plant in China (from: Jiayou et al. (1989))

The burst occured at a depth of 440 meter, where the in situ stresses at the burst site were as presented in Table 4.5. Because the out of plane stress is not given it is assumed that $\sigma_h = \sigma_z$.

Parameter rock mass	orientation	value	unit
σ_h	Horizontal, perpendicular strike drift	18	[MPa]
σ_v	Vertical	12	[MPa]
σ_z	Horizontal, out-of-plane stress	18	[MPa]

Table 4.5: Principal stresses at 440 meters depth, rounded, case China

The massive bedded limestone with a bedding plane orientation as presented in Figure 4.3. The rock mass properties are elaborated in Table 4.6.

Parameter	Value	unit
UCS	80	MPa
E_{mod}	$30,000$	MPa
ν	0.3	–
γ	27	kN/m^3

Table 4.6: Rock mass properties, case China

4.1.4 General Parameter Selection Consideration

The author considers the wire mesh to be responsible for retaining failing rock. Though, wire mesh cannot be applied tight to the excavation boundary and will deform prior to retaining the failed rock. Therefore wire mesh allows for what is called loose retention, allowing the rock mass to shift before being retained. Modelling the failing rock mass to dilate after failure may lead to overestimation of the confinement that is derived from the presence of the failed rock. This is accounted for by putting the post failure dilation (f) to 0 when modelling spalling and bursting rocks masses (Diederichs et al. (2007)).

4.1.5 Equivalent Radius Determination

In chapter 2 it is stated that a linear relationship exists between R_f/r_i and σ_{max}/σ_{ci} based on data from a range of case studies. When a non circular excavation is considered a so called equivalent radius ($r_{i,eq}$) is derived by creating a circle that encloses the excavation geometry, as displayed in Figure 4.4.

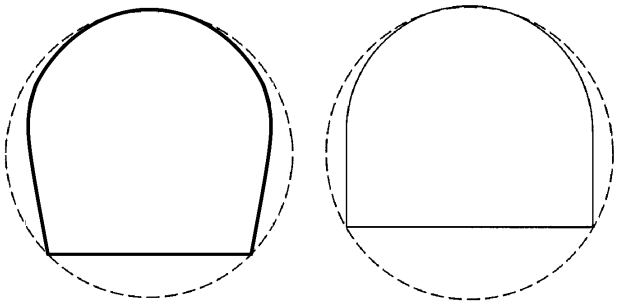

Figure 4.4: Circle with equivalent radius as proposed by Martin et al. (1999) (*adjusted*) (R) Application on excavation case Peru and Sweden (L)

Based on this methodology, the equivalent radius $r_{i,eq}$ of the excavations of the different cases are derived (Table 4.7). Logically, $r_i = r_{i,eq}$ for the Chinese case as a circular excavation is considered.

Case	Sweden	Peru	China
$r_{i,eq}[m]$	3.5	6.2	5.0

Table 4.7: $r_{i,eq}$ considered cases

Subsequently, maximum stress at the excavation boundary ($\sigma_{\theta,max}$) is calculated according to Equation 4.5 (see Appendix C).

$$\sigma_{\theta,max} = 3\sigma_1 - \sigma_3 \tag{4.5}$$

4.2 Step I: Analytic Analysis

Based on the way the derivation of the analytic solution is set up an unrealistic relation between the support stress and the size of the plastic zone is obtained. The formulation implies that $r_e \to \infty$ when no support pressure is applied ($p_i = 0$ MPa). A disussion on this is given in chapter 5. As a consequence it is not usefull to set up the model for all cases and compare the outcome. Instead, only case Sweden is considered and the outcome is treated qualitatively. A rebar bolt with a representative pullout strength of $200kN$ installed at a $1 \times 1m$ spacing supplies a support pressure of 0.2MPa when fully mobilised (Li (2017b)). Therefore a constant support pressure of 0.2MPa is applied and it is assumed that the support system successfully dissipates released energy, because the radius of the failed zone (p_i) is infinite if the support system would fail.

The convergence-confinement equilibrium for case Sweden was investigated using the Python code presented in Appendix D. An example output of this code is shown in Figure 4.5.

This code was run with a varying UCS and in situ stress p while making sure that the model limitations as presented in chapter 3 are avoided. This means that an output is not included in the presented results if one or both of the conditions are violated. The convergence curves that follow from this analysis are presented in Figure 4.6 and Figure 4.7.

The corresponding energy release per unit of failing rock E_1 and size of the failed zone V, and the total energy release E_{tot} are displayed in Figure 4.8 and Figure 4.9 respectively.

From the latter two results it follows that the total energy release goes down with an increasing UCS, regardless of the in situ stress p.

```
Case: Quartzite drift Sweden
sigma_c = 140.0 p = 40.0 s = 0.16 r_i = 3.5
```

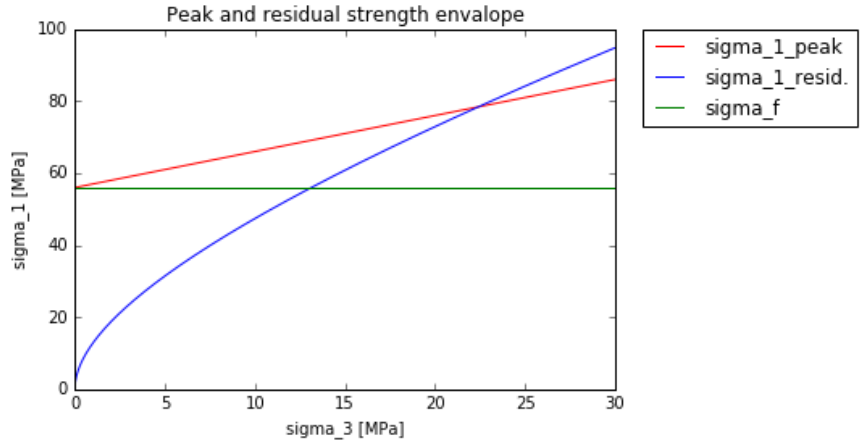


```
bolt type = Rebar ,EDC = 5.0 ,Amount = 22.0
Energy Dissipation Capacity: 110.0 [kJ]
The support pressure at equilibrium is: 0.2 MPa
```

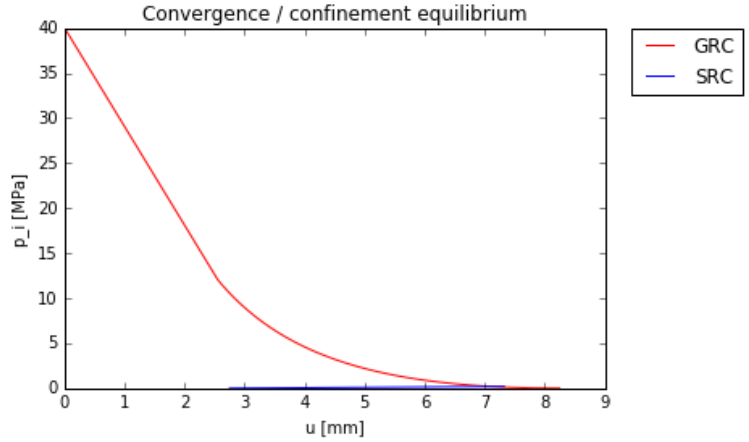

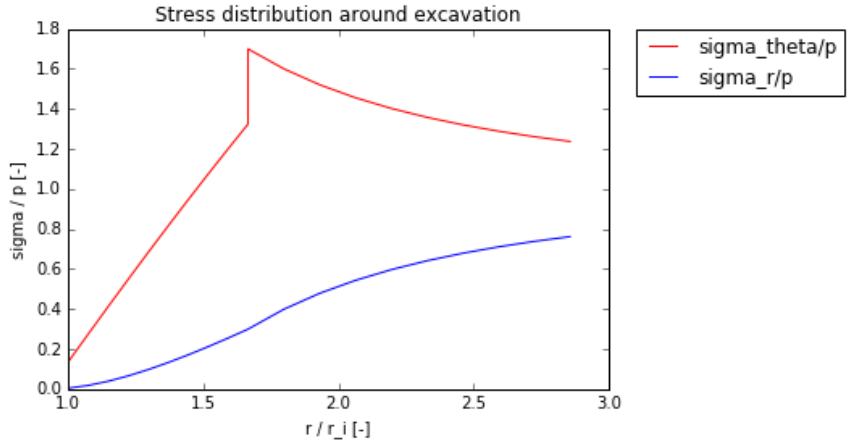


```
Radius failed zone: 5.8 m
Volume failed zone: 68.2 m^3
Released energy/m^3 failing rock: 30.7 kJ
Released energy from failed zone: 2093.2 kJ
Factor of safety: 0.05 -
(Stable/Failure): Failure
Outcome validation:
(1) UCS / Sigma_r         (bounary intact/broken): 11.7 [-] valid
(2) sigma_1_p/sigma_1_res (boundary intact/broken): 1.3 [-] valid
```

Figure 4.5: Analytic analysis output Python code case Sweden

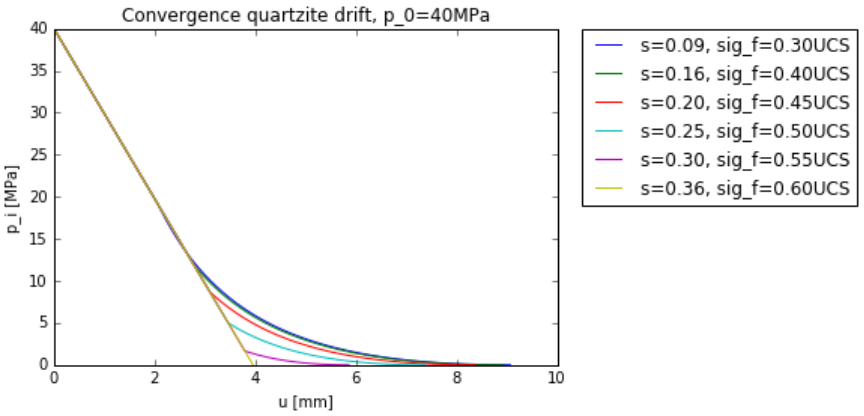

Figure 4.6: Convergence curve case Sweden, varying rock mass strength σ_f

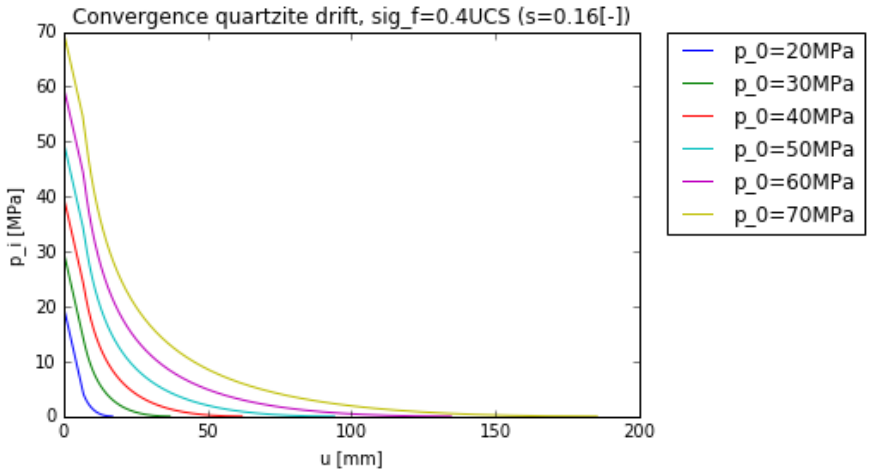

Figure 4.7: Convergence curve case Sweden, varying in situ stress p

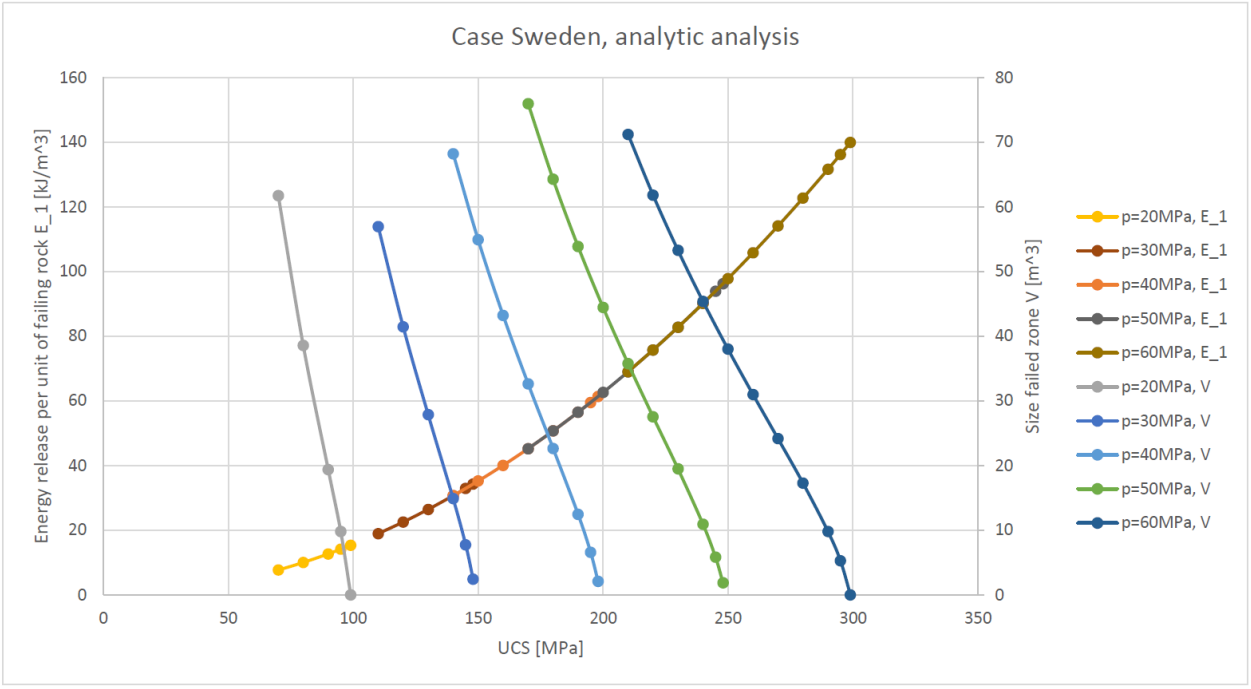

Figure 4.8: Analytic analysis output, case Sweden, E_1 and V

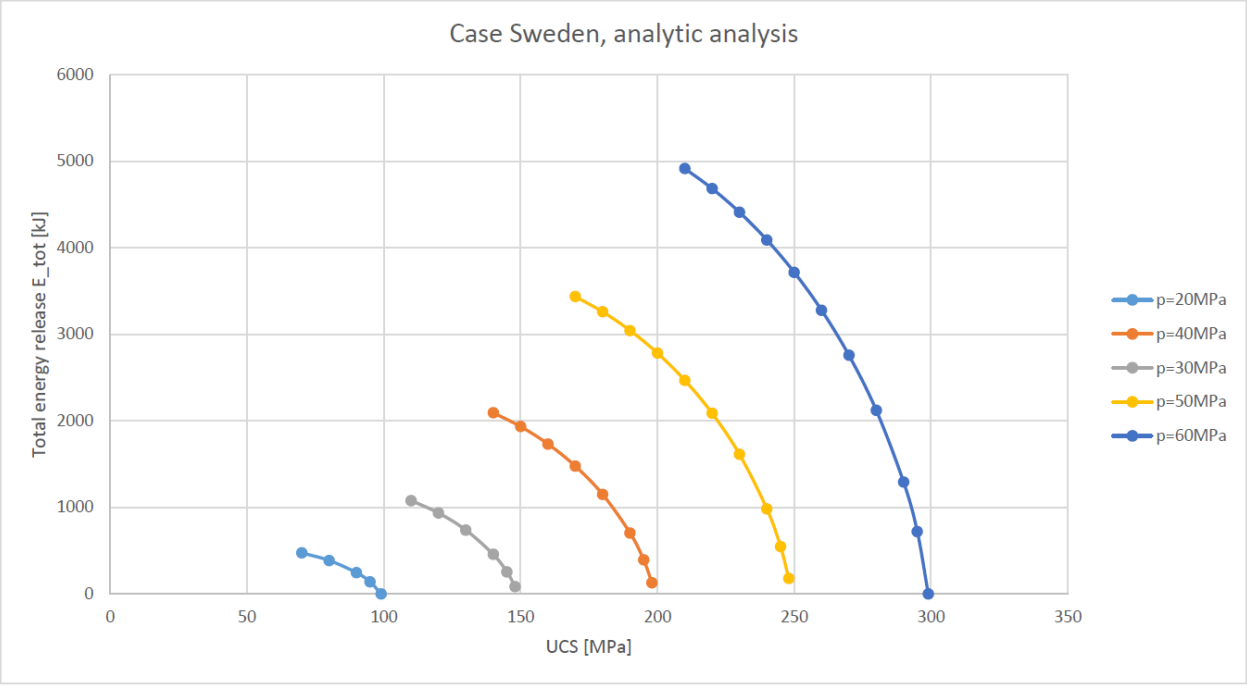

Figure 4.9: Analytic analysis output, case Sweden, E_{tot}

4.3 Step II: Numerical Analysis

In the case of localised failure (non hydrostatic) in situ stress state, the methodology described in chapter 3 is applied by means of the numerical package RS2 9.0. The output of this model for case Sweden is given in chapter 3 as an example.

As discussed in chapter 3 the number of bolts considered responsible for stabilising the ejected mass is a function of the width of the failed zone. An example of such an analysis is given in Figure 4.11 using the systematic bolting pattern option in RS2 9.0. From this image three bolts are considered responsible for arresting the failing rock.

For all cases (Sweden, China and Peru) the depth of failure was calculated and plotted as $\sigma_{\theta,max}/UCS$ against R_f/r_i (Figure 4.12). From the linear trendline it showed that the intersection with the x-axis was at a slightly lower $\sigma_{\theta,max}/UCS$ value compared to the relationship stated by Martin et al. (1999) (see Figure 2.6, right hand side, *predicted*). The reason for this difference was found when repeating the analysis for every case but with varying UCS values (Figure 4.13). The results showed that the suggested linear relationship is not satisfied for low UCS values, and the data point for case Sweden was right at the onset of this non-linearity.

When investigating the relationship between the energy release per unit of failing rock (E_1), volume of failed rock (V) and the total energy release (E_{tot}) as a function of the UCS only UCS values are considered from which a linear $\sigma_{max}/UCS - R_f/r_i$ relationship is found in Figure 4.13. The results from this analysis are displayed in Figure 4.14.

For all cases it is found that the size of the failed zone (V) reduces and the energy release per unit of failing (E_1) rock increases with an increasing rock mass strength. However, for all cases the total energy release E_{tot} reduces with an increasing rock mass strength and will go to zero if the rock mass strength is so high that the no failure will occur at all. This observation is qualitatively consistent with the results obtained from the analytic analysis (Figure 4.9).

All results are elaborated in an online Dropbox folder, which can be shared after requesting the author through his e-mail address: wik.breure@gmail.com

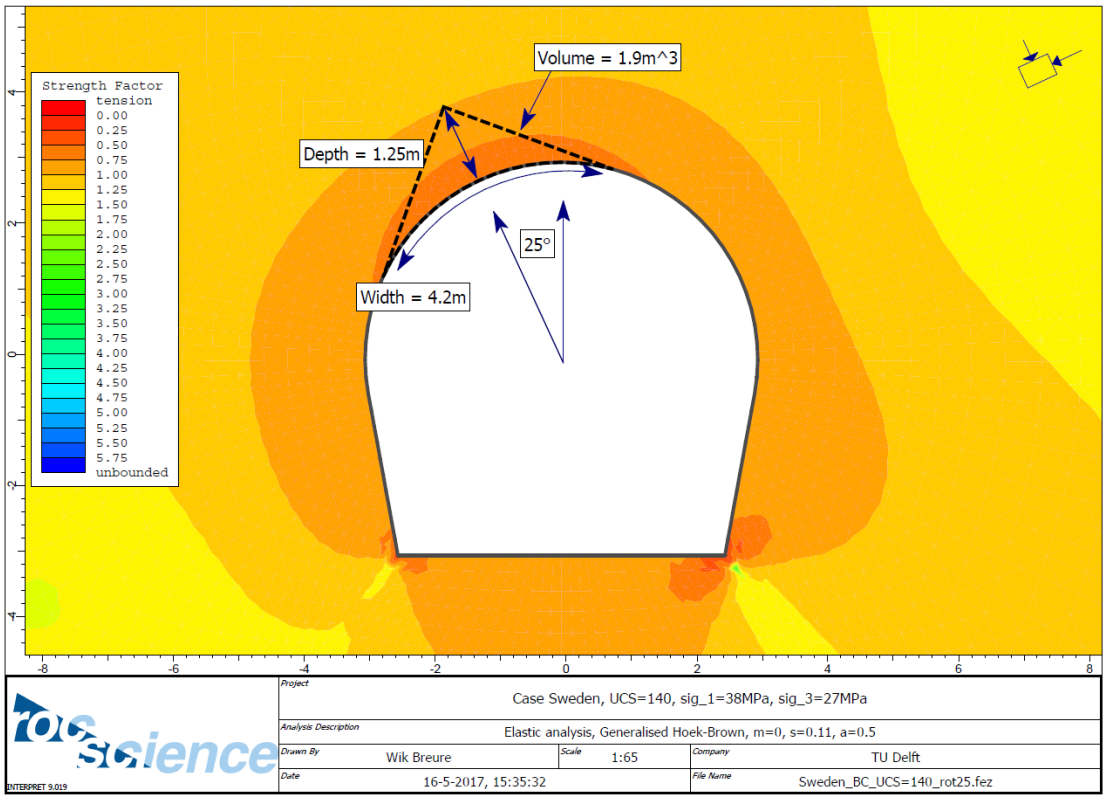

Figure 4.10: Output numerical analysis case Sweden, geometry and size failed zone

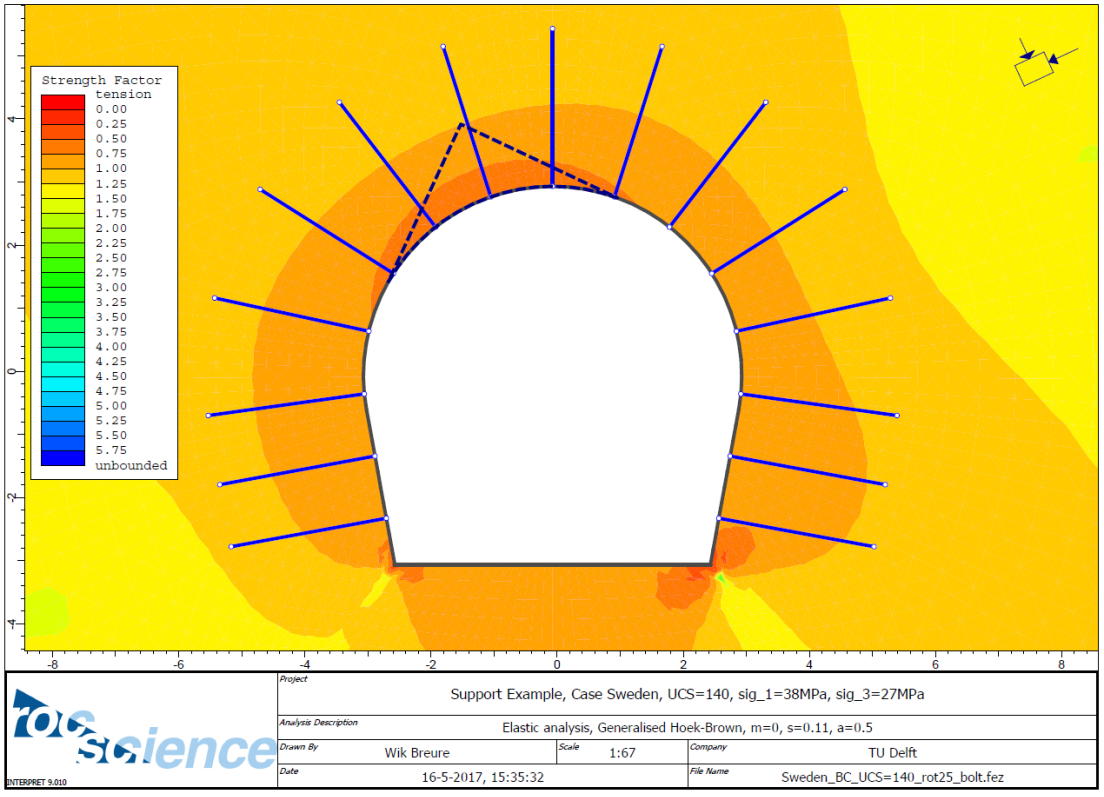

Figure 4.11: Output numerical analysis case Sweden, bolting patern with 1m spacing

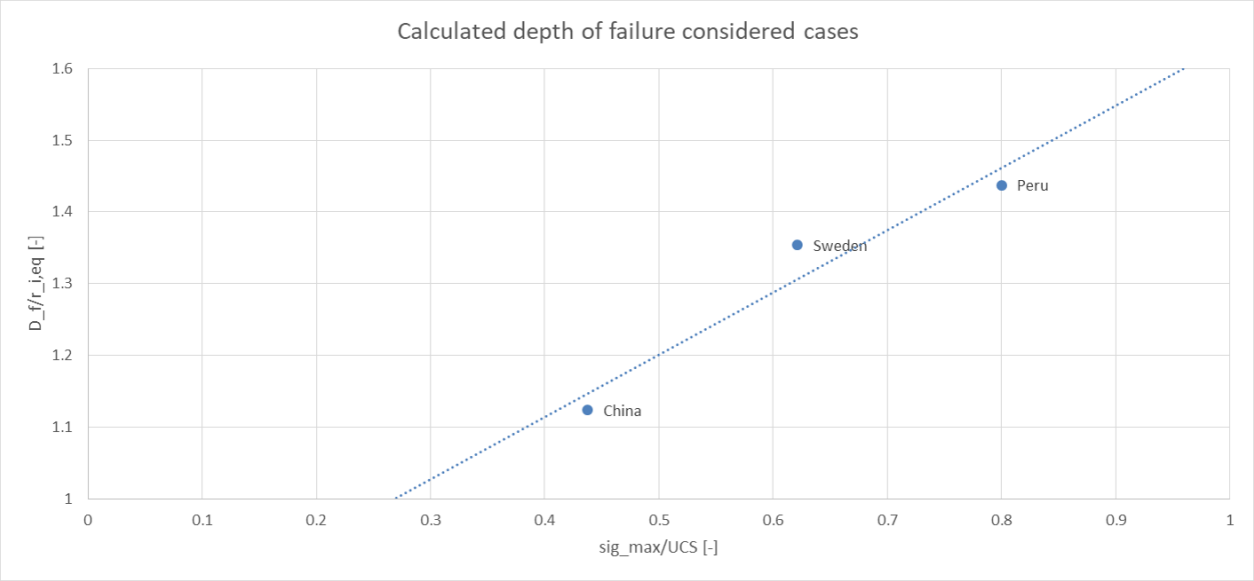

Figure 4.12: Depth of failure considered cases (Sweden, China and Peru)

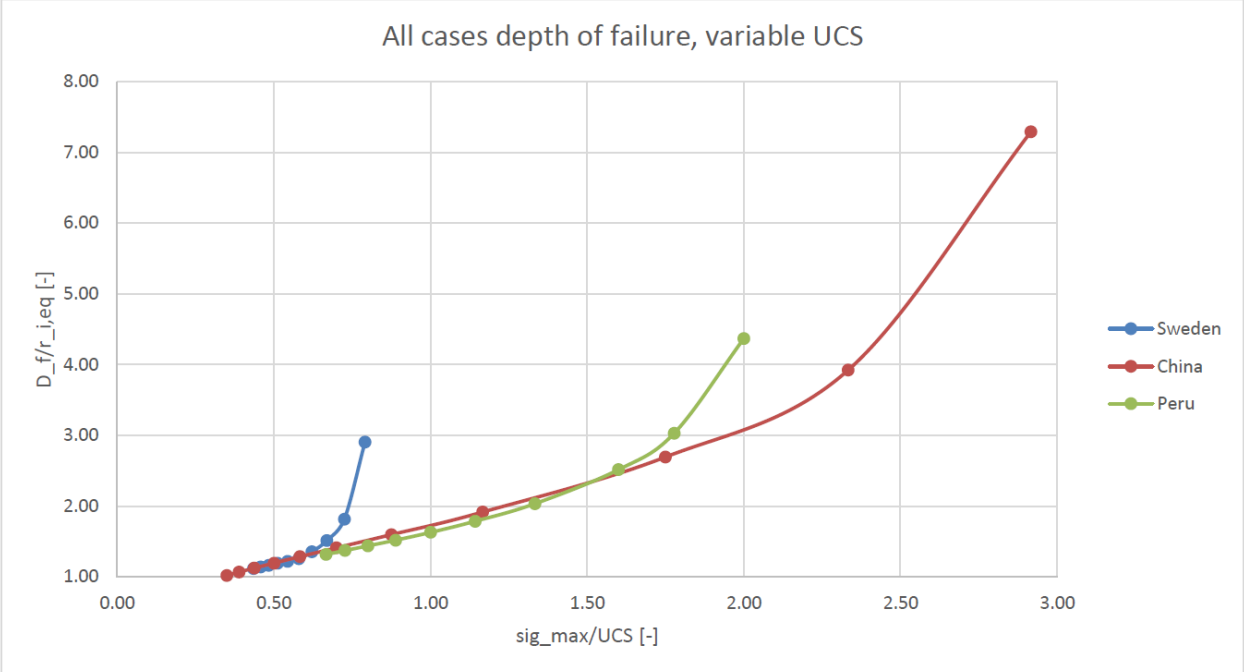

Figure 4.13: Depth of failure considered cases (Sweden, China and Peru), varying UCS

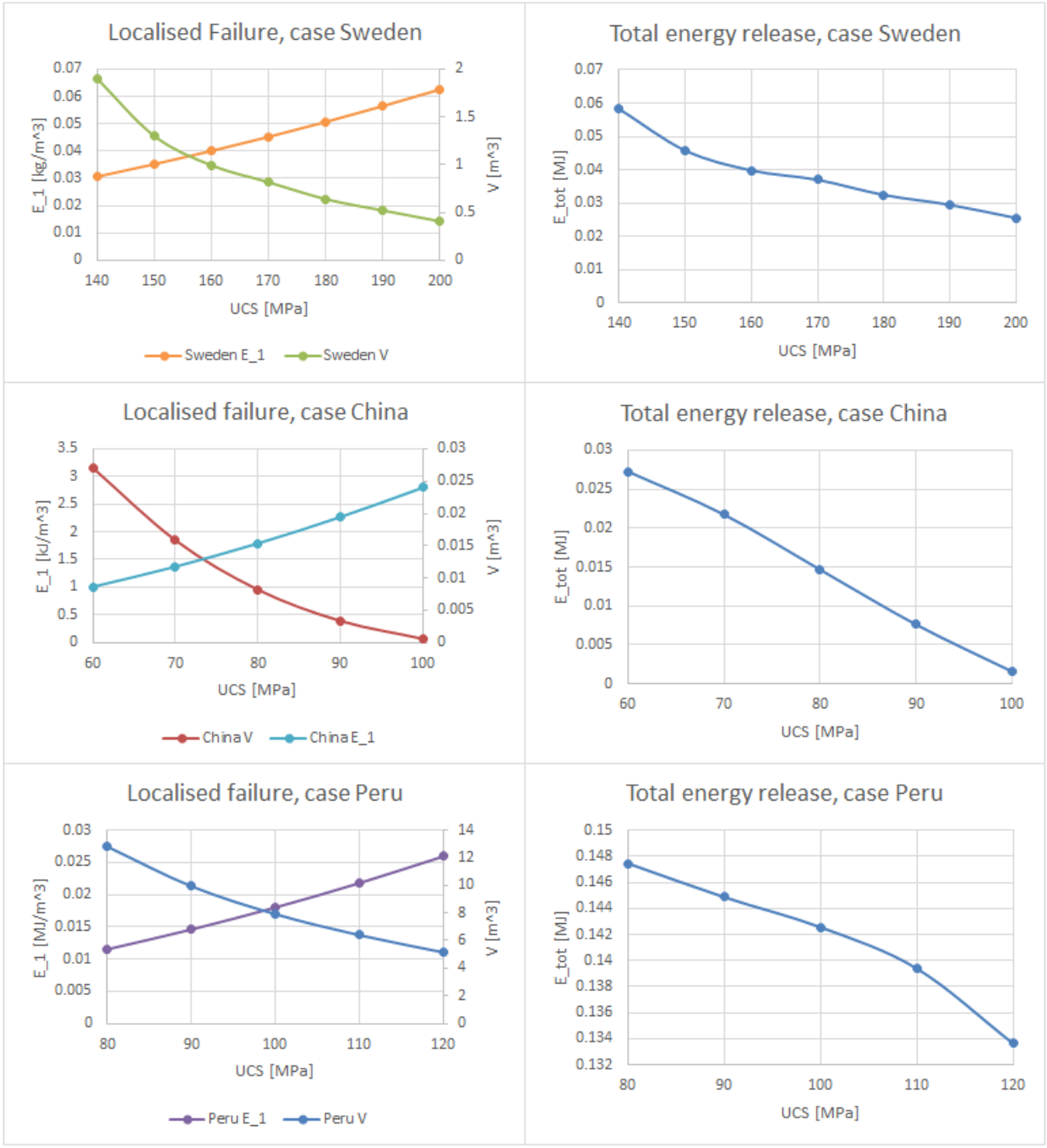

Figure 4.14: Numerical analysis voor all considered cases, energy release per unit of failing rock (E_1), volume of failed rock (V), and the total energy release (E_{tot})

4.4 Support Design

For all cases the energy release is calculated and the energy dissipation capacity of the reinforcement system using different bolt types (chapter 2). This allows for derivation of the factor of safety FOS which determines whether the failing rock is retained successfully after bursting (Table 4.8).

Rebar	$V[m^3]$	$E_1[kJ/m^3]$	$E[kJ]$	$Width[m]$	$n_{bolt}[-]$	EDC_b	EDC	FOS
Sweden	1.9	31	58.9	4.2	3	5	15	0.25
Peru	7.8	18	140.4	8	7	5	35	0.25
China	0.96	15	14.4	2.1	1	5	5	0.35
Split-set								
Sweden	1.9	31	58.9	4.2	3	27.5	82.5	1.40
Peru	7.8	18	140.4	8	7	27.5	192.5	1.37
China	0.96	15	14.4	2.1	1	27.5	27.5	1.91
D-bolt								
Sweden	1.9	31	58.9	4.2	3	56	168	2.85
Peru	7.8	18	140.4	8	7	56	392	2.79
China	0.96	15	14.4	2.1	1	56	56	3.89

Table 4.8: Calculated factor of safety for different cases using varying bolt types ($1m \times 1m$ bolt spacing)

4.5 Back Calculated Ejection Velocity

In chapter 3 a derivation is presented from which follows that the ejection velocity of the failing rock can be calculated with Equation 3.6 and Equation 3.7. From the theory presented in chapter 2 it follows that the in situ strength amounts approximately 40% of the UCS but in more recent publications it is stated that the in situ strength may be higher. In line with this observation the ejection velocities are back calculated based on $\sigma_f = 0.4\sigma_{ci}$ and an arbitrary higher in situ strength $\sigma_f = 0.6\sigma_{ci}$. From this the results presented in Table 4.9 were found. These numbers are in good agreement with the obtained ejection velocities from tests, from which it showed that results in the range of $4 - 6m/s$ may be expected.

	$\sigma_f = 0.4\sigma_{ci}$	$\sigma_f = 0.6\sigma_{ci}$
Sweden	4.8	7.2
Peru	3.7	5.5
China	3.3	5.1

Table 4.9: Back calculated ejection velocities $v_e[m/s]$

Chapter 5

Discussion and Conclusion

In this chapter the results, applied methodology and applied theory are discussed, from which the conclusion and discussion follow. Recommendations for future research are given as well.

5.1 Applicability of Analytic Analysis

In this thesis research the original LEBP analytic solution for the convergence curve based on the HB criterion proposed as by Brown et al. (1983) is applied. After the introduction of this approach several papers have been published proposing modified approaches (e.g. Wang (1996) and Sharan (2003)). In the opinion of the author non of these alternative derivations present any proof that the method introduced by Brown et al. (1983) is false. It is only stated by the more recent publications that different solutions to the problem were found, admitting that it is unknown why their derivation differs from the original.

The derivation presented in Brown et al. (1983) is a tough act to follow, which may be an explanation why other authors have derived different solutions but cannot tell why their solution differs. The author has not been able to completely reproduce the derivation either using the Hoek Brown failure criterion. However, the derivation based on the MC was succesfully reproduced (Brady and Brown (2007), Appendix D).

In both solutions (HB and MC), the support pressure (p_i) at the excavation boundary is the boundary condition for the radial stress in the rock mass at $r = r_i$. When a plastic zone is formed the unconfined residual strength of the failed rock is zero. As a consequence, no equilibrium radial stress is found at the boundary between the failed and the intact rock which in theory leads to $r_e = \infty$. When reconsidering the expression for the radius of the yielded zone r_i based on the Hoek-Brown failure criterion (see Appendix D for complete derivation):

$$r_e = \lim_{p_i \to 0} r_i \exp\left[N - \frac{2}{m_r \sigma_{ci}}(m_r \sigma_{ci} p_i + s_r \sigma_{ci}^2)^{0.5}\right] \neq \infty \tag{5.1}$$

with:

$$N = \frac{2}{m_r \sigma_{ci}}(m_r \sigma_{ci} p + s_r \sigma_{ci}^2 - m_r \sigma_{ci}^2 M)^{0.5} \tag{5.2}$$

$$M = \frac{1}{2}\left[\frac{m}{4} + m\frac{p}{\sigma_{ci}} + s\right]^{0.5} - \frac{m}{8} \tag{5.3}$$

But for Mohr-Coulomb:

$$r_e = \lim_{p_i \to 0} r_i \left[\frac{2p - \sigma_{ci}}{(1+b)p_i}\right]^{1/(d-1)} = \infty \tag{5.4}$$

As a consequence of the formulation the solution based on the HB criterion does not satisfy the observation $r_e = \infty$ when $p_i \to 0$ but the MC solution does. However, the idea that the size of the failed zone is infinite if no rock support is applied is not realistic. Therefore the relationship between the support stress at equilibrium and the formed plastic zone is not considered realistic either. Also, the size of the failed zone

being circular is only the case if a circular excavation in a completely massive rock mass subjected to a hydro static in situ stress state is considered. This is a situation that is very unlikely to be encountered in practice. Martin et al. (1999) state that due to heterogenities in the rock mass failure will always be localised.

The author suggests that in future research the solution based on the MC failure criterion should be applied when studying the analytic convergence confinement equilibrium based on LEBP rock mass behavior. This because the formulation of this model can be back figured easily and the radius of the failed zone (r_e) as a function of the support pressure p_i is formulated as may be expected from the boundary conditions.

5.2 Variability in Obtained Depth of Failure

In Figure 2.6 the depth of failure over the excavation radius as a function of the maximum tangential stress over the rock mass UCS is given, where a linear relationship is suggested. From extrapolation follows that the in situ brittle strength of massive rock masses $\sigma_f \approx 0.4$ UCS. However, in the graph a certain data scatter can be seen. This section presents a short discussion on the conditions that may cause this scatter:

- Observations presented by Ortlepp and Stacey (1994) and Broch and Sørheim (1984) show that massive rock masses are most susceptible to strain bursting. This means that when the rock mass is modeled to be completely massive a worst case scenario with regard to the susceptibility for strain bursts is considered. In line with this statement the rock mass is considered completely massive in this study. The data set considers underground excavations that were made through both massive and moderately jointed rock masses, which implies that there is a possibility that there has been a differential susceptibility to spalling failure between the considered cases.

- The generally accepted observation that the damage initiation stress is a decent estimator for the in situ brittle strength of rock masses contradicts with several observations. In both UCS testing in a lab and a rock mass situ, reaching the stress state corresponding with the onset of damage initiation is associated with acoustic emissions (Appendix A). When equating the in situ strength to the damage initiation stress would mean that the rock mass fails as soon as the first cracking sound is heard. However, observations by Prof. Dr. C.C. Li in the drift referred to as case Sweden in this report point out that continuous cracking was heard over a period of time prior to failure (Li (2017b)). This is an indication that stress larger than the damage initiation stress was building up in the rock mass prior to failure.

  This observation can possibly be explained by a hypothesis stated and researched by Cai and Kaiser (2014a) and Guo et al. (2016). Tunnels and drifts excavated by means of drilling and blasting, as in case Sweden, are likely to produce an irregular wall geometry as the result of over break. As a result, the stress concentrations at the excavation boundary will be very local, rather than along a certain stretch of a smooth excavation boundary. This discontinuous stress state causes tensile cracks under compressive loading to be formed only locally, while a higher stress is required to cause brittle failure on a larger scale (spalling). As a result, tunnels excavated by means of drilling and blasting can have a higher in situ strength than would be predicted based on current practice. To date no quantitative relation between the wall geometry and in situ strength is available. In a recent online lecture by Kaiser (2016), The co-author of the prior paper in which the hypothesis is presented, recommends using $m = 0$, $s = 0.17$ when applying the generalised Hoek-Brown criterion in LEBP numerical analysis. This corresponds with an in situ unconfined strength of 41% of the UCS, in line with previous observations (Martin et al. (1999)). The author concludes from this that the stated hypothesis is not yet confirmed or rejected, meaning that it is still recommended to use the damage initiation stress as an estimator of the in situ strength.

  A consequence of the discussed hypothesis is that excavations with a smooth wall are supposed to be more susceptible to the occurrence of strain bursts. This is consistent with a case study presented by Stacey and Thompson (1991). Massive kimberlite rock was mined at a depth of 430 meters below the surface. Some parts were excavated by means of drilling and blasting and others by means of a road header. It was observed that the roof of all excavations made with the road header showed stress

induced brittle failure, whereas damage to the tunnels excavated by drilling and blasting was much less severe and occurred less frequently. The results of this thesis research show that the total energy release (E_{tot}) is reduced with an increasing UCS. This means that a potential underestimation of the rock mass strength leads to conservative assessment of the total energy release.

- In most cases the UCS of the rock mass is stated as a given number, without a further explanation with regard the applied method to derive this value (e.g. UCS testing, triaxial testing, point load testing or a simple means methods such as response to geological hammering as suggested by Hack and Huisman (2002)). The UCS is the only rock property included in the depth of failure analysis, whereas other characteristics are likely to have an influence as well on the rock mass strength (e.g. tensile strength σ_t and GSI). As a consequence the solution logically has a high sensitivity for the UCS. However, many methods only produces an order of magnitude value for the UCS. Also, bad samples have to be removed from the dataset in order to obtain realistic UCS values for intact rock. As an example, in the considered case in Sweden the UCS of the rock mass was derived based on point load tests on drill cores from exploration drilling. In total 211 tests were conducted in which values were obtained ranging from 5 to 379 MPa. Following from this the average of 140MPa is recommended to be representative. Especially the low values are not in line with what may be expected from quartzite rock. The large range of values that is found is an indication that exclusion of bad samples or failures along pre existing planes of weakness has not been done or has not been done properly. As a consequence, the recommended UCS value is likely to be an underestimation of the actual value for intact rock.

5.3 Energy Loss

When loading the rock mass plastic deformations occur through crack formation and energy is lost breaking up the rock when bursting. When rock is retained by the reinforcement system it is observed that fine dust comes from the excavation, which means that energy is dissipated by grinding of the rock fragments (Li (2011)). In this report the energy loss is reflected in the parameter α, for which an arbitrary value of 0.9 is adopted as an educated guess (Li (2017b)). This suggests that the rock reinforcement system is subjected to 90% of the energy that is put into the failing rock through loading.

5.4 Interaction Failed / Intact Rock

Martin (1997) states that *"the development of the notch stops when the notch geometry provides sufficient confinement to stabilize the process zone at the notch tip."* It is believed that when failed rock has a certain residual strength it is capable of transferring (confining) stresses and potentially contributing to stabilisation of the notch, decreasing the size of the failed zone. The numerical method applied to assess the depth of failure (assuming linear material behavior) does not allow for support interaction analysis, as the data it is based on comes from unsupported excavations (see Figure 2.6). On the other hand, the way the analytic solution is set up assumes that the failed rock supplies confining stresses to the intact rock. As discussed in the previous section steel wire mesh supplies loose retention when the released energy is successfully dissipated. When the rock shifts before being retained, a probability exists that a void exists around the notch of the failed zone, meaning that no interaction exists and any effort to model the interaction between failed rock and intact rock will overestimate the residual rock mass strength.

5.5 Influence of Support Pressure on Development of Failure

As shown in Equation 2.3 the peak strength of rock mass is a function of the confining stress it experiences. When the rock mass is subjected to high confining stresses the in situ failure mechanism changes from spalling to shear failure (Figure 2.5). The mobilised support pressure at the excavation boundary is a confining stress. A rebar bolt with a representative pullout strength of $200kN$ installed at a $1 \times 1m$ spacing supplies a support pressure of 0.2MPa when fully mobilised (Li (2017b)). When a circular excavation subjected to a hydrostatic stress state is considered, the tangential stress at the excavation boundary amounts two times the in situ stress p. When an in situ hydro static stress of 40MPa is assumed, this means an tangential stress of 80MPa at the excavation boundary (Appendix C). Because the support stress (p_i) is much lower than the major

principal stress at the excavation boundary ($\sigma_{theta,max}$), it is assumed that the failure mechanism is not affected here.

5.6 Applicability of Shotcrete

In literature controversy exists with regard to the applicability of (reinforced) shotcrete as a mitigation measure in burst prone rock masses. It is suggested by McCreath and Kaiser (1992) and Langille and Burtney (1992) that shotcrete does provide effective support in the case of mild bursting. When heavy bursting conditions are considered the application of shotcrete is less effective. Both Kabwe et al. (2015) and Cai (2013) write that the brittle nature of shotcrete and its low energy absorbing capacity cause the shotcrete to become part of the fly rock when a burst occurs, which means that the failed rock is not retained. Also in case Sweden and case Peru shotcrete was applied and completely destroyed when the burst occured (Sayah et al. (2016), Li (2011), Li (2017b)). In order to increase the post failure deformability and strenght, steel fibres and mesh can be added to the reinforcement system. Also this reinforced shotcrete in combination with bolts does not always manage to retain the failing rock. A potential solution to prevent this lies in the application of energy absorbing bolts in combination with just steel mesh. From this it can be concluded that the shotcrete does not serve the purpose of reinforcing and retaining the failing rock but only aids to secure the connection between the bolts and the mesh. This validates the assumption to consider reinforcement systems that consist out of bolts and mesh in this research, even though shotcrete could be applied in practice.

In the introduction of this thesis report it is outlined that generally two modes of failure can occur in rock masses, being stress induced failure and structural controlled failure. At high stress conditions in more massive rock masses stress induced failure is commonly the dominant failure mechanism. This does not mean that structurally controlled failure is not possible in these conditions (e.g. wedge failure). Therefore when designing a rock reinforcement system in potentially burst prone conditions measures against structurally controlled failure should not be disregarded. When discussing the performance of shotcrete in this regards, the author does not by any means question its applicability as a measure against structurally controlled failure mechanisms.

5.7 Application of Split Set bolts

As elaborated in chapter 2 Split Set bolts mobilise their resistance through skin friction between the bolt steel and the rock mass they are installed into. When the rock mass is fractured or broken after failure this frictional resistance is reduced, which has a negative effect on the performance of the bolt. Also, split set bolts tend to be prone to deterioration over time as the result of erosion of the bolt steel (Li (2017b)). Such effects are not considered in the example calculations presented in this research. However, they should be looked at when selecting a bolt type in excavation design.

5.8 Moment of installation support and distance to the face

As shown in Figure 4.5 and Appendix E the elastic loading stiffness of the reinforcement system is much lower than the elastic unloading stiffness of the rock mass. Also, the maximum support stress mobilised by the reinforcement system is very low (rebar or D-bolt, 1m $\times$ 1m grid, $p_i = 0.2$MPa) and likely to be below the critical support stress $p_{i,cr}$ required to keep a burst from occurring (for case Sweden $p_{i,cr} = 12$MPa (see Figure 4.5 and Equation D.16). As a consequence a reinforcement system consisting out of bolts and wire mesh is unlikely to be capable of preventing the occurrence of a strain burst, even when installed at the earliest possible moment after the blast and as close as possible to the front face (then $\frac{1}{3}$rd or the total deformation has already taken place, see Figure 2.16 and Figure 2.17).

5.9 Energy Release at Failure

The assumption with regard to energy release applied in this research is that all elastic strain energy accumulated in rock is released upon failure. However, a hypothesis exists that the release of elastic strain energy is stopped when the residual strength is reached (Li (2017b)). In that case the area designated with

diagonal red stripes (BCD) shown in Figure 5.1 indicates E_1. The plastic energy consumed per volume unit of failing rock mass is represented by the triangle ABE.

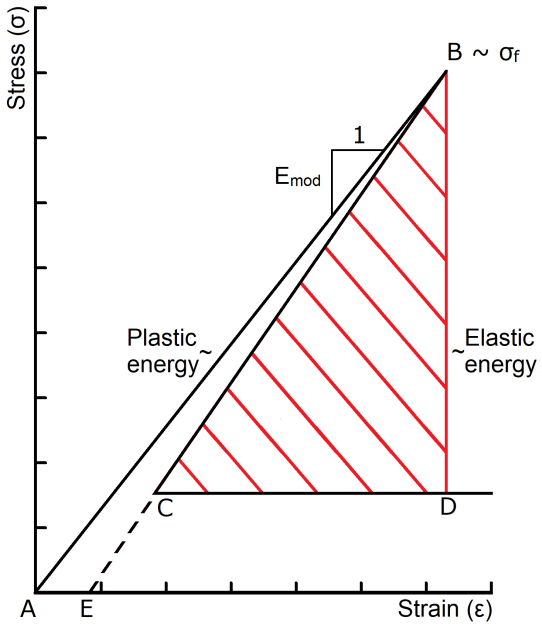

Figure 5.1: Energy released per unit of brittle failing rock (from: Li (2017b))

A residual strength exists when the failed rock is retained and confined (see chapter 2). As discussed earlier, steel wire mesh is believed to be the best option to serve as the retaining element of the rock reinforcement system. However, steel wire mesh only allows for what is called loose retention as it is not applied tight to the excavation boundary. Therefore, the failing rock mass will shift before being retained.

Strong brittle rocks generally have a high stiffness ($E \approx 300UCS$, Waltham (2009)), which means that a relatively small deformation is associated with failure. In order to keep the rock from completely unloading at failure the residual strength has to be reached within a very small reversed strain rate. According to the author the deformation of the rock mass before being retained is too high to keep all the energy from being released. In line with this statement it is more likely that the failing mass completely unloads and is reloaded to its residual strength when being retained.

5.10 Implications When Numerically Modeling LEBP Behavior

Application of LEBP rock mass behavior means is that the rock mass properties suddenly change when failure occurs. As a consequence the model might have difficulties obtaining equilibrium or a 'messy' stress distribution is obtained around the excavation after running the analysis. This problem can partially be overcome by running the analysis using low values of $0.001 - 0.01$ for s_r, m and m_{dil} rather than putting them to zero (Diederichs (2007)). It is expected that this slight change of input parameters does not influence the quality of the outcome but helps to obtain a more smooth model output. However, this adjustment does not completely take away the described issues. It is stated by Diederichs (2007) that every output of a model based on LEBP material behavior should be treated with suspicion. The obtained results in trial realisations showed irregularities the author could not explain, which has led to the search for an alternative method to assess the size and geometry of the failed zone. From this the method by Martin et al. (1999) has been selected as a reasonable alternative.

5.11 Model Validation

The proposed methodology to find the energy release when a strain burst occurs should be looked at as an initial guess based on available theory and engineering judgment of the author. The most commonly used approach in engineering design is based on the principal that there is a driving force (in this case energy) and a resisting force (in this case energy dissipation capacity of the rock reinforcement system). When the energy dissipation capacity exceeds the amount of released energy the situation is considered stable. When implementing this principal in support design it is important to comprehend that a safety factor should be considered. The magnitude of this safety factor depends on:

- When testing the dynamic response of different types of rock bolts a certain spread is to be obtained. Some bolt types tend to show great variations in response (e.g. split-set bolts (Tomory et al. (1998))) posting a uncertainty with regard to the response in situ.
- The required degree of safety and purpose of the excavation. Whether it concerns for example a highway tunnel with an expected lifespan of 100 years or a temporary underground opening such as an exploration drift leads to different requirements.
- The design of a support system by means of the methodology proposed in this research is based on a set of input parameters, for example the UCS of intact rock. When conducting a series of tests to derive the UCS a certain spread in obtained values will exist, posting an uncertainty with regard to the UCS encountered in situ. Besides uncertainties regarding the values of input parameters, the size and shape of the excavation may differ from the designed geometry. This may be the result of over break or rock blocks falling out after excavation during scaling. These uncertainties regarding the response of the excavation imply a need for a conservative design, which can be done by implementing a safety factor.
- Validating a method is done by gathering data on strain burst events (i.e. setting, applied support, stable/not stable) and back calculating whether the proposed methodology would have been able to predict this situation. As discussed the proposed method does not account for all the factors influencing strain burst effects. The uncertainty with regard to the accuracy of the outcome of a calculation should be incorporated in the safety factor. This uncertainty will decrease with an increasing amount of data gathered.

An example on how to validate a theoretical design procedure is presented by Salamon and Munro (1967). For pillar stability a suggested factor of safety based on statistical analysis was done in South African room and pillar coal mines. For a large number of coal pillars it was back calculated whether they were stable or not based on the suggested method to derive their strength, compared this with failure data and came up with a minimum required safety factor. The author suggests that such an analysis should be conducted as well to validate the proposed approach to design rock reinforcement systems exposed to loading from strain bursts.

5.12 Conclusion

The research questions presented in chapter 1 are handled separately in this section.

Can input parameters for the alternative ($E_{tot} = E_1 V$) method be derived, and how?
Relatively low support pressures can be mobilised when applying reinforcement systems consisting out of bolts and steel wire mesh. Also, such support systems have a relatively low loading stiffness compared to the unloading stiffness of the massive rock mass. As a consequence the reinforcement system cannot stop the potential occurrence of failure and only serves the purpose of retaining the ejected rock mass through dissipation of the released energy. The support pressure is a confining stress which in theory causes the size of the failed zone to be reduced. Also, such support systems allow for loose retention, which means that failing rock will shift before being retained, and that every assumption that confining stresses are transferred from the failed rock to the intact rock may lead to an overestimation of the rock mass strength and underestimation of the failed zone. As a consequence the volume of failed rock from an unsupported excavation is considered a good estimate for the volume of failed rock when a supported excavation is considered.

The size of the failed zone from localised failure in unsupported excavations can be derived in a convenient manner based on the method proposed by Martin et al. (1999) assuming linear elastic rock mass behavior using the HB failure criterion with $s = 0.11$, $m = 0$, $a = 0.5$. The energy release per unit of failing rock is a function of the UCS and the stiffness E_{mod} of the rock mass and the relationship between the lab strength and in situ strength of the rock mass.

Is the derivation procedure for the input parameters convenient?
Implementation of numerical analysis to find the geometry and volume of the failed zone is straight forward (e.g. RS2 9.0). Model outputs using the approach as proposed by Martin et al. (1999) is in decent agreement with data from test tunnels, which makes it a convenient method to adopt. From this analysis the relation between the UCS (σ_{ci}) and the in situ strength (σ_f) is also derived to be: $\sigma_f \approx 0.4\sigma_{ci}$.

Derivation of the UCS and the stiffness E_{mod} can very well be done in a lab setting. In the absence of certain lab equipment (e.g UCS or triaxial testing) decent approximations can be done based on simpler testing procedures (e.g. point load tests or geological hammering Hack and Huisman (2002)). Literature sources may be consulted as well (e.g. Waltham (2009) and Nilsen and Palmström (2000)). All together this makes the required input parameters to set up a energy release assessment analysis very accessible.

As discussed it is suggested in recent publications that for excavations made by means of drilling and blasting the in situ strength may be underestimated. The results from all considered cases (Sweden, China and Peru) show that the total energy release (E_{tot}) decreases with an increasing in situ strength σ_f. This means that a potential underestimation of the in situ strength when an excavation realised by means of drilling and blasting is considered leads to a conservative assessment of the total released energy.

Is the outcome of energy release assessment satisfactory when using the alternative method?
In order to verify whether the output of the alternative method is satisfactory, or in short *'makes sense'*, the output of the analysis is compared with a physical quantity that is measured: the ejection velocity v_e. For all cases, with an in situ strength ranging from $40 - 60\%UCS$ ejection velocities were backcalculated and values ranging from $3.3 - 7.1m/s$ were found, which is in very good agreement with the measured ejection velocities of $3 - 10m/s$.

How can the alternative method be implemented in excavation design?
A major advantage of using the alternative method is that the geometry of the failed zone is determined as a part of the solution. This allows for assessment of sufficient bolt length, and how many bolts are considered responsible for stabilising the failing rock mass (n_{bolt}). With the dynamic performance of the bolts (EDC_b) being known, deriving the dynamic performance of the system as a whole is a very straight forward exercise. The general approach in engineering is that there is a driving force and a resisting force, and as long as the resisting force exceeds the driving force a stable situation is obtained. According to this principal there is a driving energy (released energy with ejected rock mass, E_{tot}) and a resisting energy (energy dissipation capacity of the system, EDC). When EDC exceeds E_{tot} a stable situation is obtained.

5.13 Recommendations for Future Research

- In this study the only rock mass parameter the depth of failure depends on is the UCS of intact rock. Qualitative relations between other rock mass properties, such as the tenstile strength σ_t and GSI, and the susceptibility to strain bursting are presented by several authors (e.g. Diederichs (2007)). As presented in the discussion section of this report recent publications introduce the hypothesis that excavations made by means of drilling and blasting have a higher in situ strength than excavations made by means of mechanical excavation (TBM or roadheader). Also, it is suggested by Zhiming et al. (2015) that the mineral composition of the rock mass has an influence on its susceptibility to strain bursting. A better understanding of how these additional parameters influence the development of a burst and size of the failing zone will allow for more accurate determination of the released energy when a burst occurs.

- The method to assess the energy release the rock reinforcement system is subjected to presented in this thesis is theoretical. A preliminary verification is given by means of back calculating the ejection velocity v_e. Further verification is required, which can be done through the collection and analysis of

data of tunnels subjected to strain bursting in which the method proposed in this thesis work is applied. An example on how to analyse such data is given in the discussion section.

- For the depth of failure and geometry of the failed zone assessment purely linear elastic material behavior is applied in this research, even though the rock is expected to fail in a brittle manner when the in situ strength is reached. Efforts made by the author to implement LEBP behavior led to suspicious results, mainly stress concentrations in unexpected places and no solution was found during the iteration process. Successful and reliable implementation of LEBP rock mass behavior in numerical modelling would in theory lead to more accurate determination of the size and geometry of the failed zone.

- Determination of energy release per unit of failing rock (E_1) is based on the thought that the elastic strain energy in the rock mass is released at failure. Unloading of the rock mass will take place until the failing rock is retained by the reinforcement system. In this post failure state of equilibrium there is a certain stress acting on the failed rock mass, which is equal to the residual strength. In this research it is assumed that the rock mass unloads completely, which means that all the accumulated elastic strain energy is released, because the reinforcement system only supplies what is referred to as loose retention. However, it is argued in the discussion section of this report that if the failing rock mass has not unloaded completely when being retained not all the accumulated strain energy is released. In order to proceed regarding this question the interaction between reinforcement systems and failing rock should be studied more comprehensively.

- In order to prevent the occurrence or mitigate the consequences of a strain bursts procedural measures may be considered as well. After the occurence of the burst event described in case Peru (Sayah et al. (2016)) de-tension blasting ahead of the face was applied as an additional measure. Other measures, such as leaving the muck in place at the face and excavating a convex face geometry were adopted already before. What these measures mean for the support stress (p_i) derived from the presence of the face or how they influence response of a tunnel or drift after excavation is not accounted for in this research. Inclusion of the consequences of such measures in the model (e.g. reduced rock mass quality after de-tension blasting) will allow for an increased understanding whether a strain burst may be expected and at what intensity after implementation.

Bibliography

Z. T. Bieniawski. *Engineering rock mass classifications: a complete manual for engineers and geologists in mining, civil, and petroleum engineering*. John Wiley & Sons, 1989.

B. Brady and E. Brown. *Rock Mechanics: For underground mining*. Springer Netherlands, 2007. ISBN 9781402021169. URL `https://books.google.nl/books?id=s0BaKxL11KsC`.

E. Broch and S. Sørheim. Experiences from the planning, construction and supporting of a road tunnel subjected to heavy rockbursting. *Rock Mechanics and Rock Engineering*, 17(1):15–35, 1984. ISSN 1434-453X. doi: 10.1007/BF01088368. URL `http://dx.doi.org/10.1007/BF01088368`.

E. T. Brown, J. W. Bray, B. Ladanyi, and E. Hoek. Ground response curves for rock tunnels. *Journal of Geotechnical Engineering*, 109(1):15–39, 1983.

M. Cai. Principles of rock support in burst-prone ground. *Tunnelling and Underground Space Technology*, 36:46–56, 2013.

M. Cai and P. Kaiser. In-situ rock spalling strength near excavation boundaries. *Rock mechanics and rock engineering*, 47(2):659–675, 2014a.

M. Cai and P. K. Kaiser. In-situ rock spalling strength near excavation boundaries. *Rock Mechanics and Rock Engineering*, 47(2):659–675, 2014b. ISSN 1434-453X. doi: 10.1007/s00603-013-0437-0. URL `http://dx.doi.org/10.1007/s00603-013-0437-0`.

J. Crowder and W. Bawden. Review of post-peak parameters and behaviour of rock masses: current trends and research. *Rocnews, fall*, page 13, 2004.

M. Diederichs. Manuel rocha medal recipient rock fracture and collapse under low confinement conditions. *Rock Mechanics and Rock Engineering*, 36(5):339–381, 2003.

M. Diederichs, J. Carvalho, and T. Carter. A modified approach for prediction of strength and post yield behaviour for high gsi rock masses in strong, brittle ground. In *Proceedings from the 1st Canada-US Rock Mechanics Symposium*, pages 249–257, 2007.

M. S. Diederichs. The 2003 canadian geotechnical colloquium: Mechanistic interpretation and practical application of damage and spalling prediction criteria for deep tunnelling. *Canadian Geotechnical Journal*, 44(9):1082–1116, 2007.

E. Eberhardt, D. Stead, B. Stimpson, and R. Read. Identifying crack initiation and propagation thresholds in brittle rock. *Canadian Geotechnical Journal*, 35(2):222–233, 1998.

C. Fairhurst and N. Cook. The phenomenon of rock splitting parallel to the direction of maximum compression in the neighborhood of a surface. In *Proceedings of the first congress on the international society of rock mechanics*, volume 1, pages 687–692, 1966.

R. E. Goodman. *Introduction to rock mechanics*, volume 2. Wiley New York, 1989.

M. Greenspan. Effect of a small hole on the stresses in a uniformly loaded plate. *Quarterly of Applied Mathematics*, 2(1):60–71, 1944.

A. A. Griffith. The phenomena of rupture and flow in solids. *Philosophical transactions of the royal society of london. Series A, containing papers of a mathematical or physical character*, 221:163–198, 1921.

S. Guo, S. Qi, and M. Cai. Influence of tunnel wall roughness and localized stress concentrations on the initiation of brittle spalling. *Bulletin of Engineering Geology and the Environment*, 75(4):1597–1607, 2016.

R. Hack and M. Huisman. Estimating the intact rock strength of a rock mass by simple means. In *engineering geology for developing countriesproceedings of 9th congress of the International Association for Engineering Geology and the Environment, Durban, South Africa*, pages 16–20, 2002.

E. Hoek and Z. T. Bieniawski. Brittle fracture propagation in rock under compression. *International Journal of Fracture Mechanics*, 1(3):137–155, 1965. ISSN 1573-2673. doi: 10.1007/BF00186851. URL `http://dx.doi.org/10.1007/BF00186851`.

E. Hoek and E. Brown. Practical estimates of rock mass strength. *International Journal of Rock Mechanics and Mining Sciences*, 34(8):1165 – 1186, 1997. ISSN 1365-1609. doi: http://dx.doi.org/10.1016/S1365-1609(97)80069-X. URL `http://www.sciencedirect.com/science/article/pii/S136516099780069X`.

E. Hoek and E. T. Brown. Empirical strength criterion for rock masses. *Journal of Geotechnical and Geoenvironmental Engineering*, 106(ASCE 15715), 1980a.

E. Hoek and E. T. Brown. *Underground excavations in rock*. Number Monograph. 1980b.

E. Hoek and P. Marinos. A brief history of the development of the hoek-brown failure criterion. *Soils and rocks*, 2:1–8, 2007.

E. Hoek and C. Martin. Fracture initiation and propagation in intact rock a review. *Journal of Rock Mechanics and Geotechnical Engineering*, 6(4):287 – 300, 2014. ISSN 1674-7755. doi: http://dx.doi.org/10.1016/j.jrmge.2014.06.001. URL `http://www.sciencedirect.com/science/article/pii/S1674775514000559`.

E. Hoek, P. K. Kaiser, and W. F. Bawden. *Support of underground excavations in hard rock*. CRC Press, 2000.

E. Hoek, C. Carranza-Torres, and B. Corkum. Hoek-brown failure criterion-2002 edition. *Proceedings of NARMS-Tac*, 1:267–273, 2002.

L. Jiayou, D. Lihui, Z. Chengjie, W. Zebin, et al. The brittle failure of rock around underground openings. In *ISRM International Symposium*. International Society for Rock Mechanics, 1989.

E. Kabwe, Y. Wang, et al. Review on rockburst theory and types of rock support in rockburst prone mines. *Open Journal of Safety Science and Technology*, 5(04):104, 2015.

P. K. Kaiser. Rock mechanics considerations for construction of deep tunnels in brittle rock. In *Rock Mechanics in Underground Construction, ISRM International Symposium 2006, 4th Asian Rock Mechanics Symposium, Singapore*, pages 47–58, 2006.

P. K. Kaiser. Challenges in rock mass strength determination for design of underground excavations, 2016. URL `https://www.isrm.net/gca/?id=1227`.

P. K. Kaiser and B.-H. Kim. Characterization of strength of intact brittle rock considering confinement-dependent failure processes. *Rock mechanics and rock engineering*, 48(1):107–119, 2015.

P. K. Kaiser, D. McCreath, and D. Tannant. Canadian rockburst support handbook. *Geomechanics Research Centre, Laurentian University, Sudbury*, 314, 1996.

G. Kirsch. *Die Theorie der Elastizität und die Bedürfnisse der Festigkeitslehre*. Springer, 1898. URL `https://books.google.co.in/books?id=pvBuPwAACAAJ`.

H. Kirsten, J. Klokow, et al. Control of fracturing in mine rock passes. In *4th ISRM Congress*. International Society for Rock Mechanics, 1979.

C. Langille and M. Burtney. Effectiveness of shotcrete and mesh support in low energy rockburst conditions at inco's creighton mine. In *Rock support in mining and underground construction, proc. int. symp. rock support*, pages 633–638, 1992.

S. Lee, B. Park, and S. Lee. Analysis of rockbursts that have occurred in a waterway tunnel in korea. *International Journal of Rock Mechanics and Mining Sciences*, 41, Supplement 1:911 – 916, 2004. ISSN 1365-1609. doi: http://dx.doi.org/10.1016/j.ijrmms.2004.03.157. URL `http://www.sciencedirect.com/science/article/pii/S1365160904002047`. Proceedings of the ISRM SINOROCK 2004 Symposium.

C. C. Li. A practical problem with threaded rebar bolts in reinforcing largely deformed rock masses. *Rock Mechanics and Rock Engineering*, 40(5):519–524, 2007.

C. C. Li. A new energy-absorbing bolt for rock support in high stress rock masses. *International Journal of Rock Mechanics and Mining Sciences*, 47(3):396–404, 2010.

C. C. Li. Rock support for underground excavations subjected to dynamic loads and failure. *Advances in Rock Dynamics and Applications*, pages 483–506, 2011.

C. C. Li. Performance of d-bolts under static loading. *Rock Mechanics and Rock Engineering*, 45(2):183–192, 2012.

C. C. Li. Lecture handout, 2016.

C. C. Li. Principles of rockbolting design. *Journal of Rock Mechanics and Geotechnical Engineering*, 9 (3):396 – 414, 2017a. ISSN 1674-7755. doi: http://dx.doi.org/10.1016/j.jrmge.2017.04.002. URL `http://www.sciencedirect.com/science/article/pii/S1674775517300239`.

C. C. Li. Private communication, 2017b.

C. C. Li and C. Doucet. Performance of d-bolts under dynamic loading. *Rock mechanics and rock engineering*, 45(2):193–204, 2012.

C. C. Li, G. Stjern, and A. Myrvang. A review on the performance of conventional and energy-absorbing rockbolts. *Journal of Rock Mechanics and Geotechnical Engineering*, 6(4):315–327, 2014.

P. Marinos, E. Hoek, et al. Gsi: a geologically friendly tool for rock mass strength estimation. In *ISRM International Symposium*. International Society for Rock Mechanics, 2000.

C. Martin and N. Chandler. The progressive fracture of lac du bonnet granite. *International Journal of Rock Mechanics and Mining Sciences & Geomechanics Abstracts*, 31(6):643 – 659, 1994. ISSN 0148-9062. doi: http://dx.doi.org/10.1016/0148-9062(94)90005-1. URL `http://www.sciencedirect.com/science/article/pii/0148906294900051`.

C. Martin, P. Kaiser, and D. McCreath. Hoek-brown parameters for predicting the depth of brittle failure around tunnels. *Canadian Geotechnical Journal*, 36(1):136–151, 1999.

C. Martin et al. Failure observations and in situ stress domains at the underground research laboratory. In *ISRM International Symposium*. International Society for Rock Mechanics, 1989.

C. D. Martin. *The strength of massive Lac du Bonnet granite around underground openings*. University of Manitoba, 1994.

C. D. Martin. Seventeenth canadian geotechnical colloquium: the effect of cohesion loss and stress path on brittle rock strength. *Canadian Geotechnical Journal*, 34(5):698–725, 1997.

D. McCreath and P. Kaiser. Evaluation of current support practices in burst-prone ground and preliminary guidelines for canadian hardrock mines. In *Rock support in mining and underground construction, proc. int. symp. rock support*, pages 611–619, 1992.

B. Nilsen and A. Palmström. *Engineering geology and rock engineering*. Norwegian Group for Rock Mechanics, 2000.

Normet. D-bolt technical data sheet. Technical report, Normet, 2014.

W. Ortlepp and N. Gay. 40 performance of an experimental tunnel subjected to stresses ranging from 50 mpa to 230 mpa. In *Design and Performance of Underground Excavations: ISRM SymposiumCambridge, UK, 3–6 September 1984*, pages 337–346. Thomas Telford Publishing, 1984.

W. Ortlepp and T. Stacey. Rockburst mechanisms in tunnels and shafts. *Tunnelling and Underground Space Technology*, 9(1):59–65, 1994.

A. Palmström. Characterizing rock burst and squeezing by the rock mass index. In *International conference in design and construction of underground structures*, volume 10, 1995.

F. Pelli, P. Kaiser, and N. Morgenstern. An interpretation of ground movements recorded during construction of the donkin-morien tunnel. *Canadian Geotechnical Journal*, 28(2):239–254, 1991.

J. Player, E. Villaescusa, and A. Thompson. Dynamic testing of friction rock stabilisers. *RockEng09, Rock Engineering in Difficult Conditions, Toronto*, pages 9–15, 2009.

S. Qiu, X. Feng, C. Zhang, and T. Xiang. Estimation of rockburst wall-rock velocity invoked by slab flexure sources in deep tunnels. *Canadian Geotechnical Journal*, 51(5):520–539, 2014.

M. Salamon and A. Munro. A study of the strength of coal pillars. *Journal of the South African Institute of Mining and Metallurgy*, 68(2):55–67, 1967.

S. Sayah, M. Thuring, M. Braghini, and B. R. Cerro del guila hydro power plant in peru design and construction of 12 km waterways and utility tunnels in complex geology. Swiss Tunnel Congress, June 2016.

J. J. Scott et al. Friction rock stabilizers in uranium mining. In *The 18th US Symposium on Rock Mechanics (USRMS)*. American Rock Mechanics Association, 1977.

S. Sharan. Elastic–brittle–plastic analysis of circular openings in hoek–brown media. *International Journal of Rock Mechanics and Mining Sciences*, 40(6):817–824, 2003.

B. Simser. Geotechnical review of the july 29, 2001. west ore zone mass blast and the performance of the brunswick/ntc rockburst support system. Technical report, Tech Rep, 2001.

T. Stacey. Stress fracturing around a deep-level bored. *Journal of the South African Institute of Mining and Metallurgy*, 78:124, 1977.

T. Stacey and P. Thompson. A large borehole breakout? In *7th ISRM Congress*. International Society for Rock Mechanics, 1991.

G. Stjern. Practical performance of rock bolts. In *Dr.-Ing. thesis*, page 178. Norwegian Institute of Technology Trondheim, 1995.

T. Szwedzicki. A hypothesis on modes of failure of rock samples tested in uniaxial compression. *Rock mechanics and rock engineering*, 40(1):97–104, 2007.

T. Szwedzicki and W. Shamu. The effect of discontinuities on strength of rock samples. In *Proceedings of the Australasian Institute of Mining and Metallurgy*, volume 304, pages 23–28. Citeseer, 1999.

D. Tannant, G. McDowell, R. Brummer, and P. Kaiser. Ejection velocities measured during a rockburst simulation experiment. In *Proc. 3rd Int. Symp. on Rockbursts and Seismicity in Mines, Kingston, AA Balkema, Rotterdam*, pages 129–133, 1993.

P. Tomory, M. Grabinsky, J. Curran, and J. Carvalho. Factors influencing the effectiveness of split set friction stabilizer bolts. *CIM bulletin*, 91(1018):205–214, 1998.

N. Vlachopoulos and M. Diederichs. Improved longitudinal displacement profiles for convergence confinement analysis of deep tunnels. *Rock mechanics and rock engineering*, 42(2):131–146, 2009.

T. Waltham. *Foundations of engineering geology*. CRC Press, 2009.

Y. Wang. Ground response of circular tunnel in poorly consolidated rock. *Journal of Geotechnical Engineering*, 122(9):703–708, 1996.

W. Wawersik and C. Fairhurst. A study of brittle rock fracture in laboratory compression experiments. *International Journal of Rock Mechanics and Mining Sciences & Geomechanics Abstracts*, 7(5):561 – 575, 1970. ISSN 0148-9062. doi: http://dx.doi.org/10.1016/0148-9062(70)90007-0. URL `http://www.sciencedirect.com/science/article/pii/0148906270900070`.

J. Whyatt, W. Blake, T. Williams, and B. White. 60 years of rockbursting in the coeurdalene district of northern idaho, usa: lessons learned and remaining issues. In *Presentation at 109th annual exhibit and meeting, Society for Mining, Metallurgy, and Exploration*, pages 25–27. Phoenix, 2002.

Z. Zhiming, E. Ali, W. Guang, and W. Xihua. Assessment of strain energy storage and rock brittleness indices of rockburst potential from microfabric characterizations. *American Journal of Earth Sciences*, 2 (1):8, 2015.

Appendix A

Rock Behavior in Lab Tests

A.1 UCS Test

Martin and Chandler (1994) describe the different stages of the response of a sample of intact rock upon loading in a UCS test setting. In this chapter the obtained generalized behavior as displayed in Figure A.1 is discussed with the assumption that single shear is the obtained failure mechanism. Other failure mechanisms are explained as well in the other sections of this chapter.

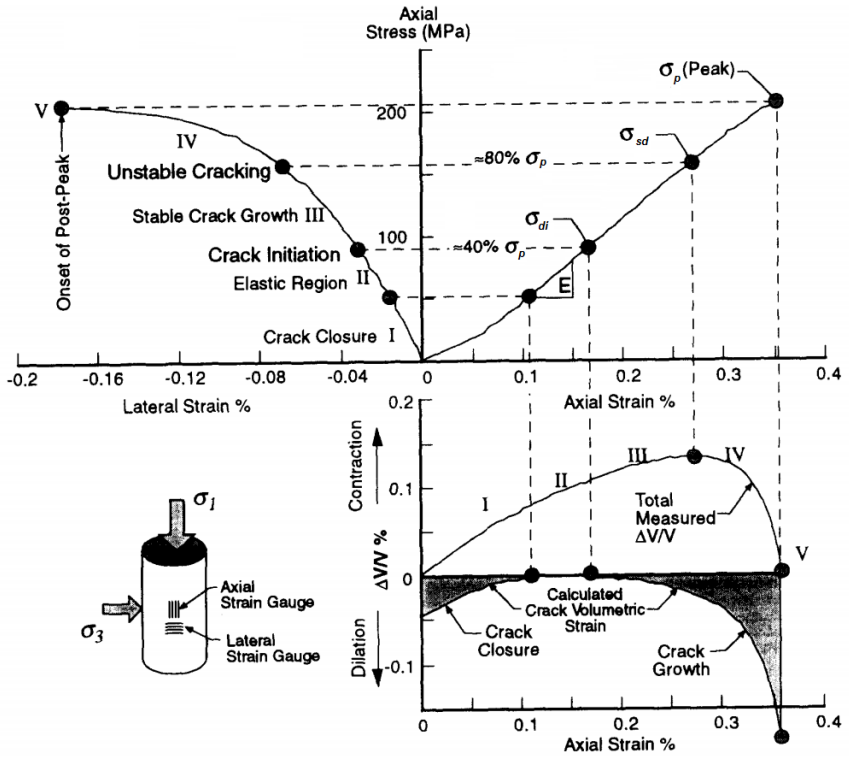

Figure A.1: Stress strain diagram from UCS test, showing crack initiation, crack damage and peak strength. *Note:* $\sigma_p = UCS$ (from: Martin and Chandler (1994), *modified*)

When a UCS test is conducted the first response of the sample is closure of already existing micro cracks (stage I). It is believed that after the closure of the micro cracks the rock behaves as a linear elastic homogeneous material. From the sress strain curve obtained in this stage (Figure A.1, stage II) the elastic properties of the tested rock can be determined. The elastic stage ends when the sample starts to dilate as the result of the initiation of cracking. The formation of a micro crask is associated with the emmision of sound, referred to as an acoustic event (AE). This is referred to as stage III in Figure A.1 and generally starts at 30-50% of the stress at failure. The stress associated with the initiation of crack growth is called the crack or damage initiation stress and referred to as σ_{di}. It has been found that the rock strength is not reduced as long as the

stress the sample is exposed to does not exceed σ_{di}. In stage III cracks grow in a stable manner, which means that crack formation is stopped when the load is removed from the sample. The start of stage IV is associated with a decrease in the total volumetric strain, which is caused by sliding along surfaces of weakness. In other words this means the start of the formation of a shear plane along which the sample will eventually fail, causing a very significant increase of microcracks (Hoek and Martin (2014)). This process starts at about 80% of the stress at failure and is denoted with σ_{sd}, in which the subscript stands for systematic damage. It has been found that σ_{sd} represents the long term strength of the tested intact rock material, as the strength that is obtained up to the stress at failure (σ_p) is the result of unstable crack growth and coalescence of cracks forming a shear plane along which failure occurs eventually.

A.2 Failure Mechanisms in UCS Testing

When conducting a UCS test in a lab setting different failure mechanisms can be obtained from the tested sample, as displayed in Figure A.2. The displayed mechanisms are explained by Szwedzicki (2007) as follows:

- Simple shear: A shear planes develops under an angle with respect to the direction of the applied compression (σ_1). Usually this shear plane intersects with the boundary of the sample in the unconfined zone (i.e. side of the sample). When simple shear is obtained this is often due to the fact that a plane of weakness exists in the sample and leads to the lowest UCS value compared to other failure mechanisms that are discussed underneath. In practice single or multiple shear is the failure mechanism that is obtained the most.
- Multiple shear: Same as explained above but multiple shear non parallel shear planes exist in the sample upon failure.
- Multiple fracture: Failure along multiple intersecting planes that can originate from shear or axial failure. Intersection of the shear and axial planes causes the sample to disintegrate. Characteristic for this mode of failure is that the failed sample is often cone shaped.
- Vertical splitting: Failure planes develop parallel to the applied pressure (σ_1). In practice this failure mechanism occurs the least upon testing and points out that there have been little microscopic discontinuities in the tested sample.

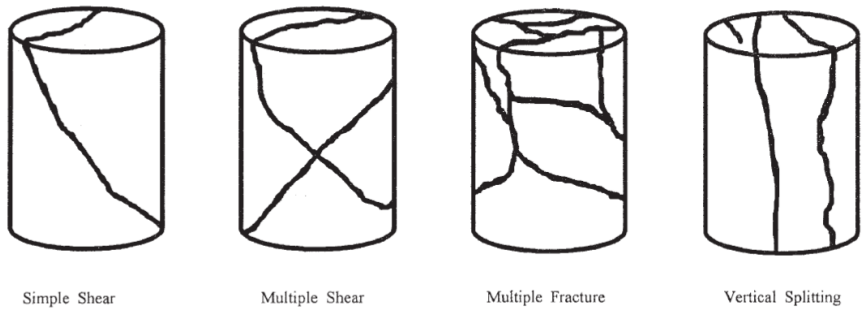

Figure A.2: Failure mechanisms obtained in UCS testing (from: Szwedzicki and Shamu (1999))

A.3 Interpreting UCS Test Results

As discussed different failure mechanisms can be obtained when conducting UCS tests on what seems to be similar samples. It is an interesting fact that a relatively simple test commonly leads to such a large spread in obtained results. An example is given by Hoek and Martin (2014), where a series of tests on Lac du Bonnet granite is presented (Figure A.3).

Hoek and Martin (2014) state that the obtained spread results from poor sample preparation. Szwedzicki (2007) does not agree with this and states that the spread is the result of the distribution of micro defects in the samples causing different failure mechanisms. Based on the theory presented in this chapter the latter explanation seems to be more accurate.

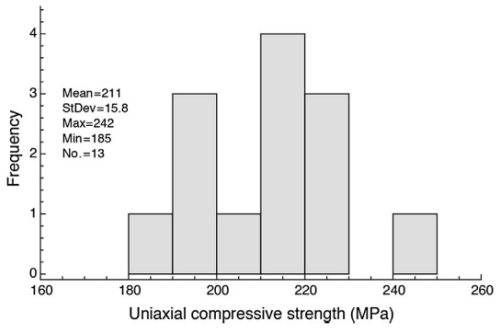

Figure A.3: Obtained failure mechanism with respect to brittleness ratio B (from: Szwedzicki and Shamu (1999))

A.4 Triaxial Testing

When sufficient confinement applied rock samples that would behave brittle in UCS testing will start to behave in a ductile manner after failure (Goodman (1989)). A practicle example is given by Wawersik and Fairhurst (1970) and illustrates that intact rock, in this case Tennesse marble, shows brittle behavior when tested in a UCS setting but behaves more and more ductile after failure as a function of the applied confinement (Figure A.4).

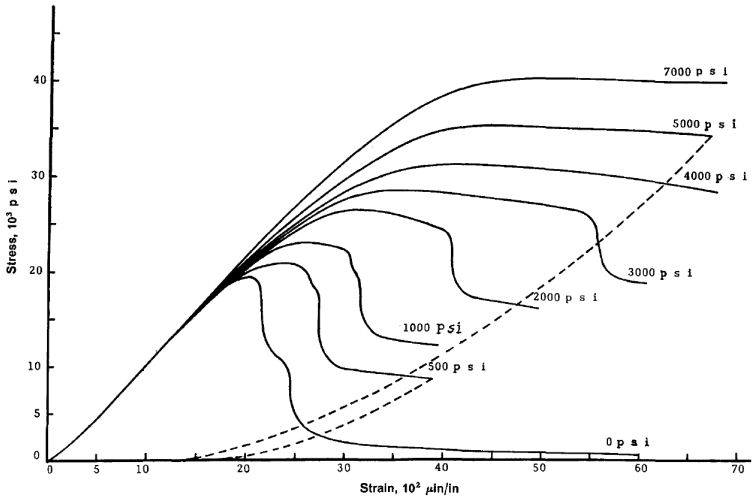

Figure A.4: Stress strain curves from tests on Tennesse marble at different degrees of confinement (1psi ≈ 6.89kPa), (Wawersik and Fairhurst (1970))

The crack initiation stress has a low susceptibility to confinement. Though, the propogation of cracks is susceptible to confinement (Diederichs (2003)). Axial splitting of a sample can only be obtained when individual cracks can propagate along the entire sample. This mechanism is suppressed when a specimen is tested in a confined setting (i.e. triaxial test). Therefore more but shorter cracks are formed in triaxial testing, leading to the development of one or multiple shear planes along which the sample fails. It is for this reason that axial splitting may be the obtained in UCS testing on a brittle rock sample but damage accumulation leading to shear failure is obtained in triaxial testing.

Appendix B

MC and HB Failure Criterion

In practise mostly the MC and HB failure criterion are applied to assess the LEBP behavior of rock masses. In this appendix both criterion will be discussed.

B.1 Mohr-Coulomb

In this section the Mohr-Coulomb failure criterion is discussed as explained by Hoek et al. (2000). According to Mohr-Coulomb the strength of a rock mass can be expressed in terms of the two strength parameters ϕ and c, denoting the friction angel and cohesion respectively. The Mohr-Coulomb failure criterion is stated in Equation B.1, in combination with Equation B.2 and Equation B.3. In this expression the parameter σ_{cm} represents the theoretical UCS of the rock mass, which is considered equal to σ_{ci} in this research as an intact rock mass is considered.

$$\sigma_1 = \sigma_{cm} + b\sigma_3 \tag{B.1}$$

$$\sigma_{cm} = \frac{2c\cos\phi}{(1-\sin\phi)} \tag{B.2}$$

$$b = \frac{(1+\sin\phi)}{(1-\sin\phi)} \tag{B.3}$$

A visual representation of the failure criterion as presented in Equation B.1 in combination with Equation B.2 and Equation B.3 is shown in Figure B.1. Note that only the part which represents failure in compression is displayed. Extrapolation of the line for negative values of σ_3 in combination of a so called tension cut off can be applied to account for the tensile strength of the rock mass.

After brittle failure the residual strength can be desribed by the same criterion by using residual strength parameters c_r and ϕ_r. The residual strength is then described by Equation B.4 in combination with Equation B.5 and Equation B.6.

$$\sigma_1 = \sigma_{cm} + b\sigma_3 \tag{B.4}$$

$$\sigma_{cm} = \frac{2c_r\cos\phi_r}{(1-\sin\phi_r)} \tag{B.5}$$

$$b = \frac{(1+\sin\phi_r)}{(1-\sin\phi_r)} \tag{B.6}$$

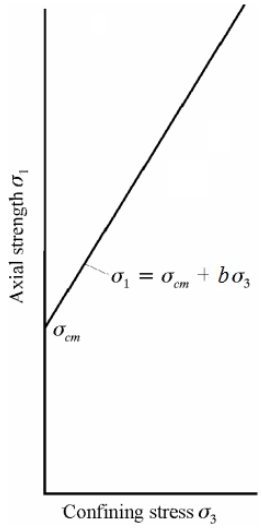

Figure B.1: Mohr-Coulomb failure criterion (from: Hoek et al. (2000))

B.2 Hoek-Brown

The Hoek-Brown failure criterion has been subjected to several adjustments sinds its introduction in 1980, as summerised by Hoek and Marinos (2007). In this section the most recent version of the failure criterion, named the generalised HB criterion, as proposed by Hoek et al. (2002) will be described. This criterion, for both intact and jointed rock masses, is displayed in Equation B.7.

$$\sigma_1 = \sigma_3 + \sigma_{ci}\left(m\frac{\sigma_3}{\sigma_{ci}} + s\right)^a \tag{B.7}$$

After brittle failure the residual strength can be described by the same criterion by using residual strength parameters s_r and m_r. The residual strength is then described by Equation B.8.

$$\sigma_1 = \sigma_3 + \sigma_{ci}\left(m_r\frac{\sigma_3}{\sigma_{ci}} + s_r\right)^{a_r} \tag{B.8}$$

Existing equations to assess appropriate values for m, s and a based on the disturbance parameter D and GSI are only applicable when the rock is failing in a confined state (i.e. right side of the spalling limit, Figure 2.5, Hoek and Brown (1997), Kaiser (2016)). This behavior is not considered in this research and therefore these equations are not elaborated.

B.3 Relation Hoek-Brown and Mohr-Coulomb

Even though the Hoek-Brown failure criterion is widely accepted, there are cases where it is considered beneficial if the strength of a rock mass is expressed in terms of the Mohr-Coulomb strength parameters ϕ and c. Hoek et al. (2002) proposes a translation from Hoek-Brown to Mohr-Coulomb strength parameter, based on the idea that the closest fit between the two criterion is found if the area on both sides of the Mohr-Coulomb criterion is balanced out (Figure B.2). The proposed expressions to derive the Mohr-Coulomb strength parameters as explained are displayed in Equation B.9, Equation B.10, Equation B.11 and Equation B.12.

$$\phi = \sin^{-1}\left[\frac{6am_b(s + m_b\sigma'_{3n})^{a-1}}{2(1+a)(2+a) + 6am_b(s + m_b\sigma'_{3n})^{a-1}}\right] \tag{B.9}$$

$$c = \frac{\sigma_{ci}\left[(1+2a)s + (1-a)m_b\sigma'_{3n}\right](s + m_b\sigma'_{3n})^{a-1}}{(1+a)(2+a)\sqrt{1 + (6am_b(s + m_b\sigma'_{3m})^{a-1})/((1+a)(1-a))}} \tag{B.10}$$

with:

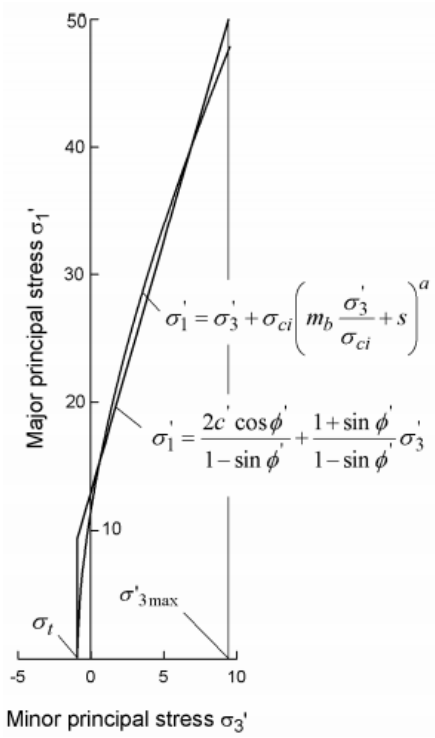

Figure B.2: Failure criterion according to Hoek-Brown and Mohr-Coulomb plotted in same stress space

$$\sigma_{3n} = \sigma_{3max}/\sigma_{ci} \tag{B.11}$$

and:

$$\frac{\sigma_{3max}}{\sigma_{cm}} = 0.47\left(\frac{\sigma_{cm}}{\gamma H}\right)^{-0.94} \tag{B.12}$$

When values of the Hoek Brown paramters m, m_r, s, s_r, a and a_r from case Sweden are converted into equivalent Mohr Coulomb parameters c, c_r, ϕ and ϕ_r using the method stated above, values as displayed in Table B.1 are found:

	c [MPa]	ϕ [◦]
peak	30.8	0
residual	2.1	30.8

Table B.1: Equivalent MC parameters base case

As discussed in chapter 2 the Hoek Brown parameters are chosen such that all cohesion is lost after failure. However, as shown in Table B.1 a certain residual cohesion is available. This is due to the fact that the Hoek Brown resedual strength envalope has a curvature in the low confinement area which causes the closest linear Mohr Coulomb criterion fit to be associated with a non zero resedual cohesion.

B.4 Hoek-Brown Schemes

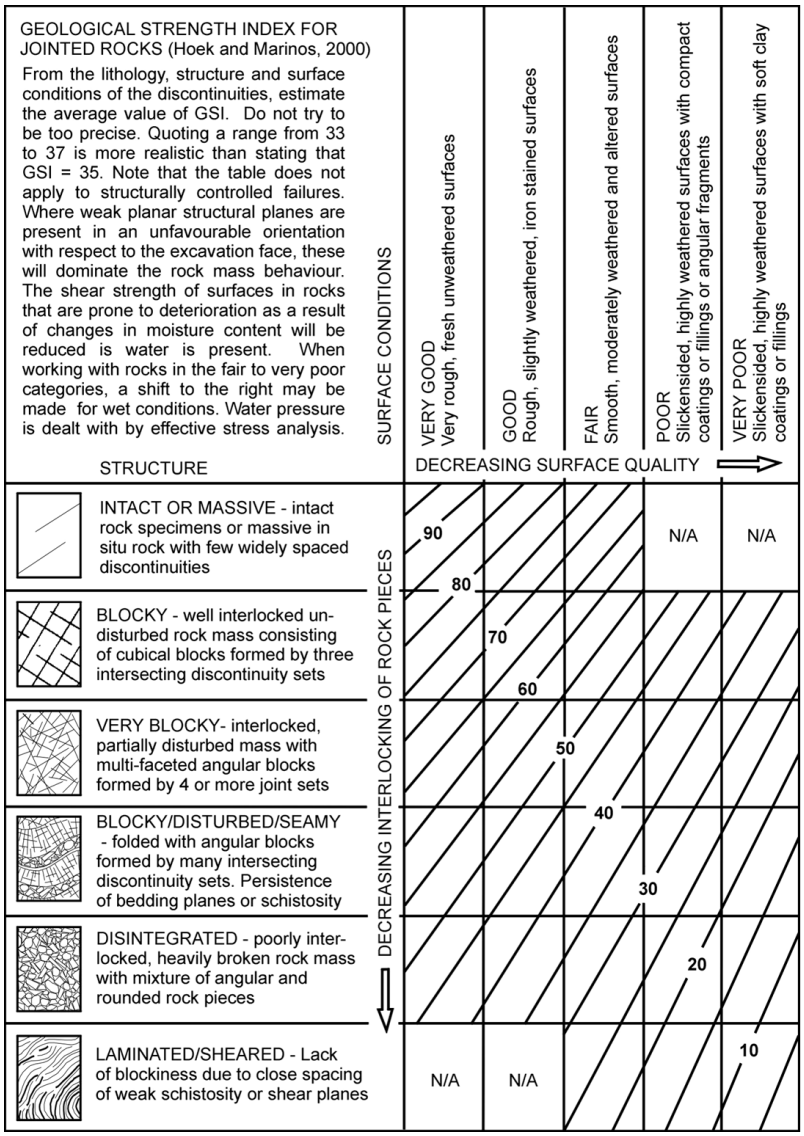

Figure B.3: Geological Strength index GSI (Marinos et al. (2000))

Rock type	Class	Group	Texture			
			Coarse	Medium	Fine	Very fine
SEDIMENTARY	Clastic		Conglomerates * Breccias *	Sandstones 17 ± 4	Siltstones 7 ± 2 Greywackes (18 ± 3)	Claystones 4 ± 2 Shales (6 ± 2) Marls (7 ± 2)
	Non-Clastic	Carbonates	Crystalline Limestone (12 ± 3)	Sparitic Limestones (10 ± 2)	Micritic Limestones (9 ± 2)	Dolomites (9 ± 3)
		Evaporites		Gypsum 8 ± 2	Anhydrite 12 ± 2	
		Organic				Chalk 7 ± 2
METAMORPHIC	Non Foliated		Marble 9 ± 3	Hornfels (19 ± 4) Metasandstone (19 ± 3)	Quartzites 20 ± 3	
	Slightly foliated		Migmatite (29 ± 3)	Amphibolites 26 ± 6	Gneiss 28 ± 5	
	Foliated**			Schists 12 ± 3	Phyllites (7 ± 3)	Slates 7 ± 4
IGNEOUS	Plutonic	Light	Granite 32 ± 3	Diorite 25 ± 5 Granodiorite (29 ± 3)		
		Dark	Gabbro 27 ± 3 Norite 20 ± 5	Dolerite (16 ± 5)		
	Hypabyssal		Porphyries (20 ± 5)		Diabase (15 ± 5)	Peridotite (25 ± 5)
	Volcanic	Lava		Rhyolite (25 ± 5) Andesite 25 ± 5	Dacite (25 ± 3) Basalt (25 ± 5)	
		Pyroclastic	Agglomerate (19 ± 3)	Breccia (19 ± 5)	Tuff (13 ± 5)	

Figure B.4: Representative values of m_i for different rock types (Marinos et al. (2000))

Appendix C

Stress Concentration Around Underground Excavations

The stresses in the roof and walls of an excavation change when the horizontal and vertical principal stress are not the same (i.e. K_0 or $k \neq 1$). Also the geometry of the underground excavation has an influence on the maximum obtained stresses in the tunnel wall and roof. This is summarised and schematised by Hoek and Brown (1980b) based on derivations presented by Greenspan (1944) and estimates the expected maximum vertical and horizontal stress in the tunnel roof and walls if the rock material behaves elastically (Figure C.1).

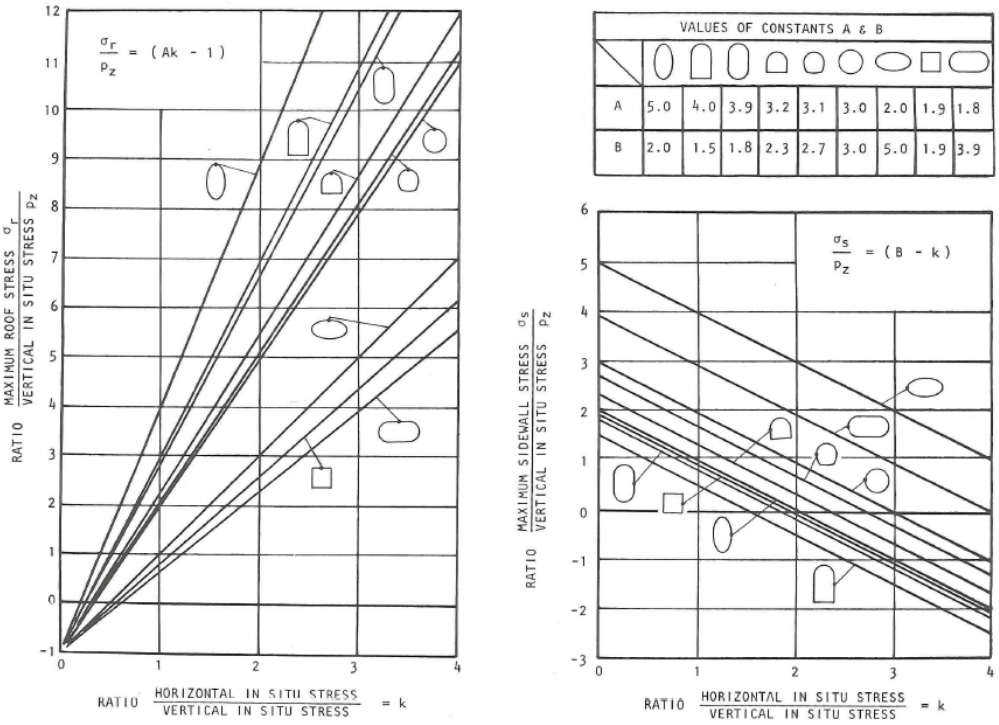

Figure C.1: Maximum roof and wall stresses based on excavation shape (Hoek and Brown (1980b)), purely elastic rock mass behavior around excavation

C.1 Equivalent In Situ Stress Analytic Solution

Case Sweden presents a situation in which a strain burst occurred in a non circular excavation subjected to a non-hydrostatic stress state. This situation is approximated using an analytic analysis in which a circular excavation subjected to a hydrostatic stress state. After excavation in either case the rock at the excavation boundary is subjected to a stress state of uniaxial compression ($\sigma_\theta \neq 0$ and $\sigma_r = 0$, as explained

in Appendix D). Figure C.1 is used to find the p at which σ_θ is equal in both cases. The calculation based on which this value for p is found is presented underneath.

In the described case the strain burst event occurred in the roof of a horse shoe shaped excavation. In Table 4.1 it is stated that the horizontal to vertical in situ stress ratio $k = \sigma_h/\sigma_v = 38/27 \approx 1.4$. In Figure C.1 $p_z = \sigma_v$, which leads to a maximum roof stress $\sigma_{\theta,max} \approx 3 \approx 80MPa$. Around a circular excavation subjected to a hydro static stress state the maximum stress $\sigma_{\theta,max} = 2p$. From this it follows that $\sigma_{\theta,max}$ is equal in both cases when $p = 40MPa$ is applied.

Appendix D

Derivation Analytic Solution Convergence Confinement Equilibrium

By creating an underground opening in the form of a drift or tunnel the original in situ stress state is disturbed and stresses are redistributed around the excavation. The stress state after excavation depends on the in situ stress in combination with the geometry of the excavation and the behavior of the rock material (i.e. elastic, LEPP, LEBP).

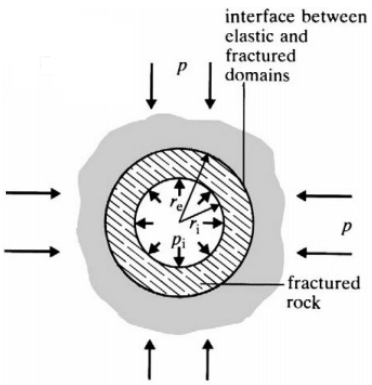

Figure D.1: Pressures that influence the radial displacement of a tunnel wall (from: Hoek et al. (2000), *modified*)

In step I of this research available analytic solutions are used to study the stress distribution around a circular excavation through a massive rock mass subjected to hydro static stresses. In the past derivations have been made for different types off rock mass behavior. In this chapter the solution with elastic behavior and linear elastic brittle plastic behavior are considered. The latter rock mass behavior is addressed based on the both the HB and MC failure criterion. When the model allows for plasticity a circular plastic zone is formed around the excavation with a radius r_e. The adressed situation is displayed in Figure D.1. The considered stress strain behavior of brittle rock masses is presented in Figure D.2. This chapter presents a comprehensive derivation of the stress distribution around the excavation based on the principal of the convergence confinement method as presented by Brown et al. (1983) and Brady and Brown (2007).

A visual representation of the required support pressure as a function of the tunnel wall displacement is referred to as the convergence curve. In theory the support stress will become zero if no rock support is applied. When the convergence curve is presented by a straight line the unloading behavior is linear. When the support pressure is reduced after the critical support pressure is reached plasticity occurs forming a plastic zone around the excavation. Deformation of the tunnel mobilises the support pressure of the reinforcement system. When equilibrium is reached tunnel wall deformation does not proceed. An example of such a convergence curve and convergence confinement equilibrium are shown in Figure D.3.

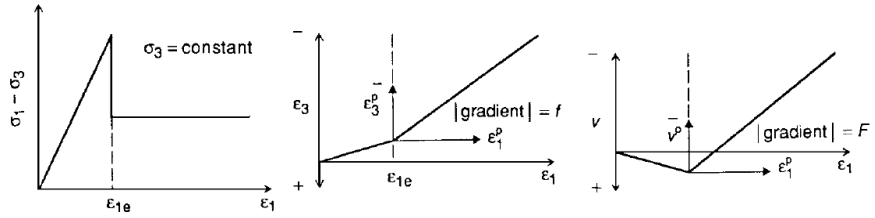

Figure D.2: Brittle rock mass behavior (from: Brown et al. (1983))

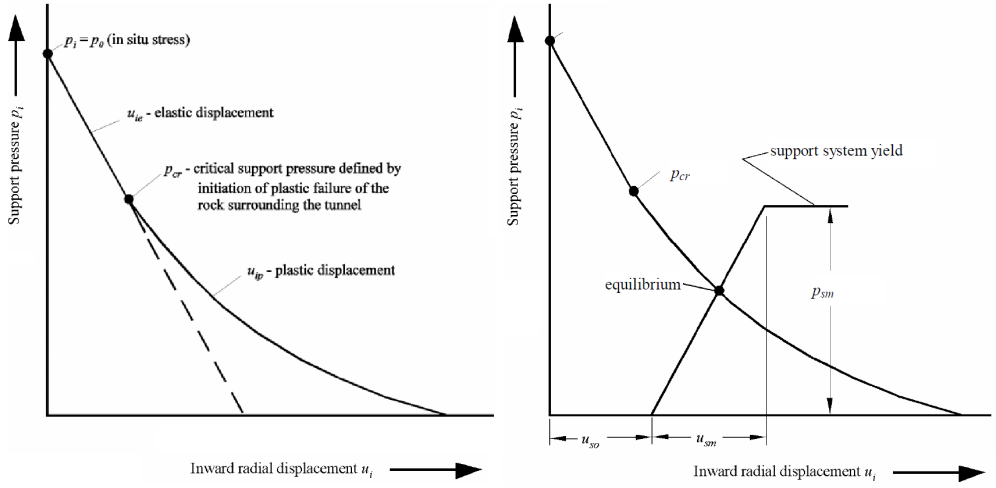

Figure D.3: Convergence of tunnel (L) Convergence-Confinement equilibrium (R) (from: Hoek et al. (2000))

When plasticity occurs the curves representing the stress state around the excavation are shaped as displayed in Figure D.4. A sudden increase in tangential stress represents the boundary between the plastic and the elastic zone.

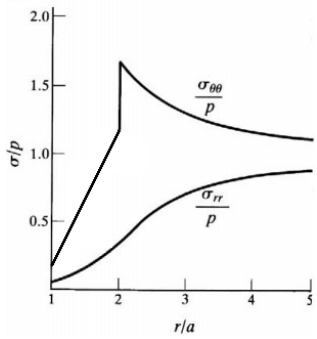

Figure D.4: Stress distribution around circular opening according to elastic brittle plastic material behavior (from: Brady and Brown (2007))

D.1 Elastic behavior

When elastic rock material behavior is assumed the stress-strain behavior is linear regardless whether the in situ strength σ_f of the rock mass is exceeded (Figure D.5).

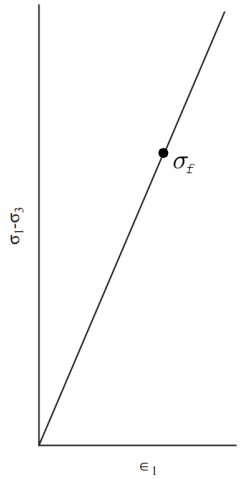

Figure D.5: Purely elastic stres strain behavior (from: Sharan (2003), *adjusted*)

A method to quantify the stresses around a two dimensional circular excavation in an elastic medium was described by Kirsch (1898), known as the Kirsch equations. The derivation of these equations will not be looked at into detail. When considering a hydrostatic stress state (i.e. $k = 1, \sigma_1 = \sigma_3 = p$) the Kirsch equations are reduced to relatively simple expressions. The tangential or circumferential stress is Equation D.2, radial or normal stress is Equation D.1 and in this simplified case the shear stresses are 0 (Equation D.3).

$$\sigma_r = p\Big(1 - \frac{r_i^2}{r^2}\Big) \tag{D.1}$$

$$\sigma_\theta = p\Big(1 + \frac{r_i^2}{r^2}\Big) \tag{D.2}$$

$$\sigma_{r\theta} = 0 \tag{D.3}$$

A visual representation of the tangential and normal stresses are shown in Figure D.6. From the Kirsch equations it follows that the tangential stress right at the excavation boundary amounts $\sigma_\theta = 3(\sigma_1 - \sigma_3) = 2p$, when the principal stresses are equal. From this it follows that the tangential stress the rock is subjected to is twice as high as the principal stress, in combination with the absence of confinement as $\sigma_r = 0$ at the excavation boundary. The deviatoric stress is equal to the stress a rock sample experiences in a UCS test.

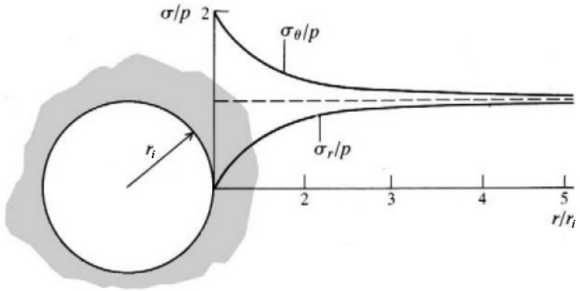

Figure D.6: Stress distribution elastic material behavior, *note:* $a = r_i$, (from: Brady and Brown (2007), *adjusted*)

D.2 Elastic Brittle Plastic Behavior - Hoek Brown

In this section a derivation for the convergence curve is explained using the Hoek Brown LEBP failure criterion as explained by Brown et al. (1983). The principal stresses are $\sigma_1 = \sigma_\theta$ and $\sigma_3 = \sigma_r$ in this axis

symmetric problem. Substitution of these principal stresses leads to the HB failure criterion being expressed as follows (Equation D.4):

$$\sigma_\theta = \sigma_r + \sigma_{ci}\left(m\frac{\sigma_r}{\sigma_{ci}} + s\right)^{0.5} \tag{D.4}$$

The empirical Hoek Brown parameters m and s reduce to residual values m_r and s_r after the rock mass has failed. The residual strength of the rock mass is described by Equation D.5. In the failed rock zone the residual strength represents the tangential stress in the rock mass.

$$\sigma_\theta = \sigma_r + \sigma_{ci}\left(m_r\frac{\sigma_r}{\sigma_{ci}} + s_r\right)^{0.5} \tag{D.5}$$

Because an axis symmetric problem is assessed the Kirsch equations can be re written such that the following condition has to be met in order to obtain a stress equilibrium in the rock mass around the excavation (Equation D.6).

$$\frac{d\sigma_r}{dr} = \frac{\sigma_\theta - \sigma_r}{r} \tag{D.6}$$

Integration of the latter equation using the conditions at the excavation boundary $\sigma_r = p_i$ and $r = r_i$ allows for the derivation of the radial stress distribution in the failed zone, as displayed in Equation D.7:

$$\sigma_r = \frac{m_r\sigma_{ci}}{4}\left[ln\left(\frac{r}{r_i}\right)\right]^2 + \left[ln\left(\frac{r}{r_i}\right)\right](m_r\sigma_{ci}p_i + s_r\sigma_{ci}^2)^{0.5} + p_i \tag{D.7}$$

The radius of the plastic zone around the excavation, r_e, can be derived using the assumption that the stress state at the boundary between the plastic and elastic zone is satisfied by the Hoek-Brown failure criterion as expressed in Equation D.4. At this boundary, the principal stress difference between σ_θ and $\sigma_r = p_1$ is:

$$\sigma_\theta - \sigma_r = 2(p - p_1) \tag{D.8}$$

Based on the failure criterion as displayed in Equation D.4, the principal stress difference can also be expressed as follows Equation D.10:

$$\sigma_\theta - \sigma_r = \sigma_{ci}\left(m\frac{\sigma_r}{\sigma_{ci}} + s\right)^{0.5} \tag{D.9}$$

Substitution of Equation D.8 into Equation D.9 leads to the expression displayed in Equation D.10:

$$2(p - p_1) = \sigma_{ci}\left(m\frac{\sigma_r}{\sigma_{ci}} + s\right)^{0.5} \tag{D.10}$$

Which can be rewritten as (Equation D.11):

$$p_1 = p - M\sigma_{ci} \tag{D.11}$$

with (Equation D.12):

$$M = \frac{1}{2}\left[\frac{m}{4} + m\frac{p}{\sigma_{ci}} + s\right]^{0.5} - \frac{m}{8} \tag{D.12}$$

The condition $\sigma_r = p_1$ has to be satisfied at $r = r_e$. Equating Equation D.7 to Equation D.11 while substituting $r = r_e$ leads to the following expression (Equation D.13):

$$p - M\sigma_{ci} = \frac{m_r\sigma_{ci}}{4}\left[ln\left(\frac{r_e}{r_i}\right)\right]^2 + \left[ln\left(\frac{r_e}{r_i}\right)\right](m_r\sigma_{ci}p_i + s_r\sigma_{ci}^2)^{0.5} + p_i \tag{D.13}$$

The latter equation is solved to find an expression for r_e, which is presented in Equation D.14 and :

$$r_e = r_i \exp\left[N - \frac{2}{m_r\sigma_{ci}}(m_r\sigma_{ci}p + s_r\sigma_{ci}^2)^{0.5}\right] \tag{D.14}$$

with (Equation D.15):

$$N = \frac{2}{m_r \sigma_{ci}}(m_r \sigma_{ci} p + s_r \sigma_{ci}^2 - m_r \sigma_{ci}^2 M)^{0.5} \tag{D.15}$$

When the support pressure p_i is lower than the critical support pressure $p_{i,cr}$ an plastic zone is formed around the excavation. From Equation D.11 it follows that $p_{i,cr}$ equals (Equation D.16):

$$p_{i,cr} = p - M\sigma_{ci} \tag{D.16}$$

After excavation the support pressure is reduced from p to p_i, leading to radial inward displacement of the rock mass. In the following derivation inwards movement of the tunnel perimeter is a negative displacement. The displacement of the elastic zone equals (Equation D.17, Equation D.18):

$$u_r = -\frac{(p - p_1) r_e^2}{2Gr} \tag{D.17}$$

In which:

$$G = \frac{E}{2(1+\nu)} \tag{D.18}$$

If a plastic zone exists, the displacement at the boundary between the elastic and the plastic zone can be found by substituting $r = r_e$ into Equation D.17, as shown underneath (Equation D.19):

$$u_r = -\frac{(p - p_1) r_e}{2G} \tag{D.19}$$

When only elastic unloading takes place no plastic zone is formed (i.e. $r_e = r$), leading to Equation D.20.

$$u_i = -\frac{(p - p_i) r}{2G} \tag{D.20}$$

As displayed in Equation D.21, Equation D.22 and Equation D.23, the strains in the plastic zone amount:

$$\epsilon_\theta = \epsilon_1 = -\frac{u}{r} \tag{D.21}$$

$$\epsilon_r = \epsilon_3 = -\frac{du}{dr} \tag{D.22}$$

$$\epsilon_3 = \epsilon_{3e} - f(\epsilon_1 - \epsilon_{1e}) \tag{D.23}$$

In the latter formula 'e' is added to the subscript to denote the strains at the boundary between the plastic and the elastic zone. The parameter f is a constant that represents the gradient between the plastic strains, as shown in Equation D.24 and Figure D.2.

$$f = \frac{\epsilon_3^p}{\epsilon_1^p} \tag{D.24}$$

The strains at the boundary between the plastic and elastic zone are (Equation D.25):

$$\epsilon_{1e} = -\epsilon_{3e} = \frac{p - p_1}{2G} \tag{D.25}$$

Substitution of Equation D.25 into Equation D.24 gives Equation D.26:

$$\epsilon_3 = -f\epsilon_1 - (1-f)\frac{p - p_1}{2G} \tag{D.26}$$

Combining Equation D.21, Equation D.22 and Equation D.26 leads to the differential equation displayed in Equation D.27:

$$\frac{du}{dr} = -f\frac{u}{r} + (1-f)\frac{p - p_1}{2G} \tag{D.27}$$

Solving the differential equation using $r = r_e$ leads to the final expression giving the inwards movement of the tunnel perimeter (Equation D.28):

$$\frac{u}{r} = -\frac{(p - p_1)}{G(1+f)}\left[\frac{f-1}{2} + \left(\frac{r_e}{r_i}\right)^{1+f}\right] \tag{D.28}$$

D.3 Elastic Brittle Plastic Behavior - Mohr Coulomb

As discussed in Appendix B the Mohr-Coulomb failure criterion defines the strength of a rock mass is described by Equation D.29, Equation D.30 and Equation D.31.

$$\sigma_1 = \sigma_{cm} + b\sigma_3 \tag{D.29}$$

$$\sigma_{cm} = \frac{2c\cos\phi}{(1-\sin\phi)} \tag{D.30}$$

$$b = \frac{(1+\sin\phi)}{(1-\sin\phi)} \tag{D.31}$$

When considering failure a loss of cohesion the residual stenght is derived from confinement due to the presence of a rock reinforcement system. In other words the term Equation B.2 is removed from the resedual strength criterion, as $c = 0$. In that case the broken rock is expected to behave as a rock fill with a certain friction angle but no cohesion (Hoek and Brown (1997)). Therefore the strength of the failed rock is described as displayed in Figure D.2. Note that the 'cohesion term' σ_{cm} is taken out of the equation compared to the failure criterion of intact rock (Equation D.32). In the latter equation ϕ_r represents the friction angle of the broken rock material.

$$\sigma_1 = d\sigma_3 \tag{D.32}$$

with:

$$d = \frac{(1+\sin\phi_r)}{(1-\sin\phi_r)} \tag{D.33}$$

In the considered case the principal stresses are $\sigma_\theta, (\sigma_1)$ and $\sigma_r(\sigma_3)$ equation Equation D.32 can be expressed as (Equation D.34):

$$\sigma_\theta = d\sigma_r \tag{D.34}$$

Like stated earlier, a circular opening is considered in this analysis. This causes the situation to be axis symmetric, which means that only one condition has to be satisfied in order to obtain an equilibrium situation (Equation D.35).

$$\frac{d\sigma_r}{dr} = \frac{\sigma_\theta - \sigma_r}{r} \tag{D.35}$$

When substituting Equation D.34 into Equation D.35, the latter equation can be written as (Equation D.36):

$$\frac{d\sigma_r}{dr} = (d-1)\frac{\sigma_r}{r} \tag{D.36}$$

Rewriting Equation D.36 in the following form allows for integration (Equation D.37):

$$(d-1)\frac{1}{r}dr = \frac{1}{\sigma_r}d\sigma_r \tag{D.37}$$

Integration of Equation D.37 by following the derivation steps displayed in Equation D.38 to Equation D.43 with the boundary conditions that apply to the fractured zone is shown underneath.

$$\int_{r_i}^{r}(d-1)\frac{1}{r}dr = \int_{p_i}^{\sigma_r}\frac{1}{\sigma_r}d\sigma_r \tag{D.38}$$

$$\left[ln(r^{d-1})\right]_{r_i}^{r} = \left[ln(\sigma_r)\right]_{p_i}^{\sigma_r} \tag{D.39}$$

$$ln(r^{d-1}) - ln(r_i^{d-1}) = ln(\sigma_r) - ln(p_i) \tag{D.40}$$

$$ln\left(\frac{r^{d-1}}{r_i^{d-1}}\right) = ln\left(\frac{\sigma_r}{p_i}\right) \tag{D.41}$$

$$\left(\frac{r}{r_i}\right)^{d-1} = \frac{\sigma_r}{p_i} \tag{D.42}$$

$$\sigma_r = p_i\left(\frac{r}{r_i}\right)^{d-1} \tag{D.43}$$

Substitution of Equation D.34 in Equation D.43 leads to the tangential stress distribution in the broken zone (Equation D.44):

$$\sigma_\theta = dp_i\left(\frac{r}{r_i}\right)^{d-1} \tag{D.44}$$

At the intersection between the fractured zone and the intact rock the radial stress is equal in both masses. Defining p_1 as the radial stress at this boundary, situated at $r = r_e$, Equation D.43 equals:

$$p_1 = p_i\left(\frac{r_e}{r_i}\right)^{d-1} \tag{D.45}$$

Which can be re-written as Equation D.46:

$$r_e = r_i\left(\frac{p_1}{p_i}\right)^{1/(d-1)} \tag{D.46}$$

The principal stresses in the elastic zone are (Equation D.47, Equation D.48):

$$\sigma_\theta = p\Big(1 + \frac{r_e^2}{r^2}\Big) - p_1\frac{r_e^2}{r^2} \tag{D.47}$$

$$\sigma_r = p\Big(1 - \frac{r_e^2}{r^2}\Big) + p_1\frac{r_e^2}{r^2} \tag{D.48}$$

At the boundary of the broken and the intact rock the conditions are (Equation D.49):

$$\sigma_\theta = 2p - p_1, \sigma_r = p_1 \tag{D.49}$$

Knowing that the condition at the intersection between the broken and the intact rock equals the stress state at failure of the rock mass, the expressions from Equation D.49 can be substituted into Equation B.1. This leads to the following expression of the failure criterion:

$$2p - p_1 = kp_1 + \sigma_{ci} \tag{D.50}$$

By rearranging the latter equation the support stress at which plasticity occurs (i.e the rock mass breaks) can be derived:

$$p_1 = \frac{2p - \sigma_{ci}}{1 + k} \tag{D.51}$$

The radius of the fractured zone is obtained when Equation D.51 is substituted into Equation D.46, as shown underneath (Equation D.52).

$$r_e = r_i\left[\frac{2p - \sigma_{ci}}{(1 + b)p_i}\right]^{1/(d-1)} \tag{D.52}$$

The displacements after excavation are the same as explained in the previous derivation using the Hoek Brown failure criterion.

D.4 Confinement Due to Rock Reinforcement

As described in the previous section the perimeter of the tunnel will start to move in the direction of the tunnel after excavation. This causes the support stress of the applied reinforcement system to be mobilised. The stress strain curve for passive rock bolts can differ based on the kind of rock bolt that is considered, which is elaborated in Appendix E.

The response of the rock support system is a function of the moment of installation, the stiffness and peak strength. Because tunnel deformation starts ahead of the face a certain deformation has already taken place when the rock reinforcement system is installed at the earliest practicable moment. In Figure D.7 this deformation is stated as u_{i0}.

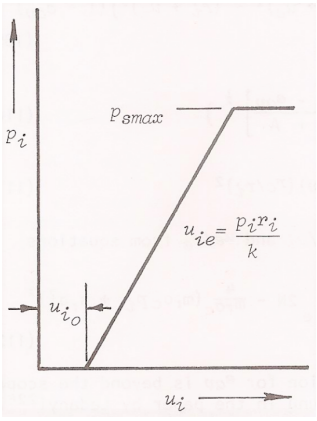

Figure D.7: Stress-Strain curve rock reinforcement system (from: Hoek and Brown (1980b))

Convergence of the tunnel after installing the rock reinforcement system will stabilise the support pressure as displayed in Equation D.53 and Equation D.54 (Hoek and Brown (1980b)).

$$p_i = k_b \frac{u_{ie}}{r_i} \tag{D.53}$$

$$u_{ie} = u_{i0} + \frac{p_i r_i}{k_b} \tag{D.54}$$

For rock bolts the values for the stiffness k_b and strength p_{smax} based on dynamic tests, where an individual rock bolt is loaded axially up till failure, in combination with the in situ bolt spacing (see Appendix E). The stress at which a bolt fails in such a test amounts T_{bf}. Besides the strength of an individual bolt the density of the bolting pattern plays a role in the support stress that can be established by the rock reinforcement system, as displayed in Equation D.55.

$$p_{smax} = \frac{T_{bf}}{s_c s_l} \tag{D.55}$$

In this thesis report rock reinforcement systems in which mesh is applied are considered. In such cases it is assumed that the mesh only serves the purpose of transferring stresses from the rock mass to the rock bolts, but does not add to the strength capacity or stiffness of the rock reinforcement system.

D.5 Python Code Analytic Convergence Confinement Equilibrium

```
# Elastic brittle behavior

import math
import numpy as np
import pylab
import matplotlib.pyplot as plt

### Tunnel Convergence ###

#Hoek-Brown input parameters
sigma_c = 140.  # UCS rock mass [MPa]
m = 0.0         # Hoek-Brown parameter m [-]
s = 0.16        # Hoek-Brown parameter s [-]
E = 46000.      # Youngs modulus [MPa]
v = 0.2         # Poissons ratio [-]
m_r = 1.        # Resedual Hoek-Brown parameter m [-]
s_r = 0.        # Resedual Hoek-Brown parameter s [-]
a = 0.5         # Hoek-Brown parameter a [-]
a_r = 0.5       # Resedual Hoek-Brown parameter a [-]

#Excavation setting
p = 40.         # Hydrostatic in situ stress [MPa]
r_i = 3.5       # Tunnel radius [m]

i = np.linspace(0, p, 10000) # Values of p_i

u = [] #values convergence (deformation)
r = [] #values radius

G = E / (2 * (1 + v)) # Shear modulus

### Equivilent M-C parameters ###

sigma_3n =  0.47 * (sigma_c / p)**-0.94 # For best fit MC-HB

phi = math.asin((6*a*m*(s+m*sigma_3n)**(a-1))/(2*(1+a)*(2+a)+(6*a*m*(s+m*sigma_3n)**(a-1))))
phi_deg = phi * 180 / math.pi
c = (sigma_c*(((1+2*a)*s+(1-a)*m*sigma_3n)*(s+m*sigma_3n)**(a-1)))/((1+a)*(2+a)
  *math.sqrt(1+(6*a*m*(s+m*sigma_3n)**(a-1))/((1+a)*(1-a))))

phi_f = math.asin((6*a_r*m_r*(s_r+m_r*sigma_3n)**(a_r-1))/(2*(1+a_r)*(2+a_r)+(6*a_r*m_r*
  (s_r+m_r*sigma_3n)**(a_r-1))))
phi_f_deg = phi_f * 180 / math.pi
c_r = (sigma_c*(((1+2*a_r)*s_r+(1-a_r)*m_r*sigma_3n)*(s_r+m_r*sigma_3n)**(a_r-1)))/((1+a_r)*
  (2+a_r)*math.sqrt(1+(6*a_r*m_r*(s_+m_r*sigma_3n)**(a_r-1))/((1+a_r)*(1-a_r))))

# Print case properties #

print "Case: Quartzite drift Sweden"
print "sigma_c =", sigma_c, "p =", p, "s =", s, "r_i =", r_i

# Plot peak and residual strenght envalope #

sigma_3 = np.linspace(0,30,1000)
sigma_1_peak = sigma_3 + sigma_c*(m*(sigma_3/sigma_c)+s)**0.5
sigma_f = (s**0.5)*sigma_c + (0*sigma_3)
sigma_1_resid = sigma_3 + sigma_c*(m_r*(sigma_3/sigma_c)+s_r)**0.5

# compose plot
pylab.plot(sigma_3,sigma_1_peak,'r',label="sigma_1_peak")
pylab.plot(sigma_3,sigma_1_resid,'b',label="sigma_1_resid.")
pylab.plot(sigma_3,sigma_f,'g',label="sigma_f")
plt.xlabel('sigma_3 [MPa]')
plt.ylabel('sigma_1 [MPa]')
plt.title('Peak and residual strength envalope')
plt.legend(bbox_to_anchor=(1.05, 1), loc=2, borderaxespad=0.)
pylab.show() # show the plot

# Parameters M & N for the elastic region
```

```
M = 0.5 * ((m / 4)**2 + (m * p / sigma_c) + s)**0.5 - (m / 8)
N = ((2 / (m_r * sigma_c)) * (math.sqrt((m_r * sigma_c * p) + (s_r * sigma_c**2)
  - (m_r*(sigma_c**2)*M))))

# Post peak dilation parameter f
f = 1. #zero volume increase after failure

for p_i in i:
    if p_i >= p - M * sigma_c:
        u.append(r_i*((p - p_i) / (2 * G)))
    else:
        r = r_i * math.exp(N - (2 / (m_r * sigma_c)) * (((p_i * m_r * sigma_c) +
        (s_r * sigma_c**2))**0.5))
        u.append(r_i*(((M * sigma_c) / (G *(f + 1))) * (((f - 1) / 2) + ((r/r_i)**(f + 1)))))

u1 = [j * 1000 for j in u]   # u = deformation tunnel wall [mm]

### Support system ###
u_f = u1[0]                  # deformation when p_i = 0 MPa
delta_0 = u_f / 3            # Tunnel deformation before instalment support [m]

# Rock bolts:
Bolt_type = 'Rebar'
T_bf = 0.2   # Strength bolt from pullout test [MN]
s_c = 1.       # Circumferential spacing bolt [m]
s_l = 1.       # longitudinal spacing bolt [m]
E_b = 205000.  # Stiffness bolt material [MPa]
EDC_bolt = 5. # Energy dissipation capacity bolt [KJ]

A_1 = r_i*2*math.pi                                    # Perimeter cross section
sp = (s_c + s_l)/2                                      # bolt spacing [m]
n = A_1/sp                                              # number of bolts [-]
EDC_tot = EDC_bolt*n                                 # total energy dissipation capacity [MJ]

print "bolt type =", Bolt_type, ",EDC =", EDC_bolt , ",Amount =", round(n,1)
print 'Energy Dissipation Capacity:', round(EDC_tot,1) , '[kJ]'

# Stiffness system rock bolts:
k_b = 150. #stiffness rock bolt [MN/m]
k_s = k_b / (s_c * s_l)

# Maximum support pressure bolts:
p_smax = T_bf / (s_c*s_l) #[MPa]

### support pressure ###

u2 = [] # deformation support[mm]

i_2 = np.linspace(0, p_smax, 500)
i_3 = np.linspace(p_smax, p_smax, 500)

i4 = []
i4.extend(i_2)
i4.extend(i_3)

for p_i in i:
    if p_i < p_smax:
       delta = (delta_0 + (((p_i * r_i) / k_s) * 1000))
       u2.append(delta)
    else:
       u2.append(np.nan)

u1 = np.asarray(u1) #turning list into array
u2 = np.asarray(u2) #turning list into array

### Equilibrium support stress ###
X = []

diff = u1 - u2
minimum = min(abs(diff))

# Find which position in array p_i represents equilibrium
```

```
142 for X1, Y in enumerate(diff):
143     if Y == minimum or Y == minimum *-1:
144         X = X1
145 
146 p_i = i4[X] #support pressure at equilibrium
147 print 'The support pressure at equilibrium is:', round(i[X],1), 'MPa'
148 
149 p_i = 0.2 #User defined p_i [MPa] if wanted.
150 
151 ### Plotting ###
152 
153 plt.plot(u1,i,'r',label="GRC")            # plotting
154 plt.plot(u2,i,'b',label="SRC")            # plotting
155 plt.xlabel('u [mm]')
156 plt.ylabel('p_i [MPa]')
157 plt.title('Convergence / confinement equilibrium')
158 plt.legend(bbox_to_anchor=(1.05, 1), loc=2, borderaxespad=0.)
159 plt.show()
160 
161 ### Stress distribution broken zone ###
162 r_e = r_i*math.exp(N-((2/(m_r*sigma_c))*((m_r*sigma_c*p_i)+(s_r*sigma_c**2))**0.5))
163 # r_e = radius broken zone
164 
165 sigma_thth = []                                 # Empty lists that will hold values
166 sigma_rr = []
167 
168 r1 = np.linspace(r_i, r_e, 10)                  # input values radius broken zone
169 
170 for r in r1:
171     sigma_rr.append(((((m_r*sigma_c)/4)*((math.log(r/r_i))**2)) + (((math.log(r/r_i))*
172     (((m_r * sigma_c * p_i)) + (s_r * sigma_c**2))**0.5) + p_i)))
173     sigma_r = ((((m_r*sigma_c)/4)*((math.log(r/r_i))**2)) + (((math.log(r/r_i))*
174     (((m_r * sigma_c * p_i)) + (s_r * sigma_c**2))**0.5) + p_i))
175     sigma_thth.append(sigma_r + (((m_r*sigma_c*sigma_r) + (s_r*(sigma_c**2)))**0.5))
176 
177 ############################
178 # stress distrubution intact zone
179 
180 r2 = np.linspace(r_e, 10, 10)   # input values radius intact zone
181 p_1 = p - (M * sigma_c)          # radial stress at boundary broken / intact rock
182 
183 for r in r2:
184     sigma_rr.append(p - ((p - p_1)*((r_e/r)**2)))
185     sigma_thth.append(p + ((p - p_1)*((r_e/r)**2)))
186 
187 ############################
188 r = []                           # a list with all r input values
189 r.extend(r1)
190 r.extend(r2)
191 
192 r_over_r_i = [i/r_i for i in r]
193 sigma_thth_over_p = [i/p for i in sigma_thth]
194 sigma_rr_over_p = [i/p for i in sigma_rr]
195 
196 plt.plot(r_over_r_i,sigma_thth_over_p,'r',label="sigma_theta/p")       # plotting
197 plt.plot(r_over_r_i,sigma_rr_over_p,'b',label="sigma_r/p")             # plotting
198 plt.xlabel('r / r_i [-]')
199 plt.ylabel('sigma / p [-]')
200 plt.title('Stress distribution around excavation')
201 plt.legend(bbox_to_anchor=(1.05, 1), loc=2, borderaxespad=0.)
202 plt.show()
203 
204 ############################
205 alpha = 0.9             #share of accumulated energy that is released at failure
206 
207 A = (r_e**2*math.pi) - (r_i**2*math.pi)              # Volume failed zone [m^3]
208 E_1 = 1000*alpha*(((sigma_c*math.sqrt(s))**2)/(2*E)) # Energy release [kJ/m^3]
209 E_tot = A*E_1    # Total Energy released at failure [kJ]
210 
211 ############################
212 FOS = EDC_tot/E_tot #FOS
213 
```

```
214 print 'Radius failed zone:',round(r_e,1), 'm'
215 print 'Volume failed zone:',round(A,1), 'm^3'
216 print 'Released energy/m^3 failing rock:',round(E_1,1), 'kJ'
217 print 'Released energy from failed zone:',round(E_tot,1), 'kJ'
218 print 'Factor of safety:',round(FOS,2), '-'
219
220 if EDC_tot > E_tot:
221     print '(Stable/Failure): Stable'
222 else:
223     print '(Stable/Failure): Failure'
224
225 ##### Validation outcome
226 sigma_f1 = (s**0.5)*sigma_c
227 sigma_1_p = p_1 + sigma_c*(m*(p_1/sigma_c)+s)**0.5
228 sigma_1_res = p_1 + sigma_c*(m_r*(p_1/sigma_c)+s_r)**0.5
229
230 print 'Outcome validation:'
231
232 check1 = []
233 check3 = []
234
235 if p_1 < (sigma_c/10):
236     check1 = 'valid'
237 else:
238     check1 = 'invalid'
239
240 if 1 < (sigma_1_p/sigma_1_res):
241     check2 = 'valid'
242 else:
243     check2 = 'invalid'
244
245 print'(1) UCS / Sigma_r
246   (bounary intact/broken):', round(sigma_c/p_1,1),'[-]', check1
247 print'(2) sigma_1_p/sigma_1_res
248   (boundary intact/broken):', round(sigma_1_p/sigma_1_res,1),'[-]', check2
```

Appendix E

Rock Reinforcement System

In this chapter the method applied to derive the static and dynamic performance of rock bolts is elaborated.

E.1 Static and Dynamic Bolt Response

In the static pull test a fracture opening up is simulated. The tested bolt is installed through two concrete blocks that are being moved apart at a low displacement rate, causing the static force-displacement behavior of the tested bolt to be obtained. An image of the set up present at the rock mechanics lab at Norwegian University of Science and Technology alongside with a schematic representation of the test is presented in Figure E.1.

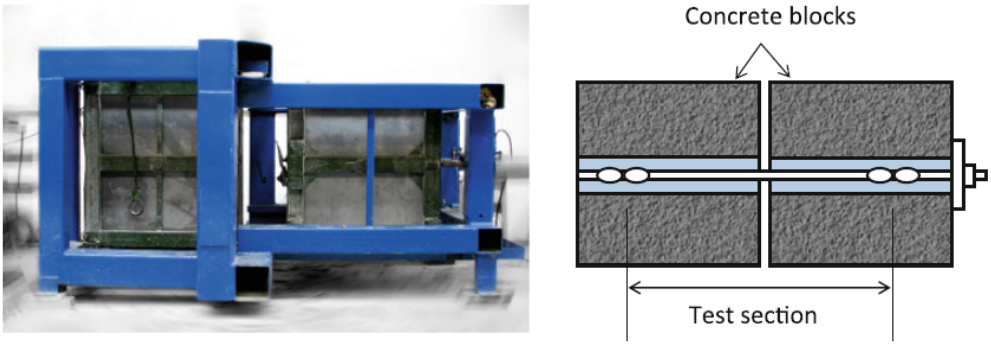

Figure E.1: Static pull test on D-bolt simulating opening up of a crack (from: Li (2012))

Dynamic tests are conducted by means of the set up presented in Figure E.2. In such tests the bolt is axially loaded by means of a block with a certain mass that is dropped from a certain height. This corresponds with a certain velocity and energy when the impact hits the bolt, according to Equation E.1 (Li and Doucet (2012)).

$$E = \frac{1}{2} m_{drop} v_{drop}^2 \tag{E.1}$$

E.2 Stiffness of the Reinforcement System

When considering the in situ stiffness of the reinforcement system in the analytic analysis the approach presented by Brady and Brown (2007) based on Hoek and Brown (1980b) is applied (Appendix D). The latter formula is presented without a derivation in literature as:

$$k_s = \frac{E_s \pi d_b^2}{4 l s_l s_c} \tag{E.2}$$

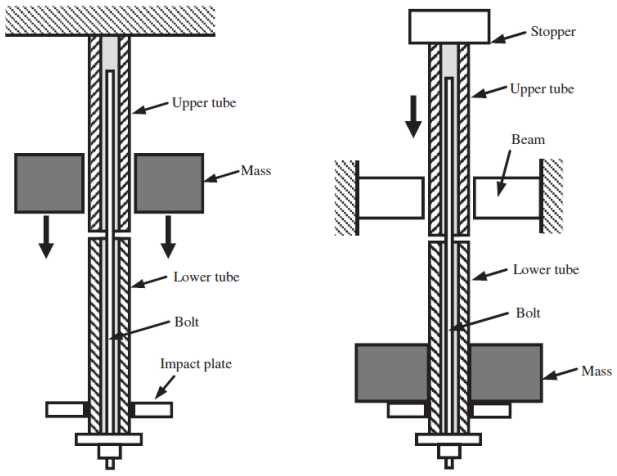

Figure E.2: Schematic dynamic test rock bolt (from: Li et al. (2014))

Simple evaluation of this formula shows that bolt is modeled as a rod with a cross section $A = \frac{1}{4}\pi d_b^2$, in which d_b represents the diameter of the cross section of the bolt steel. The formulation for the stiffness of the system (k_s) then becomes (Equation E.3):

$$k_s = \frac{1}{s_c s_l}\frac{E_s A}{l} \tag{E.3}$$

In other words, the stiffness of an individual bolt is represented by the general expression for the axial stiffness of a rod subjected to an uniform axial stress (Equation E.4):

$$k_b = \frac{E_s A}{l} \tag{E.4}$$

Based on the latter formula the stiffness of the reinforcement system k_b equals the stiffness of the bolt per unit of surface it supports (Equation E.5):

$$k_s = \frac{1}{s_c s_l} k_b \tag{E.5}$$

k_b can be derived from the force-displacement or $F - u_b$ curves that are obtained in pull out tests. The stiffness of the bolt in the elastic region (i.e. prior to yielding) equals (Equation E.6):

$$k_b = \frac{F}{u_b} \tag{E.6}$$

As shown in the introduction of this chapter the elastic response of the split set and the grouted rebar bolt is simular and the deformable section of the D-bolt is less stiff under static loading. However, Figure 2.14 shows that the D-bolt react stiffer when loaded dynamically. From visual assesment of observations presented by Player et al. (2009) it can be concluded that split set bolts are equally stiff when loaded either statically or dynamically. As far as the author is concerned no stress strain curves on the dynamic performance of grouted rebar bolts are presented in literature. Based on the aforementioned it is assumed that all three considered bolt types react equally stiff when loaded dynamically. A read off from Figure 2.11 leads to $k_b \approx 150kN/mm = 150MN/m$. Using a single value for the stiffness off all bolt types strictly spoken introduces an error into the model, because the assumption is based on the read off from a small section of the graph. However, the stiffness of the reinforcement system is a couple orders of magnitude smaller than the elastic unloading stiffness of the rock mass. For illustration, Equation D.20 representing the elastic unloading of the rock mass at the excavation boundary ($r = r_i$) is repeated underneath:

$$u_{ie} = -\frac{(p - p_i)r}{2G} \tag{E.7}$$

In this formula it shows that the linear unloading stiffness of the rock mass at the excavation boundary (k_r) equals (Equation E.8):

$$k_r = \frac{2G}{r_i} \tag{E.8}$$

and:

$$G = \frac{E}{2(1+\nu)} \tag{E.9}$$

Based on the input parameters from case Sweden $E_{mod} = 46000$ MPa, $\nu = 0.2$ $G = 19200$MPa and $r_i = 3.5$m, which leads to $k_r = 11000$ MN/m after rounding. This means that the theoretical linear elastic unloading stiffness of the rock mass is over 70 times larger than the stiffness of the reinforcement system. Based on this observation it may be assumed that the difference in stiffness between the reinforcement system and the rock mass is conserved in the model regardless of slight variations in stiffness that may exist between different bolt types.